Theses and Dissertations (ETD)   College of Graduate Health Sciences

5-2010

TDiscovery and Development of Novel Therapeutic Agents for Advanced Melanoma

Zhao Wang
University of Tennessee Health Science Center

Recommended Citation

Wang, Zhao , "TDiscovery and Development of Novel Therapeutic Agents for Advanced Melanoma" (2010). *Theses and Dissertations (ETD).* Paper 281. http://dx.doi.org/10.21007/etd.cghs.2010.0343.

www.manaraa.com

TDiscovery and Development of Novel Therapeutic Agents for Advanced Melanoma

Abstract

Malignant melanoma is the most dangerous form of skin cancer and accounts for about 75% of skin cancer deaths. Once diagnosed at the metastatic stage, it has a very poor prognosis with a median survival rate of 6 months and a 5-year survival rate of less than 5%. In addition, melanoma has become an important public health hazard owing to its rising incidence, which has been well documented over the past 50 years. Currently there is no effective way to treat melanoma. It is highly resistant to existing chemotherapy, radiotherapy, and immunotherapy. Over the past 30 years, only two drugs have been approved by the Food and Drug Administration (FDA) for metastatic melanoma: dacarbazine (DTIC) and interleukin-2 (IL-2). But even with these two drugs, fewer than 15% of patients have a favorable response and fewer than 5% of patients reach complete remission. On the other hand, the toxicity associated with DTIC and IL-2 is often significant, resulting in serious or life threatening side effects in many patients. In recent years, great efforts have been made in fighting metastatic melanoma. But neither combinations of DTIC with other chemotherapy drugs (*e.g.*, cisplatin, vinblastine, and carmustine) nor adding interferon-α2b to DTIC have shown a survival advantage over DTIC treatment alone. Extensive clinical trials with a lot of antibodies and vaccines to treat metastatic melanoma have also failed to demonstrate satisfactory efficacy. Therefore, developing more effective drugs for melanoma is urgently needed.

We started our efforts in finding new drugs for melanoma by screening a large compound library. The *in vitro* cytotoxicity data on several melanoma cell lines led us to the discovery of three active structure scaffolds: serine amides, serine amino alcohols, and arylthiazolidine-4-carboxylic acid amides (ATCAAs). Because ATCAAs showed better selectivity between cancer cells and normal fibroblast cells, the chemists in our group focused on this scaffold and performed extensive structure modifications for structure-activity-relationship (SAR) studies. The SAR results were then used to guide further synthesis in an effort to maximize activity and selectivity. Two active compounds identified during the process were sent to the U.S. National Cancer Institute for anticancer screening using 60 human tumor cell lines. Results showed that these two compounds have extensive cytotoxic activity against all nine types of cancer cells with IC_{50} values ranging from 120 nM (leukemia, CCRF-CEM cell line) to 11 µM (colon cancer, HCC-15 cell line). One compound showed particularly good activity against melanoma cells (IC_{50}=130 nM~1 mM against all eight melanoma cell lines). I then evaluated ATCAAs inhibitory effect on melanoma colony formation and *in vivo* melanoma tumor growth. The *in vivo* data were very encouraging. One tested compound significantly inhibited melanoma tumor growth at a dose of 10 mg/kg and showed higher efficacy than did DTIC at a dose of 60 mg/kg. These findings built up a strong basis for the development of novel chemotherapeutic drugs for advanced melanoma.

Furthermore, the chemists in our group also synthesized some new imidazole and imidazoline analogs by focusing on the SAR studies of the central five-member ring. Although the current compounds displayed lower potency when compared with our lead thiazolidine analogs, they may have the distinct advantage of being more stable *in vivo* with the reduced necessity of chiral separations. Some of these new compounds have activity similar to Sorafenib, an FDA-approved drug that has been tested clinically in melanoma patients.

To further expand our understanding of SARs and to potentially identify new platforms for active compounds, Dr. Li and Dr. Seibel explored a compound library from the University of Cincinnati's Drug Discovery Center. This library contains 342,910 small molecules. Based on the structure of our lead molecule, two ligand-based virtual screening approaches were used: 1) similarity search based on atom connectivity by using Scitegic Pipeline Pilot software and 2) similarity search based on molecular shape

by using Schrodinger software. Results showed that these two approaches are highly complementary and lead to different active molecular structures. These structures are quite suitable for further structural modification and provide new platforms for our anticancer drug discovery efforts.

Subsequently, further lead structure optimization led to the discovery of substituted methoxylbenzoyl-aryl-thiazole (SMART) compounds. To improve solubility and to circumvent the metabolic instability brought by the thiazole ring, our team designed and synthesized a new series of analogs: 2-aryl-4-benzoyl-imidazoles (ABIs). These two classes of compounds showed great *in vitro* cytotoxicity against melanoma, and the IC_{50} of the most active compound was below 10 nM. They also showed equal potency against multi-drug resistant melanoma cells and the sensitive parent cells, indicating that these compounds can effectively overcome multi-drug resistance, which is a major cause of cancer chemotherapy failure. *In vivo* testing on C57BL/6 mice bearing B16-F1 melanoma allograft and on double homozygous SCID (severe combined immunodeficiency) hairless outbred (SHO) mice or athymic nude mice bearing A375 human melanoma xenograft showed these two classes of compounds significantly inhibited melanoma tumor growth. Some compounds even showed substantially better activity than did DTIC, the gold standard anti-melanoma drug. Meanwhile, preliminary toxicity studies suggested that mice can tolerate tested compounds well at effective dose levels. No sign of acute toxicity was observed from the experiments. More importantly, I identified the cellular target for ABI and SMART compounds through a series of biotechniques and molecular modeling studies. Strong experimental evidence has shown that these compounds bind to tubulin at the colchicine binding site in the α/β-tubulin heterodimers to disrupt functional microtubule formation. In the meantime, I also tested the pharmacokinetic properties of some active compounds in mice together with Mr. Chien-ming Li. With their good *in vivo* anti-melanoma activity and their ability to overcome multi-drug resistance, these new classes of compounds have great potential for melanoma therapy.

Document Type
Dissertation

Degree Name
Doctor of Philosophy (PhD)

Program
Pharmaceutical Sciences

Research Advisor
Wei Li, Ph.D.

Keywords
Melanoma, tubulin, inhibitor, multi-drug resistance, imidazole, thiazole

Subject Categories
Medicinal and Pharmaceutical Chemistry | Medicine and Health Sciences | Pharmaceutics and Drug Design | Pharmacy and Pharmaceutical Sciences

Comments
Two year embargo expired May 2010

DISCOVERY AND DEVELOPMENT OF NOVEL THERAPEUTIC AGENTS FOR ADVANCED MELANOMA

A Dissertation
Presented for
The Graduate Studies Council
The University of Tennessee
Health Science Center

In Partial Fulfillment
Of the Requirements for the Degree
Doctor of Philosophy
From The University of Tennessee

By
Zhao Wang
May 2010

DEDICATION

To
My parents,
My wife, Rui Zhu
And
My daughter, Sophia Z. Wang
For
Their endless love and continuous support

ACKNOWLEDGMENTS

who graduated before me including Wenwei Lin for their guidance and support. They really made my stay in Memphis a memorable experience.

Last but not least, I would like to thank Drs. Larry Tague and Shirley Hancock for their great help in format reviewing. Their adherence to perfectionism and great efforts help our dissertation looks much more professional.

ABSTRACT

Malignant melanoma is the most dangerous form of skin cancer and accounts for about 75% of skin cancer deaths. Once diagnosed at the metastatic stage, it has a very poor prognosis with a median survival rate of 6 months and a 5-year survival rate of less than 5%. In addition, melanoma has become an important public health hazard owing to its rising incidence, which has been well documented over the past 50 years. Currently there is no effective way to treat melanoma. It is highly resistant to existing chemotherapy, radiotherapy, and immunotherapy. Over the past 30 years, only two drugs have been approved by the Food and Drug Administration (FDA) for metastatic melanoma: dacarbazine (DTIC) and interleukin-2 (IL-2). But even with these two drugs, fewer than 15% of patients have a favorable response and fewer than 5% of patients reach complete remission. On the other hand, the toxicity associated with DTIC and IL-2 is often significant, resulting in serious or life threatening side effects in many patients. In recent years, great efforts have been made in fighting metastatic melanoma. But neither combinations of DTIC with other chemotherapy drugs (*e.g.*, cisplatin, vinblastine, and carmustine) nor adding interferon-α2b to DTIC have shown a survival advantage over DTIC treatment alone. Extensive clinical trials with a lot of antibodies and vaccines to treat metastatic melanoma have also failed to demonstrate satisfactory efficacy. Therefore, developing more effective drugs for melanoma is urgently needed.

We started our efforts in finding new drugs for melanoma by screening a large compound library. The *in vitro* cytotoxicity data on several melanoma cell lines led us to the discovery of three active structure scaffolds: serine amides, serine amino alcohols, and arylthiazolidine-4-carboxylic acid amides (ATCAAs). Because ATCAAs showed better selectivity between cancer cells and normal fibroblast cells, the chemists in our group focused on this scaffold and performed extensive structure modifications for structure-activity-relationship (SAR) studies. The SAR results were then used to guide further synthesis in an effort to maximize activity and selectivity. Two active compounds identified during the process were sent to the U.S. National Cancer Institute for anticancer screening using 60 human tumor cell lines. Results showed that these two compounds have extensive cytotoxic activity against all nine types of cancer cells with IC_{50} values ranging from 120 nM (leukemia, CCRF-CEM cell line) to 11 μM (colon cancer, HCC-15 cell line). One compound showed particularly good activity against melanoma cells (IC_{50}=130 nM~1 μM against all eight melanoma cell lines). I then evaluated ATCAAs inhibitory effect on melanoma colony formation and *in vivo* melanoma tumor growth. The *in vivo* data were very encouraging. One tested compound significantly inhibited melanoma tumor growth at a dose of 10 mg/kg and showed higher efficacy than did DTIC at a dose of 60 mg/kg. These findings built up a strong basis for the development of novel chemotherapeutic drugs for advanced melanoma.

Furthermore, the chemists in our group also synthesized some new imidazole and imidazoline analogs by focusing on the SAR studies of the central five-member ring. Although the current compounds displayed lower potency when compared with our lead thiazolidine analogs, they may have the distinct advantage of being more stable *in vivo*

with the reduced necessity of chiral separations. Some of these new compounds have activity similar to Sorafenib, an FDA-approved drug that has been tested clinically in melanoma patients.

To further expand our understanding of SARs and to potentially identify new platforms for active compounds, Dr. Li and Dr. Seibel explored a compound library from the University of Cincinnati's Drug Discovery Center. This library contains 342,910 small molecules. Based on the structure of our lead molecule, two ligand-based virtual screening approaches were used: 1) similarity search based on atom connectivity by using Scitegic Pipeline Pilot software and 2) similarity search based on molecular shape by using Schrodinger software. Results showed that these two approaches are highly complementary and lead to different active molecular structures. These structures are quite suitable for further structural modification and provide new platforms for our anticancer drug discovery efforts.

Subsequently, further lead structure optimization led to the discovery of substituted methoxylbenzoyl-aryl-thiazole (SMART) compounds. To improve solubility and to circumvent the metabolic instability brought by the thiazole ring, our team designed and synthesized a new series of analogs: 2-aryl-4-benzoyl-imidazoles (ABIs). These two classes of compounds showed great *in vitro* cytotoxicity against melanoma, and the IC$_{50}$ of the most active compound was below 10 nM. They also showed equal potency against multi-drug resistant melanoma cells and the sensitive parent cells, indicating that these compounds can effectively overcome multi-drug resistance, which is a major cause of cancer chemotherapy failure. *In vivo* testing on C57BL/6 mice bearing B16-F1 melanoma allograft and on double homozygous SCID (severe combined immunodeficiency) hairless outbred (SHO) mice or athymic nude mice bearing A375 human melanoma xenograft showed these two classes of compounds significantly inhibited melanoma tumor growth. Some compounds even showed substantially better activity than did DTIC, the gold standard anti-melanoma drug. Meanwhile, preliminary toxicity studies suggested that mice can tolerate tested compounds well at effective dose levels. No sign of acute toxicity was observed from the experiments. More importantly, I identified the cellular target for ABI and SMART compounds through a series of biotechniques and molecular modeling studies. Strong experimental evidence has shown that these compounds bind to tubulin at the colchicine binding site in the α/β-tubulin heterodimers to disrupt functional microtubule formation. In the meantime, I also tested the pharmacokinetic properties of some active compounds in mice together with Mr. Chien-ming Li. With their good *in vivo* anti-melanoma activity and their ability to overcome multi-drug resistance, these new classes of compounds have great potential for melanoma therapy.

TABLE OF CONTENTS

CHAPTER 5. NOVEL IMIDAZOLES TARGET TUBULIN POLYMERIZATION AND OVERCOME MULTI-DRUG RESISTANCE IN METASTATIC MELANOMA 100

LIST OF TABLES

xiii

LIST OF FIGURES

xvi

xvii

LIST OF ABBREVIATIONS

µM	micro-molar per liter
ABI	2-aryl-4-benzoyl-imidazole
AICA	2-aryl-imidazole-4-carboxylic amide
AIMM	allovectin-7 immunotherapeutic for metastatic melanoma
AJCC	american joint committee of cancer
ASCI	antigen-specific cancer immunotherapeutic
ATCAA	arylthiazolidine-4-carboxylic acid amides
BCG	bacillus of calmette and guerin
CBDT	combination of cisplatin, DTIC, carmustine, and tamoxifen
CD	cluster of differentiation
CNS	central nervous system
CR	complete response
CTLA4	cytotoxic t-lymphocyte antigen 4
CVD	combinations of ciplatin, vinblastine, and DTIC
DC	dendritic cell
DMSO	dimethyl sulfoxide
DNP	dinitrophenyl
DTIC	dacarbazine
ECFC6	extended connectivity fingerprints counts over 6 atoms
ECFP2	extended connectivity fingerprints over 2 atoms
ECFP4	extended connectivity fingerprints over 4 atoms
EDG	electron-donating-group
ERK	extracellular-related kinase
ERK-P	phosporylated ERK kinase
ESI	electrospray ionization
EWG	electron-withdrawing-group
FCFP4	functional class fingerprints over 4 atoms
FCFP6	functional class fingerprints over 6 atoms
FDA	food and drug administration
GM-CSF	granulocyte-macrophage colony-stimulating factor
GSK	glaxosmithkline
HDFa	human dermal fibroblast (adult) cells
HSV-1	herpes simplex virus type 1
IC_{50}	50 percent inhibition concentration
ICF	infected-cell protein
ICR	imprinting control region
IFA	incomplete freund's adjuvant
IFN	interferon
IL-2	interleukin-2
LC-MS	liquid chromatography-mass spectrometry
LDH	lactate dehydrogenase
MAGE	melanoma-associated antigen
MAPK	mitogen-activated protein kinase

MDR   multi-drug resistant
MGMT   o-6-methylguanine-dna methyltransferase
MHC   major histocompatibility complex
MITF   microphthalmia-associated transcription factor
MTIC   3-methyl-(triazen-1-yl)imidazole-4-carboxamide
mTOR   mammalian target of rapamycin
NDA   new drug application
nM   nano-molar per liter
Pgp   P-glycoprotein
PI3K   phosphatidylinositol 3 kinase
PIP3   phosphatidylinositol triphosphate
pM   pico-moler per liter
PR   partial response
PTEN   phosphatase and tensin homolog
RECIST   response evaluation criteria in solid tumors
SAR   structure-activity-relationship
SCID   severe combined immunodificiency
SEM   standard error of the mean
SEM   standard error of the mean
SHO   scid hairless outbreed
SMART   4-substituted methoxylbenzoyl-aryl-thiazole
SPA   special protocol assessment
SRB   sulforhodamine b
TAA   tumor-associated antigen
TMZ   temozolomide
US   unique short region protein
VEGF   vascular endothelial growth factor

CHAPTER 1. LITERATURE REVIEW

1.1 Introduction

Melanoma is a cancer derived from melanocytes which produce pigment called melanin. This cancerous transformation can be initiated from either localized pre-existing nevi or de novo, arising from the single melanocyte that is located at the junction of the epidermis (1). Under normal condition, melanocytes proliferation and migration are regulated by keratinocytes through direct cell-cell contact or soluble growth factors (2). Upon malignant transformation, melanoma cells initially have a superficial spreading (radial growth phase), followed by tumor cells invading the dermis (vertical growth phase). Then they can advance to a more aggressive metastatic phase in which the tumor cells can metastasize lymphatically or haematologically to regional and distant sites in the body (3).

Metastatic melanoma is the most dangerous form of skin cancer, accounts for about 75% of skin cancer deaths (4). If detected at an early stage, cutaneous melanoma is curable with complete surgical excision in most patients. But once the disease progresses in regional or distant sites, it is very difficult to treat. And when disseminated, it is a devastating illness. Metastatic melanoma has a very poor prognosis, with a median survival rate of 6~10 months and a 5-year survival rate of less than 5% (5).

Melanoma has become an important public health hazard owing to its rising incidence as this has been well documented over the past 50 years. There has been a 3 to 7% worldwide annual age standardized incidence increase over the past five decades. The incidence of melanoma is rising steadily in Western populations. The number of cases has doubled in the past 20 years. The current lifetime risk is 1.9% for men and 1.37% for women (6). Melanoma is the fastest rising form of cancer among men and the second fastest rising form of cancer among women. The overall mortality from melanoma has increased because of the increase in incidence. Around 160,000 new cases of melanoma are diagnosed worldwide each year, and it is more frequent in males and Caucasians (7). According to a WHO Report, about 48,000 melanoma-related deaths occur worldwide per year. Because melanoma affects young- and middle-aged individuals, the number of years of life lost to this malignancy is high and exceeds all other adult solid tumors except testicular carcinoma (8).

1.2 Current Treatment Agents for Metastatic Melanoma

According to the current 6th edition American Joint Committee of Cancer (AJCC) staging system, melanoma can be pathologically classified to the following stages: 0, IA, IB, IIA, IIB, IIC, IIIA, IIIB, IIIC, and IV. Stage 0 is in situ melanoma. Stage I and II are growth phase of localized cutaneous melanoma with increasing thickness. Stage III has regional involvement of lymph node. Stage IV means distant metastasis. Normally stage III and IV melanoma are called metastatic melanoma. Localized melanoma is curable

with complete surgical excision in most patients. But currently there is no effective way to treat metastatic melanoma. Only two agents in current use have been approved by the Food and Drug Administration (FDA) for metastatic melanoma: dacarbazine (DTIC) and interleukin-2 (IL-2). But even with these two drugs, only less than 15% patients have response and less than 5% patients can reach complete remission. On the other hand, the toxicity associated with DTIC and IL-2 is often significant, resulting in serious or life threatening side effects in many of the patients treated.

In this section, I will focus on the usage and performance of DTIC and IL-2 first. Of cause surgery is often used as a treatment for melanoma whenever a surgical removal is possible. Radiation therapy is often used after surgical resection for patients with regionally advanced melanoma or for patients with unresectable distant metastases. But these two strategies of treatment for metastatic melanoma are beyond the scope of this review.

1.2.1 Chemotherapy Agent DTIC

Currently DTIC is the only FDA approved chemotherapy drug for metastatic melanoma. This drug gained FDA approval in May 1975 as DTIC-Dome for the treatment of metastatic melanoma. It was initially marketed by Bayer. The therapeutic effect of DTIC is believed to be produced through alkylation of DNA. While its anticancer mechanism of action is still not fully understood, DTIC is believed to be first metabolically bioactivated through a series of reactions involving CYP450. Initial demethylation to MTIC [3-methyl-(triazen-1-yl)imidazole-4-carboxamide] is followed by formation of diazomethane, the active moiety of DTIC and a potent methylating agent (9).

DTIC has produced response rates of from 15% to 25% in single-institution trials. But the overall response rate has fallen over the years from 15% to 7% and less than 5% of responses are complete in phase 3 trials. The median response durations to DTIC are 5 to 6 months. Long-term follow-up of patients treated with DTIC alone shows that only <2% can be anticipated to survive for more than 6 years. In recent phase 3 trials that used strict response assessment criteria, the response rates with single-agent DTIC did not exceed 12% (10).

Over the past 30 years after its approval by the FDA, DTIC remains the only currently used cytotoxic drug for the treatment of metastatic melanoma. Despite its low single-agent activity, DTIC has remained the mainstay of many combination chemotherapy regimens and evaluations of resistance-reversing agents. After more than 20 years of research, DTIC is still the standard against which most new chemotherapy agents are compared (11).

As for the dose, it has been demonstrated that 850~1000 mg/m^2 single dose of DTIC is tolerated. This single dose administration appears to deliver clinical improvements similar to those observed with multiple doses that provide the same total

dose per cycle. This should be the reference standard for randomized trials comparing new therapies with DTIC (12).

1.2.2 Immunotherapy Agent IL-2

In 1998, the FDA approved intermittent high-dose bolus IL-2 based on its ability to mediate durable complete response in metastatic melanoma patients (13). IL-2 is a type of cytokine immune system signaling molecule, which is a leukocytotrophic hormone that is instrumental in the body's natural response to microbial infection and in discriminating between foreign (non-self) and self. It's a glycosylated 15,500 dalton single protein molecule. IL-2 mediates its effects by binding to IL-2 receptors, which are expressed by lymphocytes, the cells that are responsible for immunity. It is one of the only two FDA approved agents for the treatment of metastatic melanoma. Although the overall response rate is only about 15% and less than 5% of patients achieve complete remission with IL-2, its performance on melanoma is better than DTIC.

One of the major immunologic effects of IL-2 upon the immune system is to expand the total number of T-lymphocytes (CD4+ and CD8+) and to prevent lymphocyte apoptosis. Another key role of IL-2 is to provide the appropriate cytokine milieu necessary to overcome tumor-induced immune tolerance. But the exact molecular and genetic mechanisms involved in this complex interaction between the tumor and the host immune response is still largely unknown (14).

There is currently a wide spectrum of dosing schedules and regimens for IL-2 therapy, with the current standard used by most oncologists being 600,000 to 720,000 IU/kg/dose, given at 8 h intervals. Although the optimal dosing schedule resulting in the best clinical response is currently unknown, previous data would suggest that the higher dose regimens as well as the number of total doses received correlates best with clinical response. Thus, several groups have begun to look at alternative dosing strategies to achieve an increased drug tolerance and tolerability profile, such as the continuous infusion of IL-2 (18 mIU/m^2/day) over an extended period of 72 h (15). But the multiorgan toxicity of many IL-2 regimens limits its use. In addition, the tumor-killing cytotoxic T cells and natural killer cells, which are the presumed target cells for IL-2, are frequently inefficient in the tumor environment, partly due to suppressive and apoptosis-inducing signals from tumor-infiltrating mononuclear phagocytes (16).

1.3 Recent Research Efforts in the Treatment for Metastatic Melanoma

Because of effective treatment shortage, the prognosis for metastatic melanoma patients remains very poor. Over the past 30 years, great efforts have been attempted to search for better agents or strategies to fight this deadly disease. Hundreds of different stages of clinical trials have been carried out. Although most of them have failed, some did show very promising results. Some new treatment strategies have resulted in

3

paradigm shift in our approach to therapy of melanoma patients. These shining examples may markedly change our philosophy about melanoma treatment.

1.3.1 Chemotherapy

1.3.1.1 Temozolomide

Temozolomide (TMZ) is an orally active alkylating agent. It's a prodrug of MTIC and congener of DTIC. It has been available in the US since August 1999 and in other countries since the early 2000s. The therapeutic benefit of temozolomide depends on its ability to alkylate/methylate DNA, which most often occurs at the N-7 or O-6 positions of guanine residues. This methylation damages the DNA and triggers the death of tumor cells. However, some tumor cells are able to repair this type of DNA damage, and therefore diminish the therapeutic efficacy of temozolomide, by expressing an enzyme called O-6-methylguanine-DNA methyltransferase (MGMT) or O-6-alkylguanine-DNA alkyltransferase (17).

The single agent activity of TMZ in metastatic melanoma has been established in several phase 1 and 2 studies (18). In a randomized trial of 305 patients with advanced melanoma, TMZ showed efficacy at least equivalent to that of DTIC in terms of objective response rate, time to progression, and overall disease-free survival (19). TMZ was tolerated very well and showed an advantage in terms of improvement in the quality of life. More patients showed improvement or maintenance of physical functioning at Week 12. That trial excluded patients who had brain metastases. Because the trial design was intended to demonstrate the superiority of TMZ over DTIC, rather than equivalence, the FDA did not accept the results of that trial as grounds for approving a melanoma indication for TMZ. But in clinical practice, patients with metastatic melanoma often are treated off-label with TMZ.

TMZ has demonstrated efficacy in the treatment of variety of solid tumors, especially in brain malignancies, which is a manifestation of its far greater ability to penetrate the central nervous system (CNS). Taking into account the high rate of CNS recurrence as a site of failure after cytotoxic chemotherapy, TMZ may represent a viable alternative to DTIC, which is ineffective against melanoma CNS metastases.

1.3.1.2 Sorafenib

Sorafenib (BAY43-9006, developed by Bayer Pharmaceuticals, West Haven CT, trade name Nexavar) is an orally administered tyrosine kinase inhibitor that is a potent inhibitor of the B-Raf kinase that is frequently mutated in melanoma, as well as an inhibitor of the Vascular Endothelial Growth Factor (VEGF) receptor and other kinases. It targets the adenosine triphosphate-binding site of the B-Raf kinase and inhibits both wild-type and mutant B-Raf *in vitro*. Sorafenib was approved by the FDA in December

2005 for use in the treatment of advanced renal cancer. Preclinical studies demonstrated a significant retardation in the growth of human melanoma tumor xenografts with Sorafenib. In a phase 1 study, the maximum tolerated dose of Sorafenib as a single agent was established at 400 mg twice daily, and the most common toxicities were gastrointestinal (mainly diarrhea), dermatologic (skin rash, hand-foot syndrome), and fatigue (20).

But in further phase 2 clinical trials, Sorafenib had shown relatively little activity in metastatic melanoma when using alone. In a phase 2 trial that was conducted in 20 patients with refractory metastatic melanoma, Sorafenib showed modest activity with 1 partial response and 3 patients who achieved stable disease (21). In another phase 2, randomized, discontinuation trial, no objective responses were achieved, and 19% of patients achieved stable disease (22).

Sorafenib combined with other chemotherapy drugs were also tested clinically. In a phase 1 and 2 study that combined carboplatin and paclitaxel with escalating doses of Sorafenib in 35 patients, a promising response rate of 31% was observed, and another 54% of patients experienced stable disease that lasted longer than 3 months. That study recently was updated to include 105 patients, and the current response rate is 27% (23). On this basis, 2 phase 3 trials have been launched to assess the efficacy of carboplatin and paclitaxel plus Sorafenib versus placebo in chemotherapy-naive patients and in previously treated patients. In December 2006, Bayer reported the combinations failed to show significant improvement of progression-free survival in melanoma patients (24).

1.3.1.3 Other Single Chemotherapy Agents

Cisplatin and carboplatin have shown modest activity as single agents in patients with metastatic melanoma. Cisplatin as single-agent therapy induced a 15% response rate with a short median duration of 3 months (25). A response rate of 19% has been reported in 26 chemotherapy-naive patients with metastatic melanoma who received carboplatin. In those patients, there were 5 partial responses, and thrombocytopenia was the dose-limiting toxicity (26). *In vitro* studies suggested that oxaliplatin may be more active than cisplatin or carboplatin. But a small phase 2 trial in 10 patients who had received and failed prior chemotherapy produced no objective responses (27).

The nitrosoureas (carmustine, lomustine, and semustine) induce objective responses in 13~18% patients. They can cross the blood-brain barrier. But at conventional doses, little or no activity was observed against melanoma brain metastases (28). Another drawback of the nitrosureas is they induce prolonged myelosuppression. Despite these, they have been included frequently in multi-agent chemotherapy combinations, presumably for their ability to penetrate into the CNS and lack of viable alternatives for metastatic melanoma.

5

The vinca alkaloids (vindesine and vinblastine) have produced responses in approximately 14% of patients (29). The taxanes have produced responses in 16~17% patients (30). All of these response rate data were obtained from phase 2 trials. None of those drugs have been evaluated as single agents in phase 3 trials. Based on the experience with DTIC, it is likely that the phase 3 trial objective response rates would be less than the rates reported from phase 2 trials. All of these drugs are rarely used currently as single-agent therapy in metastatic melanoma, but they frequently have been incorporated into combination chemotherapy and biochemotherapy regimens.

1.3.1.4 Chemotherapy Drug Combinations

Theoretically drug combination should be based on laboratory or clinical evidence of synergistic effect. But since single-agent chemotherapy regimens only provided modest activity against metastatic melanoma and lack of viable alternatives, many combination regimens have been evaluated in clinical trials. Initially two-agent combinations were tested in which DTIC was combined with a nitrosourea, vinca alkaloid, or platinum compound. In most of these trials, only 10~20% response rates were observed. There was little evidence to suggest superiority of these combinations compared with DTIC treatment alone (31-33).

In order to improve response rates, more aggressive multi-drug combinations using 3 or 4 different drugs were also tested clinically. Two most widely studied combinations are cisplatin, vinblastine, and DTIC (CVD) and the Dartmouth regimen. The later is a 4-drug combination of cisplatin, DTIC, carmustine, and tamoxifen (also called CBDT). Both combinations showed improved response rates that ranged from 30% to 50% in single-institution phase 2 studies (34, 35). But in further randomized phase 3 trials which involved more patients, they all showed much lower efficiency: In a randomized trial comparing CVD with single-agent DTIC that involved approximately 150 patients, the CVD arm produced a 19% response rate compared with 14% for the DTIC arm, and there was no differences in either response duration or survival. In another randomized phase 3 trial, the CDBT combination was compared with single-agent DTIC. That cooperative group trial involved 240 patients, and the response rate was 10% for the DTIC regimen compared with 19% for the CDBT regimen (P=0.09). The median survival was 7 months, with no significant difference between the 2 treatment arms (11).

The main reason for such discrepancies between the findings from single-institution studies and the findings from large, multicenter, cooperative trials probably is selection bias. Differences in performance status, percentages of patients with visceral involvement, and number of metastatic sites easily could account for some of the observed differences. In fact, all of those factors are known to have an impact on both response rate and survival (36).

Overall, controlled trials have produced no compelling evidence to support the value of combination chemotherapy, with or without tamoxifen, in patients with

6

metastatic melanoma. Toxicity was substantially greater for the combination regimen, with bone marrow suppression, nausea, emesis, and fatigue significantly more frequent with CDBT than with DTIC (11). So it is difficult to justify the use of either CVD or CBDT instead of single-agent DTIC or TMZ for the treatment of most patients with metastatic melanoma.

1.3.2 Immunotherapy

1.3.2.1 Interferon α

Interferons (IFNs) are proteins made and released by the cells of most vertebrates in response to the presence of pathogens or tumor cells. They allow communication between cells to trigger the protective defenses of the immune system that eradicate pathogens or tumors. IFNs belong to the large class of glycoproteins known as cytokines. They are named after their ability to "interfere" with viral replication within host cells. IFNs have other functions: they activate immune cells, such as natural killer cells and macrophages; they increase recognition of infection or tumor cells by up-regulating antigen presentation to T lymphocytes; and they increase the ability of uninfected host cells to resist new infection by virus.

Based on the type of receptor through which they signal, human interferons have been classified into three major types. The type I interferons present in human are IFN-α, IFN-β and IFN-ω (37). High-dose IFN therapy using IFN-α was the first form of medical therapy to be approved by the FDA for use in high-risk melanoma in the adjuvant setting. Adjuvant normally means using IFN- α weeks after the surgical excision of the melanoma tumor. Common treatment scheme is IFN-α2b at 20 million units (MU)/m^2/day intravenous injection 5 days a week for 4 weeks, then 10 MU/m^2/day subcutaneous injection 3 days a week for the next 48 weeks for a full year's. But IFN-α2b can also be used one month before definitive surgical lymphadenectomy. This is called 'neoadjuvant' treatment (38).

The first randomized comparison of high-dose IFN versus observation found the median relapse-free survival was 1.72 years in the high-dose IFN arm versus 0.98 year in the observation arm (P=0.0023) and the median overall survival was 3.82 versus 2.78 years (P=0.0237) respectively (39). But in a later pooled analysis of more patients in more clinical trials, the relapse-free survival benefit was maintained but no overall survival benefit was seen (40).

The exact mechanism of IFN IFN-α's anti-tumor efficacy is still unknown. But it was found that the STAT1/STAT3 expression ratios rose in association with IFN treatment. The clinical effects of IFN-α2b in human melanoma are also found to be inversely related to STAT3 expression (41). Induction of apoptosis has been shown to be important *in vitro*, if not *in vivo*. IFN-α can induce apoptosis in transformed cell lines as well as primary tumor cells (42).

7

High-dose IFN is the standard of care for high-risk melanoma patients in the adjuvant setting. However, it is associated with significant toxicity. The incidence and severity of these adverse events is clearly dose-related. Consequently, there has been a great deal of interest in intermediate- and low-dose regimens administered through subcutaneous injection. However, none of the trials using intermediate or low dosing so far have been able to demonstrate any reliable benefit in terms of relapse-free survival or overall survival (43).

1.3.2.2 Anti-CTLA4 Antibodies: Ipilimumab and Tremelimumab

Cytotoxic T-Lymphocyte Antigen 4 (CTLA4) also known as CD152 (Cluster of differentiation 152) is a member of the immunoglobulin super family, which is expressed on the surface of Helper T cells and transmits an inhibitory signal to T cells that eventually shuts off the activated state. The rationale for involving this in treatment of metastatic melanoma is to block the negative signal sending by CTLA4 by using anti-CTLA4 antibodies, thus reduce the sensitivity of activated T cells to negative regulatory signals and enhance the immune response of the host to tumor cells.

As of October 2007 there are two fully human monoclonal anti-CTLA4 antibodies in advanced clinical trials, one from Medarex, Inc. (Princeton, NJ) and Bristol-Myers Squibb (New York), called ipilimumab (MDX-010), and one from Pfizer (New York), called tremelimumab (formerly ticilimumab, CP-675,206) (44). These antibodies were produced using different types of mice with engineered immune systems, and are thus fully human, with long half-lives of 2– 4 weeks.

Ipilimumab (MDX-010) is an IgG1 monoclonal antibody. Preclinical and early clinical studies of patients with metastatic melanoma show that ipilimumab promotes antitumor activity as monotherapy and in combination with treatments such as chemotherapy, vaccines, or cytokines. The initial success with these antibodies has encouraged the rapid development of new agonistic and antagonistic antibodies that alter immune regulation, such as anti-PD-1, anti-4-1BB, anti-CD40, and anti-OX-40. On December 10, 2007, Bristol-Myers Squibb and Medarex released the results of three studies on ipilimumab (44). The three studies tested 487 patients with metastatic melanoma. Short-term tumor progression prior to delayed regression has been observed in ipilimumab-treated patients, and objective responses may be of prolonged duration. In some patients clinical improvement manifests as stable disease, which may also extend for months or years. One of the three studies failed to meet its primary goal of shrinking tumors in at least 10% of the study's 155 patients. Overall the medication produced weaker-than-anticipated efficacy on melanoma patients.

In the meantime, the side effect profile was high in the ipilimumab treated group, with the generation of autoimmune-like effects, such as diarrhea, dermatitis and effects upon the thyroid and pituitary glands. Several patients also experienced vitiligo, indicative of anti-melanocyte autoimmunity. However, the majority of the side effects were noted to be transient (except the vitiligo), improving or disappearing after the

8

completion of therapy. Early clinical data suggest a correlation between these side effects and response to ipilimumab treatment and most likely reflect the drug mechanism of action and corresponding effects on the immune system (44).

Tremelimumab is an IgG2 monoclonal antibody produced by Pfizer. It blocks the binding of the antigen-presenting cell ligands B7.1 and B7.2 to CTLA-4, resulting in inhibition of B7-CTLA-4-mediated down-regulation of T-cell activation. Subsequently, B7.1 or B7.2 may interact with another T-cell surface receptor protein, CD28, resulting in a B7-CD28-mediated T-cell activation unopposed by B7-CTLA-4-mediated inhibition. Tremelimumab is thought to stimulate patients' immune systems to attack their tumors. It has been shown to induce durable tumor responses in patients with metastatic melanoma in phase 1 and phase 2 clinical studies (45).

On April 2, 2008, Pfizer announced that it has discontinued a phase 3 clinical trial for patients with metastatic melanoma after the review of interim data showed that the trial would not demonstrate superiority to standard chemotherapy (46). Studies for other tumors are planned as of October 2009, namely for prostate cancer and bladder cancer.

1.3.2.3 Anti-Integrin Antibody: Etaracizumab

Etaracizumab (also known as etaratuzumab, MEDI-522, trade name Abegrin) is an IgG1 humanized monoclonal antibody directed against the αVβ3 integrin. αVβ3 is essential for endothelial cell proliferation, maturation, and survival. When it is blocked, proliferating endothelial cells undergo apoptosis and regress. In addition, αVβ3 is highly expressed in melanomas and is associated with tumor growth and invasion. In preclinical studies using αVβ3 antagonists, inhibition of melanoma tumor growth independent of its antiangiogenic effects was reported (47). Etaracizumab has been investigated in 3 phase 1, dose-escalation studies in patients with refractory melanoma. In the phase 2 trial, 57 patients received etaracizumab alone, and 55 patients received etaracizumab plus DTIC. Etaracizumab with or without DTIC generally was well tolerated and was active in patients with metastatic melanoma. The median survival was 12.6 months for the group that received etaracizumab with DTIC and 9.4 months for the group that received etaracizumab without DTIC (48). These results encouraged people to further test this antibody in more clinical trials.

Early 2010, a study by the Etaracizumab Melanoma Study Group was reported. In this study, 112 patients were randomized to receive etaracizumab alone or etaracizumab plus DTIC. None of the patients in the etaracizumab alone study arm and 12.7% of patients in the etaracizumab plus DTIC study arm achieved an objective response. Stable disease occurred in 45.6% of patients in the etaracizumab alone study arm and 40.0% of patients in the etaracizumab plus DTIC study arm. Despite a modest increase in survival, 12.6 months in the etaracizumab alone arm, versus 9.4 months in the etaracizumab plus DTIC arm, the researchers concluded that the survival results in both treatment arms of this study were considered unlikely to result in clinically meaningful improvement over

9

DTIC alone (49). At the present time, clinical development of etaracizumab has been interrupted

1.3.2.4 Vaccines Based on Tumor Cells: Canvaxin, Melacine, and MVax

The basic idea is to use tumor cell-based vaccine to stimulate and activate the host immune system to recognize, contain and eliminate cancer cells. This effect may be based on the following two pathways: direct migration of the tumor cells to the draining lymph node basin after injection, or uptaking of apoptotic or necrotic tumor cells by host dentritic cells located within the skin (50).

The most extensively studied tumor cell-based vaccine is a polyvalent, antigen-rich whole cell vaccine called Canvaxin (CancerVax Corp., Carlsbad, CA). It is comprised of three melanoma cell lines that contain over 20 immunogenic melanoma tumor antigens, given intradermally every two weeks for 3 to 5 doses, followed by monthly injections for the remainder of the first year. However, several small, single-institution phase 1 and 2 clinical trials of Canvaxin have not yielded a striking clinical benefit in most patients when administered with BCG as an immunoadjuvant (51). But the rare complete responder to Canvaxin therapy has prompted the initiation of two multicenter phase 3 randomized trials of Canvaxin therapy in 1998. In these trials, patients who have undergone complete resection of regional (stage III) or distant (stage IV) metastatic melanoma receive postoperative adjuvant immunotherapy with Canvaxin plus Bacillus of Calmette and Guerin (BCG) or BCG alone. In April 2005, CancerVax announced the discontinuation of their phase 3 clinical trial of Canvaxin in patients with Stage IV melanoma based upon the clinical funding that it was unlikely that the trial would provide significant evidence of a survival benefit for Canvaxin-treated patients versus those receiving placebo. On October 3, 2005, CancerVax announced the discontinuation of another phase 3 clinical trial of Canvaxin in patients with Stage III melanoma base on the similar reason (52).

The second tumor cell-based vaccine that has been well studied since 1988 is Melacine. It is an allogeneic melanoma cell lysate combined with an immunologic adjuvant which is composed of a mixture of detoxified endotoxin, cell wall cytoskeleton and monophosphoryl lipid A. Early phase 1 and 2 clinical trials in 1987 and 1988 revealed some promising results, with one complete and three partial responses seen in 25 patients treated with Melacine. These results prompted the completion of seven open-label phase 2 trials involving 139 patients with stage III/IV melanoma and a multicenter phase 3 clinical trial of Melacine versus the Dartmouth regimen. The objective response rates for all of the above studies have been between 5 and 10%. Based largely upon these former results and the clinical results of other phase 3 trials, a phase 3 observation controlled trial of Melacine in melanoma patients was conducted. But the results revealed no evidence of a benefit from Melacine in patients with melanoma (53).

One very promising autologous cell vaccine is MVax which is now in active phase 3 clinical trial sponsored by AVAX Technologies, Inc. This vaccine is derived from autologous tumor cells that have been irradiated and then modified with the hapten

dinitrophenyl (DNP) (54). In February 2004 the Journal of Clinical Oncology published an article by Dr. David Berd on the treatment of 214 Stage IIIb and IIIc melanoma patients that showed a five-year survival rate of 44%. Comparison to published results of similar patients treated with surgery alone showed five-year survival figures of 22%. In stage IV patients MVax has demonstrated significant response rates as a monotherapy and in published reports MVax plus adjuvant IL-2 have reported response rate of 35% (13% Complete Response, 22% Partial Response). This compares to published response rates in low dose IL-2 of 3% (55).

In October 2006, AVAX obtained a Special Protocol Assessment (SPA) agreement with the FDA for its phase 3 protocol. The SPA allows for the start of the phase 3 registration clinical trial for MVax for the treatment of patients with metastatic melanoma. In addition, the SPA addressed AVAX's ability to use a surrogate endpoint as a basis for accelerated approval. Based on this SPA, a phase 3 trial for stage IV melanoma was started on May 2007. AVAX plans to enroll up to 387 patients who will be assigned in a double-blind fashion at a 2:1 ratio to MVax or placebo vaccine. The MVax arm will consist of an initial dose of MVax followed by cyclophosphamide and then six weekly doses of MVax administered with BCG. Following vaccine administration patients will receive a specific schedule of low dose IL-2. Patients assigned to the control group will receive a treatment identical to the MVax group, except that a placebo vaccine will replace MVax. The primary endpoints of the study are best overall anti-tumor response rate and the percentage of patients surviving at least 2 years. Secondary endpoints of the study will include overall survival time, response duration, percentage complete and partial responses, progression free survival and treatment related adverse events (56).

1.3.2.5 Vaccines Based on Peptides: MDX-1379, Astuprotimut-R, and Others

The identification of tumor antigens that are present on the surface of melanoma cells is the basis for developing cancer vaccines that utilize peptide based immunotherapy. There are several melanoma differentiation antigens known involved in the synthesis of melanin and recognized by melanoma-reactive T cells, for example, gp100, MART-1/Melan-A, tyrosinase, TRP-1 and TRP-2, NY-ESO-1and the melanoma-associated antigen (MAGE) *etc.* One big advantage of peptide based-vaccination is that it has few toxic side effects or adverse reactions. Data suggests that most tumor cell lines established from fine needle aspiration biopsies of patients with metastatic melanoma exhibit a relatively homogeneous co-expression of MART-1 and tyrosinase, with a much more heterogeneous expression of other tumor antigens, such as gp100, NY-ESO 1 and the MAGE antigens (57).

Rosenberg and his colleagues developed a with a peptide based-vaccine using modified immunodominant peptide of the gp100 antigen, g209-2M. They used this agent vaccinated stage IV melanoma patients subcutaneously every three weeks. Following two immunizations, 10 of 11 (91%) of patients showed a consistently high level of immunization against the native g209~217 peptide, but not against the control peptide

11

g280~288. This study also demonstrated that the majority of patients immunized with the g209-2M peptide in incomplete Freund's adjuvant (IFA) consistently developed high levels of circulating immune precursors reactive against the native g209~217 peptide. Clinically, one of nine patients who received the g209~217 peptide in IFA experienced an objective cancer regression that lasted 4 months. Three of the eleven patients exhibited mixed responses with complete or partial regression of several lesions. However, all patients eventually developed progressive disease (58).

MDX-1379 vaccine consists of two gp100 melanoma peptides. These peptides are part of a protein normally found on melanocytes, or pigmented skin cells, and on melanoma cells. These melanoma peptides are recognized by cytotoxic T cells in melanoma patients that are positive for HLA-A2, a human immune system compatibility antigen that is expressed in approximately half of the melanoma population. Phase II data show limited evidence of MDX-1379's clinical activity although there is strong proof-of-concept for therapeutic vaccines based on gp100 in melanoma. Medarex is currently conducting a phase 3 clinical trial with ipilimumab and MDX-1379 combination therapy in stage III and IV melanoma at multiple sites within the United States. Preliminary data showed MDX-1379 plus ipilimumab induced a modest percentage of durable response in stage IV melanoma. But autoimmune events could make the risk/benefit ratio for MDX-1379 plus ipilimumab unfavorable (59).

Astuprotimut-R (also called recombinant MAGE-A3 antigen-specific cancer immunotherapeutic GSK1203486A) is a cancer vaccine consisting of a recombinant form of human melanoma antigen A3 (MAGE-A3) combined with a proprietary adjuvant with potential immunostimulatory and antineoplastic activities. Upon administration, astuprotimut-R may stimulate a cytotoxic T-lymphocyte response against tumor cells expressing the MAGE-A3 antigen, resulting in tumor cell death. MAGE-A3, a tumor-associated antigen (TAA) originally discovered in melanoma cells, is expressed by various tumor types including melanoma, non-small cell lung cancer, head and neck cancer, bladder cancer, with no expression in normal cells. MAGE-A3 protein has been in-licensed by GlaxoSmithKline (GSK) from the Ludwig Institute for Cancer Research. The proprietary immunostimulating adjuvant in this agent is composed of a specific combination of immunostimulating compounds selected to increase the anti-tumor immune response to MAGE-A3. Using this vaccine as intramuscular administration together with GSK's two proprietary adjuvant systems, AS15 or AS02B, they have developed a treatment regimen for cancer patients called Antigen-Specific Cancer Immunotherapeutic (ASCI).

In 2008, GSK reported a randomized, open-label phase 2 study designed to evaluate Astuprotimut-R. A total of 72 patients with measurable metastatic MAGE-A3-positive cutaneous melanoma (unresectable or in transit stage III or stage IV M1a) were randomized to receive immunization with MAGE-A3 protein combined with either AS15 or AS02B as first-line metastatic treatment. Patients were to receive a maximum of 24 immunizations over four years. Clinical activity is assessed by the Response Evaluation Criteria In Solid Tumors (RECIST) criteria, the international standards for evaluation of solid tumors. Complete response (CR) and partial response (PR) *i.e.*, disappearance or

12

significant reduction of tumor, were reported in 4 patients in the AS15 group (3 CR and 1 PR) with two of these ongoing for more than two years; in the AS02B arm, 1 patient showed a partial response which lasted for 6 months. The safety profile was similar in both groups with the majority of reported adverse events being mild or moderate local or systemic reactions (60). Currently this agent still is under phase 2 clinical development for progressive metastatic cutaneous melanoma.

Because melanoma tumors are heterogeneous in their antigenic profile, it is very difficult to make vaccines that can elicit cytotoxic T-cell responses universally in all the host immune systems. Rosenberg's group analyzed 28 different peptide-based vaccines utilized in stage IV melanoma patients. A total of 381 patients were treated with 370 patients showing no response, 9 patients showing a partial response and 2 patients with a complete response, for an overall objective response rate of only 2.9%. This suggested the lack of effectiveness with this single peptide based vaccination approach (61).

Next logical step is to make vaccines with multiple peptides to overcome tumor cell antigenic heterogeneity. A recent randomized phase 2 trial was performed in 26 patients with metastatic melanoma, vaccinating with four melanoma peptides. Although a high level of specific T-cell responses were noted (in 42% of the peripheral blood, 80% of sentinel lymph nodes), only three patients had a clinical response (62).

Here is the biggest issue in this area, actually many peptide based-vaccinations have resulted in a significant increase in the number of lymphocyte precursors reactive against a variety of tumor differentiation antigens by immunization with native or modified peptides. However, such immunological responses to peptide-based therapy have not translated into meaningful clinical responses for the vast majority of patients. To date, there is no study that has clearly shown a direct correlation between an immunologic response to therapy (immune cell activation) and a clinical response (regression of established tumor).

1.3.2.6 Vaccines Based on Dendritic Cells

In the normal human epidermis and dermis, dendritic cells (DC) are present as relatively immature antigen presenting cells, exhibiting relatively low levels of class II major histocompatibility complex (MHC) molecules and co-stimulatory molecules. But these immature DC are quite capable of capturing various soluble protein antigens, such as apoptotic and necrotic tumor cells and then cross-presenting such tumor-associated antigens to cytotoxic CD8+ T cells. When relatively immature DC in the skin is triggered to enter afferent lymphatic channels, this migrating pathway also initiates a phenotypic conversion that has profound immunological consequences [30]. When the DC arrives in the lymph node, it is characterized by an abundant levels of class II MHC antigens, as well as high surface levels of costimulatory molecules, such as CD40, CD54, CD80, CD83, and CD86. The matured DC is then capable of forming stable MHC class II-peptide complexes available to activate antigen specific CD4+ T cells (63).

13

To make the dendritic cell-based vaccine, the monocyte-derived, autologous DC can be pulsed *in vitro* with either whole irradiated, autologous tumor cells or tumor cell lysate. Once the tumor cells are "fed" to the DC *in vitro*, the apoptotic or necrotic cells are then processed and tumor-specific peptide antigens are then transported to the surface in both an MHC class I- and II-restricted fashion. Both immature and mature DC can be administered to patients as vaccine safely with few adverse side effects. The administration of DC via various routes of vaccination (intradermal, intranodal and intravenous) is also feasible. The first published clinical trial of DC vaccination was in 1995 and has since been followed by 98 additional clinical trials describing more than 1,000 DC-based vaccines performed in 15 different countries. Twenty-eight trials focused on patients with various advanced stages of melanoma. The safety profile was again noted to be quite remarkable, however, despite the treatment of over 1,000 patients with DC-based vaccines, the record of effectiveness have been disappointing (64).

One pretty successful DC-based trial for patients with advanced, metastatic melanoma was reported by Nestle *et al*. He used plastic adherent monocytes matured with a xenogenic-based 10% fetal calf serum, subsequently pulsed with either tumor cell lysate or multiple HLA-matched peptides injected intranodally. This trial involved 16 patients who were immunized on an outpatient basis. Overall, 5 of 16 patients experienced an objective response, 2 complete and 3 partial responses. The side effects were noted to be minimal in all cases, with the development of vitiligo in a few patients. One dramatic feature of this treatment was the durability of the clinical responses, with the 2 complete responders remaining free of disease for over 15 months (65).

One phase 3 clinical trial about using DC-based vaccine to treat metastatic melanoma was report by Schadendorf and colleagues recently. The trial was a prospective, randomized trial that analyzed the therapeutic effects of an autologous peptide-pulsed DC-based vaccine in patients with stage IV melanoma compared to standard chemotherapy with DTIC alone. The results revealed that the overall response in the vaccine group was 3.8% compared to 5.5% in the DTIC group, with no statistically significant differences noted in response, toxicity, overall and progression-free survival between the two groups. The median time to progression was 2.8 months versus 3.2 months respectively and the median survival was 11 months for the DTIC arm but only 9 months for the vaccine arm (66).

Although disappointed by many trials, several new avenues of DC-based immunotherapy are actively being pursued and in various stages of development, focusing on different ways to enhance the therapeutic efficacy of DC in combination with various immunoadjuvants and other anticancer agents.

1.3.2.7 Individual Therapy Based on Activated T-Cells

One very promising approach to treat metastatic melanoma is to use fully activated anti-tumor T-cells as warhead. This regimen involves the adoptive autologous transfer of highly selective tumor-reactive T-cells directed against over-expressed self-

derived differentiation antigens after lymphodepleting chemotherapy. Rosenberg group reported in 2004 a clinical trial using this method. Cancer regression in patients with refractory metastatic melanoma with large, vascularized tumors was noted in a remarkable 18 of 35 patients (51% response rate), including four patients with a complete regression of all metastatic disease. Such results may stem from the ability to infuse a large number of fully activated tumor infiltrating lymphocytes with anti-tumor activity into a host that is depleted of regulatory T-cells (67).

1.3.3 Gene Therapy

The recent developments in the field of gene transfer have advanced the use of gene therapy as a novel strategy against a variety of human malignancies. Because of its unique set of characteristics, melanoma represents a suitable target for gene therapy. Several strategies have been used by gene therapy to treat melanoma. First is to target melanoma cells to introduce "suicide" genes. Second is to transfer tumor suppressor genes. Third is to inactivate aberrant oncogene expression. Fourth is to introduce genes encoding immunologically relevant molecules. Last is to target the host's immune cells to redirect immune responses against melanoma. Clinical trials have shown the feasibility and safety of gene therapy against malignant melanoma. Although no major successes have been reported, the positive results observed in some patients support the potential for gene therapy in the management of this disease. To make gene therapy as an effective modality of treatment for malignant melanoma, better vector technology as well as increased understanding of the "bystander effect" triggered by gene transfer approaches are needed (68).

The gene therapy in our discussion is to introduce oligonucleotide or DNA sequence into host body thus to stimulate immune response to tumor cells. So it is also called DNA vaccination. This approach has been shown to induce long-lasting immunity against infectious agents and protection from tumor outgrowth in several animal models (69). Likewise, intramuscular injections of DNA (composed of naked DNA expression plasmids) into humans have also resulted in the development of an immunologic response (70). It is hypothesized that one mechanism of tumor antigen expression may involve the DNA introducing the appropriate genes into dendritic cells for subsequent processing and presentation to the host immune system. One of the obvious advantages of DNA vaccinations is that they can be administered to patients regardless of HLA-phenotype and without identifying immunogenic epitopes.

1.3.3.1 Anti-BCL2 Antisense Oligonucleotide Genasense

Genasense (Oblimersan sodium developed by Genta Inc. which is a biopharmaceutical company based in Berkeley Heights, New Jersey) is a phosphorothioate antisense oligonucleotide directed against the first six codons of the Bcl-2 messenger RNA. Binding of the drug to the mRNA recruits RNAse H, resulting in cleavage of the mRNA. As a result, further translation is halted and intracellular protein

15

concentrations of Bcl-2 decrease with time. Melanoma cell lines having Bcl-2 overexpression have been shown to enhance activity of metastasis-related proteinases, *in vitro* cell invasion, and *in vivo* tumor growth (71). Many *in vitro* studies have demonstrated increased sensitivity of melanoma cells to chemotherapy when combined with antisense Bcl-2 therapy (72). Genasense is the first oncology drug of its kind to directly target the biochemical pathway (known as apoptosis) whereby cancer cells are ultimately killed by chemotherapy. Genasense is believed to inhibit the production of Bcl-2, a protein that is believed to be a fundamental cause of resistance to anticancer therapy. By inhibiting Bcl-2, Genasense may greatly improve the activity of anticancer therapy.

Encouraged by previous data, numerous clinical trials were started to evaluate the addition of oblimersan to chemotherapy in various solid tumors, including melanoma. Updated analysis from a randomized phase 3 trial, comparing DTIC combined with oblimersan, with DTIC alone in 771 patients with Stage IV or unresectable Stage III melanoma who had not previously received chemotherapy has shown a response rate of 12.4% in the former compared with 6.8% in the latter group (P=0.007) (73). Median progression-free survival for the oblimersan group was 2.4 months as compared with 1.6 months for the DTIC group, with a relative risk reduction of 27% (P=0.0003). The median survival was increased from 7.8 months in the DTIC arm to 9 months in the oblimersan arm with a P value of 0.077, which became significant when the patients with normal baseline LDH were analyzed. In terms of toxicity, no new or unexpected adverse events were observed in this study, which had not been seen with DTIC alone.

However, in May 2004, a new drug application (NDA) based on 6-months of minimum follow-up data from this trial failed to receive an affirmative vote for approval by an advisory committee to the FDA. Genta subsequently withdrew that application, and the Company has not yet made a decision regarding re-filing the U.S. application (74).

1.3.3.2 DNA Plasmid-Lipid Complex Allovectin-7

Allovectin-7 is a bicistronic plasmid formulated with a cationic lipid system containing the DNA sequences encoding HLA-B7 and beta-2 microglobulin, which together form a MHC1 antigen. Injection of Allovectin-7 directly into tumors is designed to stimulate an immune response against both local and distant metastatic tumors. Allovectin-7 is a novel gene therapy approach for cancer with a unique mechanism of action that is fundamentally different from currently approved treatments. The following three mechanisms were believed to play roles in this agent's efficacy. Mechanism one, in HLA-B7 negative patients, a vigorous allogeneic immune response may be initiated against the foreign MHC class I antigen. Mechanism two, in all patients, ß2 microglobulin may reconstitute normal class I antigen presentation and/or increase tumor antigen presentation to the immune system. Mechanism three, in some patients, an innate pro-inflammatory response may occur that induces tumor responses following intralesional injection of the DNA/lipid complex. The final outcome of all these mechanisms is to initially cause recognition of the tumor at the local site to allow a then

16

sensitized immune response to recognize un-injected tumors at distant metastatic sites (75).

In 2001, Dr. Richards and his colleagues began a high-dose, 2 mg, phase 2 trial evaluating the Allovectin-7 immunotherapeutic alone for patients with stage III or stage IV melanoma, who have few other treatment options. The high-dose phase 2 trial completed enrollment in 2003. The data showed that the trial had a total of 15 responders among the 127 patients receiving the high dose (11.8%), with four of the patients having complete responses and 11 having partial responses. The Kaplan-Meier estimated median duration of response was 13.8 months. The Kaplan-Meier median survival was 18 months. The safety profile was excellent with no reported Grade 3 or Grade 4 adverse events associated with Allovectin-7 (76).

Allovectin-7 has been granted orphan drug designation for the treatment of invasive and metastatic melanoma by the FDA's Office of Orphan Products Development. Orphan drug designation provides U.S. marketing exclusivity for seven years if marketing approval is received from the FDA

Vical is conducting the AIMM (Allovectin-7 Immunotherapeutic for Metastatic Melanoma) trial, a phase 3 pivotal trial of Allovectin-7 as first-line therapy in approximately 375 patients with Stage III or IV recurrent metastatic melanoma in accordance with a SPA agreement completed with the FDA. The trial is being conducted at approximately 60 clinical sites worldwide. They designed the trial to include patients most likely to benefit from our treatment, and specifically excluded patients with brain or liver metastases, patients previously treated with chemotherapy, and patients with elevated lactate dehydrogenase (LDH) levels.

In January 2010 Vical announced that the company has completed enrollment of the planned 375 subjects in its multinational phase 3 trial of Allovectin-7 in patients with metastatic melanoma. Allovectin-7®'s safety profile is excellent with no drug-related serious adverse events reported to date in the phase 3 trial (75).

1.3.3.3 Herpes Simplex Virus Based OncoVEX

OncoVEX (GM-CSF) is an enhanced potency, immuneenhanced oncolytic herpes simplex virus type 1 (HSV-1). It is deleted for infected-cell protein gene 34.5 (ICP34.5), providing tumor selective replication, and ICP47 gene which otherwise blocks antigen presentation. In addition, ICP47 deletion increases unique short region protein 11 (US11) gene expression thereby enhancing virus growth and replication in tumor cells. The coding sequence for human granulocyte-macrophage colony-stimulating factor (GM-CSF) is inserted, replacing ICP34.5, to enhance the immune response to tumor antigens released following virus replication.

OncoVEX is developed by BioVex (Woburn, MA). It is a first-in-class oncolytic, or cancer destroying virus, that works by replicating and spreading within solid tumors

17

(leaving healthy cells unaffected), thereby causing cancer cell death and stimulating the immune system to destroy un-injected metastatic deposits. Both modes of action have been clearly validated in the clinic, where multiple patients with metastatic disease progressing at enrollment have been declared disease free.

BioVex recently concluded a 50-patient phase 2 trial for OncoVEX (GM-CSF) as a stand-alone therapy in patients with Stage IIIc and Stage IV melanoma. The trial was designed to measure overall objective response, which is defined as a complete response, where disease is completely eliminated, or partial response, where there is a >50% reduction in disease burden. 74% of patients who entered the study were progressing after having failed prior therapy. 13 objective systemic responses (26% objective response rate) were achieved including eight CRs, seven of which remain free of disease. 12 responses have so far continued for more than 6 months (ranging from 6 to more than 29 months). Responses were observed in patients with all stages of disease, including the complete resolution of un-injected visceral deposits. Adverse effects were primarily limited to transient flu-like symptoms (77).

In April 2009, BioVex Inc. announced that its OPTiM (OncoVEX Pivotal Trial in Melanoma) phase 3 study with OncoVEX (GM-CSF) in previously treated patients with Stage III and Stage IV melanoma had initiated. The study has commenced recruiting patients in the U.S. and with sites in the United Kingdom, Germany and Australia. The OPTiM trial is a multi-national, open label, randomized study designed to assess the efficacy and safety of treatment with OncoVEX (GM-CSF) as compared to subcutaneously administered GM-CSF in patients with unresectable stage III (b-c) and stage IV (M1a-c) disease. Patients will have received at least one prior therapy for active disease which includes any type of therapy including investigational drugs. A total of 360 patients will be enrolled (240 to the OncoVEX (GM-CSF) arm and 120 to the control arm). The study design was agreed with the FDA under the special protocol assessment process (78).

1.4 Possible Reasons for Failure

Despite an epic number of clinical trials to test a wide variety of anticancer strategies, the average survival rate for patients with metastatic melanoma remains unimproved during the past 30 years (41). Though constant clinical trials effort, although some approaches showed promising intermediate results, still no any agents for approaches have been granted a FDA approval for the treatment of metastatic melanoma. There are several reasons that may be accountable for the extremely high resistance of metastatic melanoma to current treatment modalities.

1.4.1 Reasons for Chemotherapy Failure

Melanoma cells are quite resistant to most chemotherapy reagents. This is associated with the specific feature of melanoma cells. In nature, these cells have low

levels of spontaneous apoptosis *in vivo* compared with other tumor cell types, and they are relatively resistant to drug-induced apoptosis *in vitro* (4). The natural role of melanocytes is to protect inner organs from UV light, a potent DNA damaging agent. Therefore, it is not surprising that melanoma cells may have special DNA damage repair systems and enhanced survival properties (79). Moreover, recent studies showed that, during melanoma progression, it acquired complex genetic alterations that led to hyperactivation of efflux pumps, detoxification enzymes, and a multifactorial alteration of survival and apoptotic pathways. All these have been proposed to mediate the multi-drug resistant phenotype of melanoma (80).

1.4.2 Barriers for Successful Immunotherapy

The major barrier is immunosuppressive effects activated by tumors. Tumor cell can escape immune rejection and induce immunosuppression through the following five major paths. Firstly, tumor cells may lose or down-regulate either the melanoma associated antigens or MHC molecules. Secondly, tumor cells may produce a plethora of immunosuppressive factors such as interleukin-10, VEGF and transforming growth factor. These factors create an inherently unfavorable microenvironment that limits the host immune response, in addition to tolerating the T-cell response to established tumor. Third possible reason is intrinsic inefficiency of DC whereby the appropriate co-stimulatory molecules are not being presented on the cell surface. Fourth possible reason is tumor-related alterations in T-cell signaling and a skewing of the immune response from a Th1 (immunoactivating) to a Th2 response (immunotolerant). Lastly, the concept of tumor cell escape and immune tolerance is an exceedingly complex process. We need to further understand these mechanisms before we can have successful immunotherapy to melanoma (14).

Specifically for cancer vaccines, there are some further barriers. First is the characterization of vaccines potency and toxicity. This is especially important in the transition from phase 2 to phase 3 trials. To select a meaningful and validated end point for trials is a big challenge most of the time. Second barrier is selection of the maximum tolerated dose of cancer vaccine, particularly compared with traditional anticancer agents. Cancer vaccines are typically not very toxic. So the optimum dose often has to be based on the immune response of patients. But if the patients have previously been heavily treated with other anticancer agents, this can lead to a compromised immune system that makes it difficult to detect an evoked immune response. The third barrier is appropriate trial design and statistical data process. This is also a key part and can substantially affect final trial outcome (54).

1.5 Future Directions

With the rapidly rising incidence and the high resistance to current therapeutic agents, developing more effective drugs for metastatic melanoma is urgently needed. But

19

before we can thoroughly understand all the major molecular pathological changes associated with melanoma malignancy, it is very difficult to reach a cure for it.

Melanoma is an extremely complicated disease, with many gene mutation and signaling pathway changes. Elevated signaling pathway in melanoma including mitogen-activated protein kinase (MAPK) pathway, phosphatidylinositol 3 kinase (PI3K)-AKT pathway, Wnt-Frizzled-β-catenin pathway, JAK/Stat pathway and α-MSH-MC1R or microphthalmia-associated transcription factor (MITF) pathway. The first two are crucial pathway accounting for melanoma malignance. Gene mutation involved in melanoma including the following oncogenes: B-raf, N-ras, akt3; tumor suppressors: CDKN2A, PTEN, p53, APAF-1, p16, p15, p19; others: Cyclin D1, MITF etc (81).

The binding of growth factors to their respective receptors leads to activation of RAS proteins. Ras will then activate Raf. Raf activate mitogen-activated protein kinase (MEK), which then act on extracellular-related kinase (ERK). Phosporylated ERK kinases (ERK-P) translocate to the nucleus and activate transcription factors, which promote cell cycle progression and proliferation. The PI3K-AKT pathway mediates cell survival signaling via growth factors. Phosphatase and tensin homolog (PTEN) inhibits growth factor signaling by inactivating phosphatidylinositol triphosphate (PIP3) generated by PI3K. Activated PI3K converts the plasma membrane lipid phosphatidylinositol 4,5-bisphosphonate to PIP3, which acts as a second messenger leading to the phosphorylation AKT and subsequent up-regulation of cell cycle, growth, and survival proteins. AKT can also up-regulate mTOR (mammalian target of rapamycin), S6K, and NFκb leading to cell growth and inhibition of apoptosis.

Knowing the huge complexity of melanoma, it's easy to understand why so many random trials of single agents or combinational treatment have failed. So targeted therapy in a systemic way based on the understanding about melanoma molecular pathology seems to be a reasonable way to fight this disease.

In learning from our efforts in the past, we must continue to challenge the current paradigms of treatment as we forge new paths to more effective treatment options. This will likely involve a multimodal approach to therapy utilizing all of the available tools in our arsenal. Several agents given in unique combinations may then synergize with standard chemotherapeutic regimens resulting in prolonged clinical responses and long term survival. Like the example of Sorafenib, its failure maybe largely because of it only blocked the Raf-MEK-ERK signaling pathway. Melanoma cells still can survive by compensatory up-regulating other survival pathway like the PI3K-AKT pathway. Then it can develop drug resistance with time by over expressing MDR gene. Ideally, if we can use drugs to synergistically block all the major pathways for melanoma cell survival and then educate our immune system to fight the tumor cells, we will have a very high chance to conquer this deadly disease.

Individualized T-cell-based therapy is a very promising approach. If combined with other suitable tumor killing agents, it maybe can improve the patient survival rate and time. But the selective tumor-reactive T-cells isolated from the patients only can be

20

used for themselves. Thus there is a pretty high cost associated with it. It may not be available to all the patients in the near future.

Since all the combinational treatments are based on the performance of each individual agent, developing more effective single agents is essential. In the next several chapters, I will summary our efforts in identifying more active small molecule drugs for melanoma. That's the basis for our future treatment. It also can provide more choice for combination treatment.

For the dissertation research, my overall hypothesis was by synthesizing novel small molecule and further structure modification, we can find compounds that can inhibit melanoma tumor cell growth both *in vitro* and *in vivo*. My experimental plan was first establishing an *in vitro* method to test compounds activity in inhibiting melanoma cell growth. Then I would use this method to screen a large compound library to identify active lead structure. Next step was to further modify this structure to inpromve activity. Finially I would test active compounds' *in vivo* activity. In the meantime, compounds's pharmacokinetic properties would be also measured.

CHAPTER 2. DISCOVERY OF NOVEL THIAZOLIDINE, IMIDAZOLE, AND IMIDAZOLINE ANALOGS AS CYTOTOXIC AGENTS FOR MELANOMA*

2.1 Introduction

In a continuous effort in our laboratory, our team discovered that, by replacing the glycerol backbone in lysophosphatidic acid (LPA, 1-acyl-sn-glycerol-3-phosphate), the resulting 2-arylthiazolidine-4-carboxylic acid amides (ATCAAs) were potent cytotoxic agents for melanoma (82-87). Two of earlier derivatives (*2RS, 4R*)-2-phenyl-thiazolidine-4-carboxylic acid octadecylamide 1a and (*2RS, 4R*)-2-(4-acetamidophenyl)-thiazolidine-4-carboxylic acid hexadecylamide 1b (**Figure 2-1**) were sent to the U.S. National Cancer Institute for anticancer drug screen using 60 human tumor cell lines (NCI-60). The NCI-60 screening data indicated that compounds 1a and 1b strongly inhibited the growth of all nine types of cancer cells with IC_{50} values ranging from 120 nM (leukemia, CCRF-CEM cell line) to 11 μM (colon cancer, HCC-15 cell line). 1b was very potent against melanoma (IC_{50}=130 nM~1 μM against all eight tumor cell lines) and prostate cancer (IC_{50}=170~270 nM against two tumor cell lines). Based on these preliminary cytotoxic screenings, extensive structure-activity relationship (SAR) and *in vivo* studies were carried out. In this chapter, I will discuss the biological evaluation and SAR studies of ATCAA analogues based on 1a and 1b for both melanoma. These analogs were further assessed for their ability to inhibit melanoma colony formation. The *in vivo* efficacy of compound 1b was tested in a xenograft model using human A375 melanoma tumors. This class of compounds showed potent antitumor activity and selectivity, which could represent the basis for their development into novel chemotherapeutic drugs.

2.2 Materials and Methods

2.2.1 Compound Library

Ninety-one compounds were selected to form a library for biological testing. Their activity was compared with the existing drugs, Taxol and DTIC (Sigma-Aldrich, Inc., St. Louis, MO). In addition, Sorafenib (Bay43-9006) has recently been used extensively in clinical trials for advanced melanoma and is well tolerated in patients (22). Hence, Dr. Wei Li also synthesized Sorafenib based on published procedures (88), and

---

*Portions of this chapter adapted with permission from the following:
 1. Li W, Wang Z, Gududuru V, *et al*. Structure-activity relationship studies of arylthiazolidine amides as selective cytotoxic agents for melanoma. Anticancer Res 2007;27:883-8.
 2. Li W, Lu Y, Wang Z, *et al*. Synthesis and antiproliferative activity of thiazolidine analogs for melanoma. Bioorg Med Chem Lett 2007;17:4113-7.
 3. Chen J, Wang Z, Lu Y, *et al*. Synthesis and antiproliferative activity of imidazole and imidazoline analogs for melanoma. Bioorg Med Chem Lett 2008;18:3183-7.
 4. Lu Y, Wang Z, Li CM, *et al*. Synthesis, *in vitro* structure-activity relationship, and *in vivo* studies of 2-arylthiazolidine-4-carboxylic acid amides as anticancer agents. Bioorg Med Chem 2010;18:477-95.
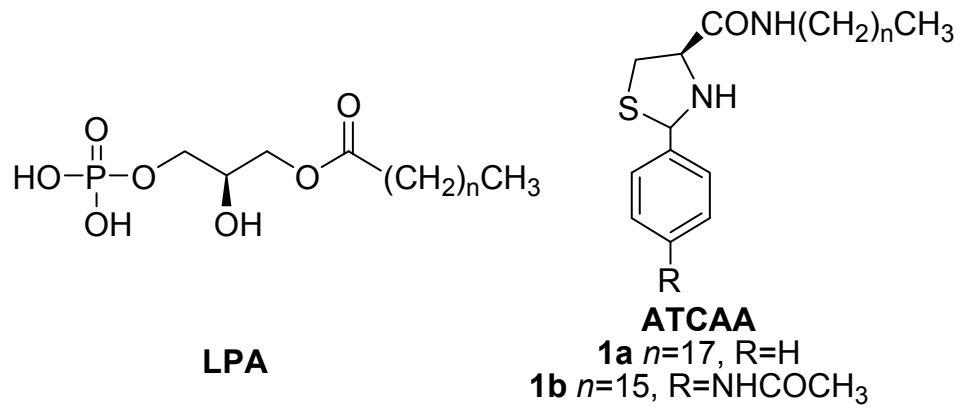
Figure 2-1. Structures of LPA and ATCAA.

used its activity as a standard to assess our lead compounds. Thiazolidine analogues were synthesized by Dr. Yan Lu. Imidazole and imidazoline compounds were synthesized by Mr. Jianjun Chen. I worked for the biological part.

2.2.2 Cell Culture

SK-MEL-188 cells were derived from primary tumors and cultured in Ham's F10 medium (Gibco Invitrogen, Inc., Grand Island, NY) plus 5% fetal bovine serum (FBS) (Cellgro Mediatech, Inc., Herndon, VA) and 1% antibiotic/antimycotic mixture (Sigma-Aldrich, Inc., St. Louis, MO) (89). WM-164 cells were derived from metastatic tumors and were a gift from Dr. Meenhard Herlyn (Wistar Institute, Philadelphia, PA). A375 cells and B16-F1 cells were purchased from ATCC (American Type Culture Collection, Manassas, VA). Both WM-164 and human dermal fibroblast cells (purchased from Cascade Biologics, Inc., Portland, OR) were cultured in DMEM (Cellgro Mediatech), supplemented with 5% FBS, 1% antibiotic/antimycotic mixture and bovine insulin (5 μg/mL; Sigma-Aldrich Inc., St. Louis, MO). Human dermal fibroblast (adult) cells (HDFa) were used as a control to examine the effect of compounds on the stromal environment. Thus, the effect of drugs on melanoma cells versus fibroblasts would document their potential selectivity.

2.2.3 Sulforhodamine B Assay

Cells were seeded into 96-well plates at 5000 cells/well. After 12 h, media were changed and serial dilutions of compounds were added (1 nM~100 μM). Cells were incubated with each compound for 48 h. Fresh media containing the testing compound were changed every 24 h. Thereafter, total cell protein corresponding to cell numbers (both viable and non-viable cells) was measured using the sulforhodamine B (SRB) assay according to the manufacturer's protocol (Sigma-Aldrich Inc., St. Louis, MO) (79, 90). Briefly, cells were fixed with trichloroacetic acid, washed, and incubated with sulforhodamine B for 30 min. After another wash, dye incorporated into the cells was solubilized and measured using a plate reader at 565 nm.

2.2.4 Lactate Dehydrogenase Release Assay

SK-MEL-188 cells were seeded at a density of 5000 cells per well in 96-well flat-bottom microtiter plates. Media were changed after 12 h, and the testing compound was added at serial dilutions. Media were changed with fresh compound every 24 h. After incubation for 48 h, supernatants were collected and transferred to a new plate. Lactate dehydrogenase (LDH) in supernatants was measured using Cytotox 96 Non-Radioactive Cytotoxicity Assay (Promega, Madison, WI). Briefly, substrate mix solution (containing tetrazolium salt) was added to each well and incubated at room temperature for 30 min. At the end of incubation, stop solution was added to each well and the plate was read at 490 nm. Cytotoxicity of compounds was calculated using the following formula: %

24

cytotoxicity=(experimental LDH release/maximum LDH release). Experimental LDH release was calculated by subtracting the absorbance corresponding to the media alone from the absorbance corresponding to control or compound-treated cells. Maximum LDH release was calculated by subtracting the absorbance corresponding to the media with added lysis solution from the absorbance corresponding to cells lysed with lysis solution.

2.2.5 DNA Content Analysis

Flow cytometry analysis was performed as described elsewhere (91). Briefly, SK-MEL-188 cells were seeded in 10 cm Petri dishes at a density of 10^6 cells per dish; at 12 h the medium was changed to 5% FBS with different concentrations (0, 6 and 60 μM) of the testing compound. Cells were incubated for 48 h and media with compounds were changed every 24 h. Cells were trypsinized, washed with PBS, and fixed in ice-cold 70% ethanol. Ethanol was removed by centrifugation and cells were incubated in phosphate-citrate buffer (0.2 M Na_2HPO_4, 4 mM citric acid, pH 7.8) for 1 h. Finally, cells were centrifuged and 1 mL of propidium iodide solution (50 μg/mL) and RNAse (0.1 mg/mL) in PBS was added (92). Samples were shaken for 30 min and analyzed with a FACS Calibur cytometer (Beckton Dickinson, San Diego, CA). Data were analyzed and graphs prepared using the Modfit 2.0 program (Verity Software House, Topsham, ME).

2.2.6 Cell Cycle Analysis

Flow cytometry analysis was performed to study cell cycle phase distribution. Briefly, A375 cells (4×10^6) were seeded in 10 cm dishes; Cells were synchronized using 0.5% charcoal-stripped DMEM medium for 72 h. After that, the medium was changed to the media containing 10% FBS with different concentrations (0, 1, 5, 10 and 20 μM) of testing compounds. Cells were incubated for additional 24 h. All cells were collected by trypsinization. Cell pellets were washed by PBS. The supernatant was discarded, and the pellets were fixed in ice-cold 70% ethanol at 4°C overnight. Ethanol was removed by centrifugation and cell pallets were washed with PBS twice. 1 mL of PBS containing 100 μg/mL RNAase A was then added and cell pallets were incubated for 1 h. Cells were centrifuged and re-suspended in 1 mL of PBS containing propidium iodide (50 μg/mL). Cell cycle analysis was conducted with a FACS Calibur Autometer (Beckton Dickinson, San Diego, CA). Data were analyzed and graphs were prepared using the Modfit 2.0 program (Verity Software House, Topsham, ME).

2.2.7 Colony-Formation Assay

To measure colony formation and growth of melanoma, A375 cells were plated at a colony-forming density (2000 cells per well on 6-well plates). Cells were grown in DMEM supplemented with FBS (Atlanta Biologicals, Lawrenceville, GA) and an antibiotic–antimycotic solution (Sigma, St. Louis, MO) at 37°C in an atmosphere of 95% air and 5% CO_2 (93). Cells were treated with compounds 1b and 3ad at different

25

concentrations (2, 20, and 100 μM). Compounds were added to the medium from 1 mM DMSO stock solutions, and corresponding dilution of DMSO was used as negative (vehicle) control. Cells were grown for 14 days, and colonies were stained with 0.1% crystalline blue for 30 min and rinsed with distilled water to remove excess dye. Plates were photographed, and the number of colonies was measured by Artek 880 Automated Colony Counter (Artek Systems Corporation, Farmingdale, NY).

2.2.8 *In Vivo* Evaluation of Anti-Melanoma Efficacy

Compound 1b was dissolved into a co-solvent system that was composed of 80% Tween 80 (Sigma-Aldrich, St. Louis, MO) and 20% Captex 200 (Abitec Corporation, Columbus, OH). Dacarbazine (DTIC) (Sigma-Aldrich, St. Louis, MO) was dissolved in saline solution. Male athymic nude mice aged 4-5 weeks were purchased from Harlan Laboratories (Harlan Laboratories, Indianapolis, IN). The laboratory housing the animals met all Association for Assessment and Accreditation and Laboratory Animal Care specifications. All of the procedures were conducted in accordance with the guidelines of our Institutional Animal Care and Use Committee.

A375 cells in a logarithmic growth phase were prepared in FBS-free DMEM medium (Cellgro Mediatech) at a concentration of 5×10^7 viable cells/mL and placed on ice. The cell suspension was mixed with BD Matrigel (BD Biosciences, Waltham, MA) at a 1:1 ratio. This cell suspension (100 μL) was injected subcutaneously in the right dorsal flank of each mouse. When tumor sizes reached about 150 mm^3, about 7 days after cell inoculation, all mice bearing tumors were divided into control and treatment groups based on tumor size (n=8 per group). Each group had similar average tumor size. Mice in control groups were injected intraperitoneally with 50 μL vehicle solution only (negative control) or DTIC at 60 mg/kg (positive control) once daily. Tumor volume was measured twice weekly with a Traceable® electronic digital caliper (Fisher Scientific, Inc., Pittsburgh, PA) and calculated using the formula $a \times b^2 \times 0.5$, where *a* and *b* represented the larger and smaller diameters, respectively (94). Tumor volume was expressed as cubic millimeters. Data were expressed as mean ± SE for each group and plotted as a function of time. Percentage tumor reduction at the conclusion of the experiment (22 days after initiating treatment) was calculated from the formula $100-100 \times [(T-T_0)/(C-C_0)]$, where T represents mean tumor volume of a treated group on a specific day, T_0 represents mean tumor volume of the same group on the first day of treatment, C represents mean tumor volume of a control on a specific day, and C_0 represents mean tumor volume of the same group on the first day of treatment (95). Animal activity and average body weight of each group were monitored during the entire experiment period to assess compound toxicity. At the end of treatment, all mice were euthanized by CO_2 followed by cervical dislocation, and tumors were harvested for further studies.

26

2.2.9 Statistical Analysis

Data are presented as mean ± SEM (n=6~8). IC_{50} (*i.e.*, concentration that inhibited cell growth by 50% of untreated control) values were obtained by nonlinear regression analysis (GraphPad Prism, San Diego, CA). Statistical analyses were performed with the Student's *t*-test (*$p<0.05$, **$p<0.001$).

2.3 Results and Discussion
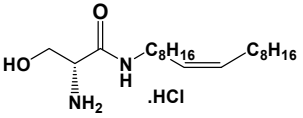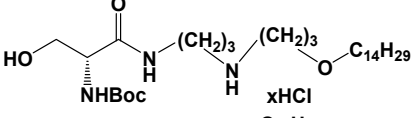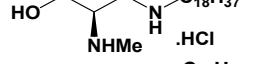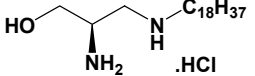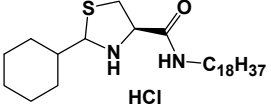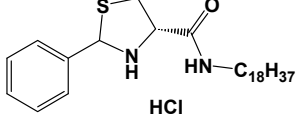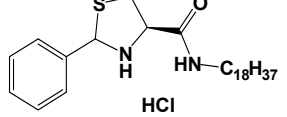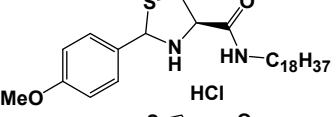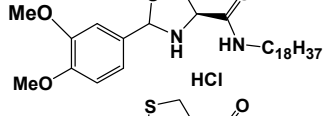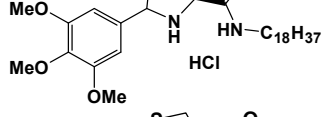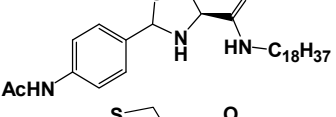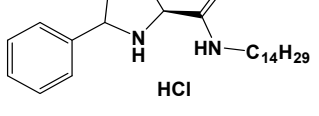
2.3.1 Identification of Lead Structures for Melanoma

In the first step of lead identification, cells were exposed to each compound at 10 µM to identify those which are active for both SK-MEL-188 and WM-164 cell lines. The IC_{50} values of the seven most active compounds with 50% or more growth inhibition at 10 µM were subsequently measured on both cancer cell lines and on the control cells (fibroblast cells). Activities of several compounds with similar structures to the active compounds were also measured in order to understand the structure-activity relationships (SAR). Sorafenib, DTIC and Taxol were assayed in the same way for comparison and served as internal quality controls in the different assay batches. The results for all three cell types are summarized in **Table 2-1**.

Overall, three basic structures were found very active in inhibiting both melanoma cell lines: (A) serine amides (*e.g.* VG-III-15), (B) serine amino alcohols (VG-II-197)**,** and (C) arylthiazolidine-4-carboxylic acid amides (ATCAA, *e.g.*, VG-III-39) (**Figure 2-2**). Analogs of (A) and (B) did not possess acceptable selectivity for cancer cells. Thiazolidine derivatives (C) displayed the highest potency and selectivity with IC_{50} values in the nano-mole range for cancer cells (**Table 2-1**, VG-III-39). Not surprisingly, data from this *in vitro* assay indicated that DTIC is inactive ($IC_{50}>100$ µM) against both cancer cell lines due to the lack of bio-activation. This is consistent with the currently proposed mechanism of action for DTIC, as well as findings by Daidone and co-workers (96). Clearly, *in vivo* assay is needed to assess the true activity of DTIC and similar structures. While Taxol is outstanding in inhibiting cancer cell growth, it is not effective in killing melanoma cells (cytostatic). In contrast, all the lead compounds from these preliminary studies killed the cells completely at higher concentrations. The mechanisms of action of our compounds are clearly different from that of DTIC and Taxol.

Sorafenib effectively killed all the melanoma cells at high concentrations, similar to that of our lead compounds. When measured by IC_{50} values, VG-III-39 is about 10 times as potent as Sorafenib. Its selectivity, defined as the ratio of IC_{50} in fibroblast cells over IC_{50} in melanoma cells, is moderate when compared with that of Sorafenib (10 *vs.* larger than 3). Together with the clinical finding that Sorafenib has low toxicity and is well tolerated by patients (22). The potency and selectivity of Sorafenib provide an excellent standard to assess the activities of our compounds and represent the future goal for optimization of our lead structures.

Table 2-1. IC$_{50}$ of the lead compounds, Sorafenib, DTIC and Taxol.

Structure	Name	IC$_{50}$ (µM) (n=3)		
		SK-MEL-188	WM-164	HDFa
	VG-II-189	>10	>10	ND
	VG-III-15	4	3	3
	VG-II-197	3	4	2
	VG-II-201	3	4	3
	VG-III-215	ND	>50	ND
	VG-III-41	24	18	28
	VG-III-149	40	>50	>50
	VG-III-83	10	13	28
	VG-III-267	2	3	>10
	VG-III-265	2	2	5
	VG-III-271	3	6	>10
	VG-III-39	**570 nM**	**460 nM**	**6**
	Sorafenib	**4**	**5**	**15**
	Taxol	4 nM	6 nM	12 nM
	DTIC	>100	>100	>100

ND: not determined.
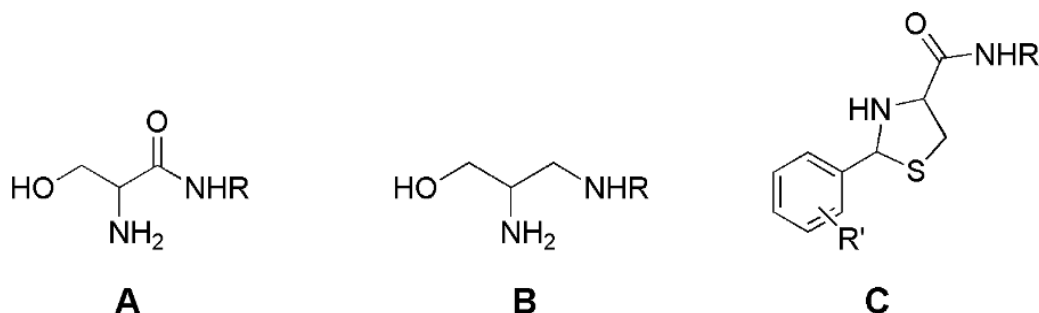
Figure 2-2. Identified active lead structures for melanoma.

Several important SARs were revealed in examining the 91-member library. Firstly, amides were less active than the corresponding alcohols (**Figure 2-2A and B** respectively). Heteroatoms on the side chain substantially increased the potency (VG-III-15), but unsaturation on the side chain had the opposite effect (VG-II-189). Secondly, an alkyl amine (VG-II-197) was about equipotent to the un-substituted amine (VG-II-201), suggesting that cyclization of the amine and alcohol may be possible. However, none of the open chain compounds displayed acceptable selectivity against cancer cells. Thirdly, the presence of the aromatic ring in the heterocyclic compounds improves selectivity and cytotoxicity of structure C (**Figure 2-2**) (VG-III-215 *vs.* VG-III-149). Fourthly, the potency of the compounds depended strongly on the chirality at C-4 position (VG-III-41 *vs.* VG-III-149), the substitution on the aromatic ring (VG-III-149 *vs.* VG-III-265), and the chain length (VG-III-39 *vs.* VG-III-149). With a similar C18 chain, the *S*-isomer at the C-4 position (VG-III-41) showed higher potency than the *R*-isomer (VG-III-149). More electron donating substitutions on the aromatic ring progressively increased the potency of analogs of structure C (VG-III-149 *vs.* VG-III-83, VG-III-267, and VG-III-265). N-substitution with the C14 chain was much more potent and selective against cancer cells than that of the C18 chain compound (VG-III-39 *vs.* VG-III-149). Clearly, further structural optimization is warranted and will likely improve both potency and selectivity for this class of compounds against melanoma.

It is interesting to compare the activity in melanoma with that in prostate cancer for these compounds. In general, their activities are consistent in these two types of cancer cells, demonstrating potentially broad anticancer properties for ATCAA analogs. Compounds that are active or inactive in prostate cancer also displayed similar behavior in melanoma, but there are a few exceptions. For example, although VG-III-149 (C18 chain length) showed excellent activity (IC$_{50}$<3 μM) against prostate cancer cells, it was not active in both melanoma cell lines (IC$_{50}$>40 μM). In addition, for compounds which are active in both cancer types, their relative potency and selectivity are not the same. For example, in prostate cancer studies, a compound with a C14 side chain was found to be slightly less active than that with a C18 chain. Substitutions on the aromatic ring with mono-, di- or tri-methoxyl groups were found to be favorable in prostate cancer cell lines. Both the potency and selectivity increased as more methoxyl substitutions were added to the aromatic ring (82). In melanoma, however, methoxyl substitutions did not have significant selectivity benefits when compared with nonsubstituted analogs (*e.g.* VG-III-

83 *vs.* VG-III-265). A C14 chain displayed much better activity and selectivity than C18 chain compounds (*e.g.* VG-III-39 *vs.* VG-III-265). Interestingly, Taxol behaves very differently in prostate cancer cells and melanoma cells. While Taxol killed all the prostate cancer cells, it only killed about half of the melanoma cells when compared with controls based on our *in vitro* assay. This may suggest different oncogenic properties between these two types of cancer.

2.3.2 VG-III-39 Induced DNA Degradation and LDH Release

To examine more closely the cell death induced by our compounds, I measured lactate dehydrogenase (LDH) release by colorimetric assay and analyzed DNA content by flow cytometry.

LDH is a stable cytosolic enzyme that is released upon cell lysis. Treatment of cells with VG-III-39 resulted in a dramatic dose-dependent increase of LDH released to the cellular environment (**Figure 2-3A**).

Analysis of the DNA content of control cells (**Figure 2-3B**) showed peaks corresponding to the cells in G1/0-cell phase (62%), S-phase (32%) and G2/M-phase (6%), a typical distribution of cells in culture (92). Treatment of cells with VG-III-39 at 6 μM and 60 μM led to the disappearance of peaks corresponding to viable, proliferating cells and the appearance of single peaks corresponding to debris/degraded DNA.

2.3.3 Early Stage SAR Study of Thiazolidine Derivatives

The ability of thiazolidine derivatives to inhibit the growth of two melanoma cancer cell lines and fibroblast cells is summarized in **Table 2-2**. Sorafenib (Velcade) has been used extensively in clinical trials for melanoma. Hence I selected this compound and DTIC as reference standards to assess the activity of our compounds. At this early stage, all compounds were used as a diastereomeric mixture if they contain chiral centers in order to select the most promising compounds for further development.

Examination of antiproliferative effects for a variety of substitutions on the phenyl ring revealed the chain-length dependence for these compounds (1~5, 6~9, 10~13, 14~19). Short chain length such as a C10 chain (*e.g.*, compound 2, 6, 10) displayed low potency for both cancer cells and fibroblast cells. As chain length increased, potency increased, as well as toxicity as measured on fibroblast cells except when the acetyl amino group was substituted on the phenyl ring (compound 14~17). Both C15 and C16 chains with this substitution displayed both high potency and high selectivity against cancer cells, with an IC_{50} for melanoma cells as low as 600 nM (compound 17). Further chain increases, however, reduced potency and selectivity. At a chain length of C18 (compound 19), the IC_{50} value was higher than 10 μM for all three cell lines. Interestingly, adding either a *cis-* or *trans-* double bond in the C18 side chain restored potency dramatically (compound 20Z and 20E), demonstrating that both length
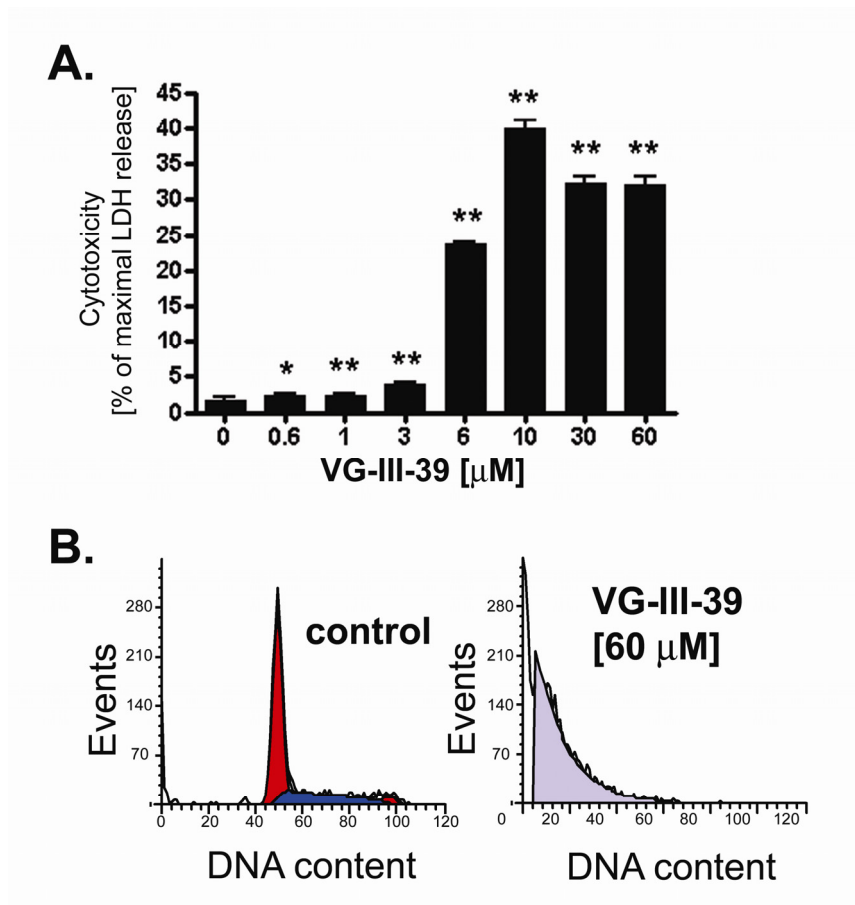
Figure 2-3. Compound VG-III-39 induced DNA degradation and LDH release. SK-MEL-188 melanoma cells were incubated with VG-III-39 for 48 h. A: LDH released from the cells after treatment was then analyzed. Data is presented as mean±SEM (n=8), *p<0.05, **p<0.001. B: DNA content was analyzed using flow cytometry. Results are representative of two separate experiments.

31

Table 2-2. Cytotoxic activity of thiazolidine analogs, Sorafenib and DTIC.
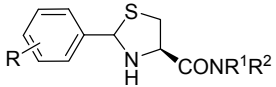
Structure	Compound	R	R^1	R^2	IC$_{50}$±SEM (µM) (n=3)		
					SK-MEL-188	WM-164	HDFa
	1	3,4,5-trimethoxyl	n-C$_8$H$_{17}$	H	17±1	20±1	21±10
	2	3,4,5-trimethoxyl	n-C$_{10}$H$_{21}$	H	15±3	2±0	7±4
	3	3,4,5-trimethoxyl	n-C$_{12}$H$_{25}$	H	2±0	2±0	2±1
	4	3,4,5-trimethoxyl	n-C$_{14}$H$_{29}$	H	2±1	2±0	3±0
	5	3,4,5-trimethoxyl	n-C$_{16}$H$_{33}$	H	2±0	1±0	2±0
	6	3,4-dimethoxyl	n-C$_{10}$H$_{21}$	H	12±6	6±3	6±1
	7	3,4-dimethoxyl	n-C$_{12}$H$_{25}$	H	3±1	2±1	5±2
	8	3,4-dimethoxyl	n-C$_{14}$H$_{29}$	H	2±1	1±0	3±1
	9	3,4-dimethoxyl	n-C$_{16}$H$_{33}$	H	2±0	1±0	2±1
	10	3,4 -OCH$_2$O-	n-C$_{10}$H$_{21}$	H	7±1	5±0	8±3
	11	3,4 -OCH$_2$O-	n-C$_{12}$H$_{25}$	H	4±0	3±0	5±1
	12	3,4 -OCH$_2$O-	n-C$_{14}$H$_{29}$	H	2±0	1±0	4±1
	13	3,4 -OCH$_2$O-	n-C$_{16}$H$_{33}$	H	2±0	2±0	6±2
	14	NHCOCH$_3$	n-C$_{12}$H$_{25}$	H	2±0	1±0	4±0
	15	NHCOCH$_3$	n-C$_{14}$H$_{29}$	H	2±0	1±0	4±1
	16	NHCOCH$_3$	n-C$_{15}$H$_{31}$	H	2±0	1±0	14±2
	17	**NHCOCH$_3$**	**n-C$_{16}$H$_{33}$**	**H**	2±0	1±0	19±8
	18	NHCOCH$_3$	n-C$_{17}$H$_{35}$	H	9±0	2±0	36±5
	19	NHCOCH$_3$	n-C$_{18}$H$_{37}$	H	22±3	12±1	>60
	20Z	**NHCOCH$_3$**	**(Z)-Octadec-8-enyl**	**H**	1±0	1±0	11±1
	20E	**NHCOCH$_3$**	**(E)-Octadec-8-enyl**	**H**	3±0	1±0	18±4
	21	H	n-C$_{14}$H$_{29}$	H	2±1	1±0	3±0
	22	H	n-C$_{16}$H$_{33}$	H	2±0	1±0	2±0
	23	H	OCH$_3$	CH$_3$	>100	>100	>100
	26	NH$_2$	n-C$_{12}$H$_{25}$	H	2±0	1±0	4±1
	27	NH$_2$	n-C$_{16}$H$_{33}$	H	2±0	1±0	7±1

32

Table 2-2. (continued)

Structure	Compound	R	R^1	R^2	IC$_{50}$±SEM (µM) (n=3)		
					SK-MEL-188	WM-164	HDFa
	24	3,4,5-trimethoxyl	n-C$_{14}$H$_{29}$	H	2±0	1±0	4±1
	25	NHCOCH$_3$	n-C$_{16}$H$_{33}$	H	3±0	1±0	23±3
	28	H	n-C$_{14}$H$_{29}$	H	42±5	>50	>50
	29	3,4-dimethoxyl	n-C$_{14}$H$_{29}$	H	19±2	43±10	>50
	30	NHCOCH$_3$	n-C$_{16}$H$_{33}$	H	29±1	>100	>100
	31	3,4,5-trimethoxyl	N/A	N/A	>50	>50	>50
	DTIC				>100	>100	>100
	Sorafenib				5±1	5±0	15±1

NA: not available.

33

and composition of the side chain are critical for their activity. There is no significant difference in their activity between the *cis-* and *trans-* isomers.

Removing the acetyl amino group on the phenyl ring (compound 21 and 22) resulted in the loss of selectivity, although potency was similar to those with this substitution (compounds 15 and 17). Replacing the alkyl chain with a methoxyl group completely abolished potency (compound 23). Changing the chirality from an *R* to *S* configuration at the C4 position on the thiazolidine ring did not substantially affect either potency or selectivity (compound 4 *vs.* 24 and compound 17 *vs.* 25). Selectivity has a strong dependence on the substitutions in the phenyl ring. For example, with a C12 chain, potency is similar for all the substitutions I studied (compounds 3, 7, 11, 14, and 26). However, selectivity improves dramatically when proper substitutions are present (compound 17 *vs.* compounds 5, 9, 13, 22, and 27).

When the amino group in the thiazolidine ring is substituted (compound 30) or a double bond is introduced (compounds 28 and 29), the resulting compounds are largely inactive with IC_{50} values above 20 µM. I also tested the intermediate compound in which the amino group is protected by a Boc group, and that compound is inactive also (data not shown). Furthermore, when Dr Yan Lu removed the aliphatic chain and the amino group by synthesizing a dimer, she obtained an inactive compound (compound 31). These results clearly demonstrate the importance of the amino group in the thiazolidine ring.

2.3.4 Further SAR Studies with New Thiazolidine Derivatives

The diastereomeric mixtures of compounds 3aa-15c were used to evaluate their *in vitro* inhibitory activity and toxicity against two human melanoma cell lines (A375 and WM-164), one mouse melanoma cell line (B16-F1), fibroblast cells (control cell line for melanoma). Because preparing pure diastereomers was not easy to achieve, the IC_{50} values were obtained on diastereomeric mixtures to select the most promising compounds. The standard sulforhodamine B (SRB) assay was used to evaluate the antiproliferative activity of different compounds in melanoma cells. The results are summarized in **Table 2-3**. Compound 1a and 1b were chosen as control compounds for both tumor cell lines in these *in vitro* studies. Cisplatin (CDDP), DTIC, and Sorafenib (Nexavar, Bay43-9006, which had been granted Fast Track designation by FDA to treat advanced melanoma) were used as reference compounds for melanoma (97). The antiproliferative data showed that all three melanoma cell lines were resistant to cisplatin. DTIC was inactive because of the lack of bioactivation *in vitro* (98, 99). The average IC_{50} value of Sorafenib on three melanoma cell lines is 5 µM, and the selectivity of Sorafenib between fibroblast cells and melanoma cells is 3-fold. Our purpose in modifying chemical structure was to enhance the selectivity between tumor cells and control cells and to increase or maintain antitumor potency. Thus, I used the average IC_{50} value of all melanoma and prostate cancer cells for comparison. Selectivity is defined as the ratio of IC_{50} values in the control cell line and the average in tumor cell lines. From Tables 2.3, the most selective compound (3id) had a selectivity of 11.3-fold in melanoma cells against fibroblast cells.

34

Table 2-3. Cytotoxic activity of ATCAA on three melanoma cell lines and a fibroblast cell line.

R^1 — (phenyl) — $\overset{S}{\underset{\underset{R^4}{N}}{}}$ — XR^2R^3
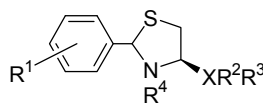
ID	X	R^1	R^2	R^3	R^4	IC$_{50}$±SEM (µM) (n=3)			
						B16-F1	A375	WM-164	HDFa
3aa	CON	3, 4, 5-trimethoxy	n-C$_{18}$H$_{37}$	H	H	6±0	5±0	3±0	5±0
3ab	CON	3, 4, 5-trimethoxy	(*Z*)-octadec-8-enyl	H	H	5±0	2±0	1±0	5±0
3ac	CON	3, 4, 5-trimethoxy	(*E*)-octadec-8-enyl	H	H	3±0	2±0	1±0	4±0
3ad	CON	3, 4, 5-trimethoxy	n-C$_{16}$H$_{33}$	H	H	2±0	1±0	1±0	2±0
3ba	CON	3, 4-dimethoxy	n-C$_{18}$H$_{37}$	H	H	14±1	7±0	3±0	20±1
3bb	CON	3, 4-dimethoxy	(*Z*)-octadec-8-enyl	H	H	3±0	2±0	1±0	18±1
3bc	CON	3, 4-dimethoxy	(*E*)-octadec-8-enyl	H	H	3±0	1±0	1±0	16±1
3ca	CON	2-OMe	n-C$_{16}$H$_{33}$	H	H	4±0	3±0	2±0	7±0
3da	CON	3-OMe	n-C$_{16}$H$_{33}$	H	H	3±0	2±0	1±0	3±0
3ea	CON	4-OMe	n-C$_{16}$H$_{33}$	H	H	2±0	2±0	1±0	8±1
3fa	CON	4-NMe$_2$	n-C$_{16}$H$_{33}$	H	H	7±1	2±0	2±0	21±3
3ga	CON	2-NHAc	n-C$_{16}$H$_{33}$	H	H	8±0	9±1	4±1	28±4
3ha	CON	3-NHAc	n-C$_{16}$H$_{33}$	H	H	2±0	2±0	1±0	6±0
3ia	CON	4-NHAc	n-C$_{18}$H$_{37}$	CH$_3$	H	19±1	21±2	11±1	>100
3ib	CON	4-NHAc	1-adamantanyl	H	H	97±4	138±4	128±3	>100
3ic	CON	4-NHAc	2-adamantanyl	H	H	108±5	66±2	64±3	>100
3id	**CON**	**4-NHAc**	**9H-fluoren-2-yl**	**H**	**H**	**4±0**	**2±0**	**2±0**	**29±1**
3ie	CON	4-NHAc	anthracen-2-yl	H	H	6±0	3±0	1±0	14±1
3if	CON	4-NHAc	4-biphenyl	H	H	6±0	6±0	4±0	33±4
3ig	CON	4-NHAc	2-benzothiazolyl	H	H	55±3	46±4	>100	>100
3ih	CON	4-NHAc	(*Z*)-hexadec-9-enyl	H	H	2±0	2±0	2±0	14±1
3ii	CON	4-NHAc	nonadec-10-ynyl	H	H	2±0	3±0	1±0	7±0
3jb	CON	H	(*Z*)-octadec-8-enyl	H	H	6±1	5±1	2±0	12±1
3jc	CON	H	(*E*)-octadec-8-enyl	H	H	10±1	5±0	2±0	12±1
4	CON	4-NHAc	n-C$_{16}$H$_{33}$	H	Ac	15±1	13±1	20±1	58±1
5	COO	4-NHAc	n-C$_{16}$H$_{33}$	H	H	42±3	28±2	19±0	>100
8a	CH$_2$N	H	n-C$_{16}$H$_{33}$	H	H	5±0	13±0	5±0	60±1
8b	CH$_2$N	4-NHAc	n-C$_{16}$H$_{33}$	H	H	12±0	14±0	3±0	85±3
15a	CON	4-NHSO$_2$CH$_3$	n-C$_{16}$H$_{33}$	H	H	114±2	51±2	19±1	>100
15b	CON	4-NHCOCH$_2$Cl	n-C$_{16}$H$_{33}$	H	H	93±4	20±1	6±0	25±1
15c	CON	4-NHCONH$_2$	n-C$_{16}$H$_{33}$	H	H	6±1	4±0	2±0	7±0
1a	CON	H	n-C$_{18}$H$_{37}$	H	H	16±1	15±1	4±0	30±2
1b	CON	4-NHAc	n-C$_{16}$H$_{33}$	H	H	2±0	2±0	1±0	16±3
DTIC						>100	>100	>100	>100
CDDP						>100	>100	>100	>100
Sorafenib						5±0	5±1	5±0	15±1

2.3.4.1 SAR of Different Amide Chains and Chain Length of ATCAA

ATCAA molecules were designed from LPA structure, which contains a long aliphatic chain. To examine whether the fatty chain played an essential role in cytotoxicity, we explored the possibilities of mimic fatty chain with bulky ring or aromatic systems such as adamantanyl, fluorenyl, and anthrancenyl. Although the antiproliferative data showed that 1- or 2-adamantanyl amides and 2-benzothiazolylamide (3ib, 3ic, and 3ig) had lower activity against most melanoma cells, introducing certain aromatic bulky groups such as 9H-fluoren-2-yl (3id), anthrancen-2-yl (3ie), and 4-biphenyl (3if) retained their proliferative activity. Of particular interest, while introducing 9-fluoren-2-yl (3id) showed a comparable IC_{50} value of 3 µM with 1b (2 µM) on melanoma cells, the selectivity of 3id increased to 11 fold from 9 fold in 1b. This structural modification provided us a new approach to optimize the drug-like properties of ATCAA molecules, in which the hydrophobic fatty lipid chain could be modified with other groups (100).

Hexadecyl chains (3ad) displayed both the highest potency and selectivity against cancer cells among the examined chains, with an IC_{50}=1 µM for WM-164 cells. However, further increasing chain length (18 carbons, 3aa) reduced potency and toxicity. Interestingly, adding either a *cis*- or *trans*- double bond in the C18 side chain restored potency dramatically (*cis*- and *trans*-octadec-8-enyl), demonstrating that both length and composition of the side chain are critical for their activity. *Trans*-octadec-8-enyl chain (3ac, 3bc, 3jc) showed slightly better activity than did the *cis*-isomers (3ab, 3bb, 3jb) against melanoma cells. Introducing a *cis*-double bond in the C16 fatty chain (3ih) or an alkyne in the C18 chain (3ii) did not increase overall potency. Introducing a branched aliphatic chain (3ia) decreased the potency in both melanoma cells (average IC_{50}=17 µM, 9.3 fold decrease) compared with 1b (average IC_{50}=2 µM).

2.3.4.2 SAR of Substitutions on 2-Phenyl of ATCAA

The antiproliferative effects indicated that when methoxy, 3, 4-dimethoxy, and 3, 4, 5-trimethoxy were introduced to 2-phenyl (3aa-3ea), potent activity was preserved or increased compared with that of 1a. For example, (2RS, 4R)-2-(3, 4, 5-trimethoxy-phenyl) thiazolidine-4-carboxylic acid octadecylamide (3aa) (average IC_{50}=5 µM) was 3 fold more potent than was 1a (average IC_{50}=12 µM). Subsequently, different groups were introduced to the *para*-phenyl position. Replacements of 4-NHCOCH₃ (1b) with 4-N(CH₃)₂ (3fa) showed comparable activity on A375 (IC_{50}=2 *vs*. 2 µM) and WM-164 cells (IC_{50}=2 *vs*. 1 µM) but slightly lower selectivity on fibroblast cells (IC_{50}=21 *vs*. 16 µM).

Although 4-N (CH₃)₂ (3fa) substituted ATCAAs were more potent than was 1a (average IC_{50}=3 µM for 3fa, and 12 µM for 1a), they were less potent than 1b (average IC_{50}=2 µM and selective ratio=8.9 for 1b). Methanesulfonamide (15a) or 2-chloroacetamide (15b) were less potent (IC_{50}=6~114 µM) and less toxic (IC_{50}= 25~>100 µM) on melanoma cell lines compared with 1b. Introducing an ureido, 4-NHCONH₂

(15c) instead of a 4-NHCOCH₃ kept partial potency (average IC$_{50}$=4 µM) but resulted in loss of selectivity against melanoma cells (1.8-fold for 15c *vs*. 8.9-fold for 1b).

We also investigated the importance of *o*-, *m*-, and *p*- substitutions in the 2-phenyl ring relative to acetylamino and methoxy groups. Interestingly, *o*-, *m*-, and *p*- isomers showed different activities. *P*-Isomers (3ea, 1b) had the best selectivity and activity. *M*-Isomers (3da, 3ha) had similar average IC$_{50}$s against melanoma compared with *p*-isomers, but their toxicity also increased on fibroblast (3 µM). *o*-MeO and *o*-NHAc analogues (3ca, 3ga) showed slightly less potency and selectivity.

2.3.4.3 SAR of 4-Linkage of ATCAA and Thiazolidine Ring

To investigate the importance of amide linkage on C4 of ATCAA, the carboxamide was replaced with an ester and amine. The isosteric replacement of the amide by an ester resulted in 5 with markedly decreased activity against all cancer cell lines. The amine derivatives 8a and 8b also failed to show any increased potency, although they did show lower toxicity (60-85 µM) than did 1a (30 µM) and 1b (16 µM) in fibroblast cells.

Thiazolidine-4-carboxylic acid has been reported to be effective for treating advanced cancers (101, 102). To examine the importance of a central thiazolidine ring, Dr Yan Lu synthesized 3-acetyl-thiazolidine compound 4 and a series of thiazolidine ring-opened compounds 16a-16d. The structure of these ring-open and their relationship is shown if **Figure 2-4**. Antiproliferative activity of 16a-16d against melanoma is summarized in **Table 2-4.** When acetyl was introduced to 3-NH of thiazolidine, activity decreased in both cancer cell lines (average IC$_{50}$=16 and 10 µM against melanoma and prostate cancer, respectively). Cleavage of both the C-S and C-N bond (16a) led to substantial decrease in both potency (13~14 µM on melanoma cell lines) and toxicity (61 µM on the control cells) compared with 1b and 3ja (1~2 µM on cancer cells, 2~16 µM on control cells). Opening the thiazolidine ring from the C-S bond (16b) caused a loss of potency on both cancer and control cells (>100 µM). Cleavage of the C-N bond in the thiazolidine ring (16c) also resulted in decreased activity (13~15 µM) and no improvement on selectivity compared with 3ja. Removing the C-S bond (16d) reduced the activity of 1b from IC$_{50}$=1~2 µM to 10~12 µM. These results suggested that the presence of the thiazolidine ring is critical for activity. Attempts to reduce the amide with LAH or B$_2$H$_6$ resulted in the C-S bond cleavage in thiazolidine. A disulfanyl dimer, which completely lost anticancer activity, was obtained, and this result is consistent with the above finding that the thiazolidine ring played an essential role in ATCAA potency.
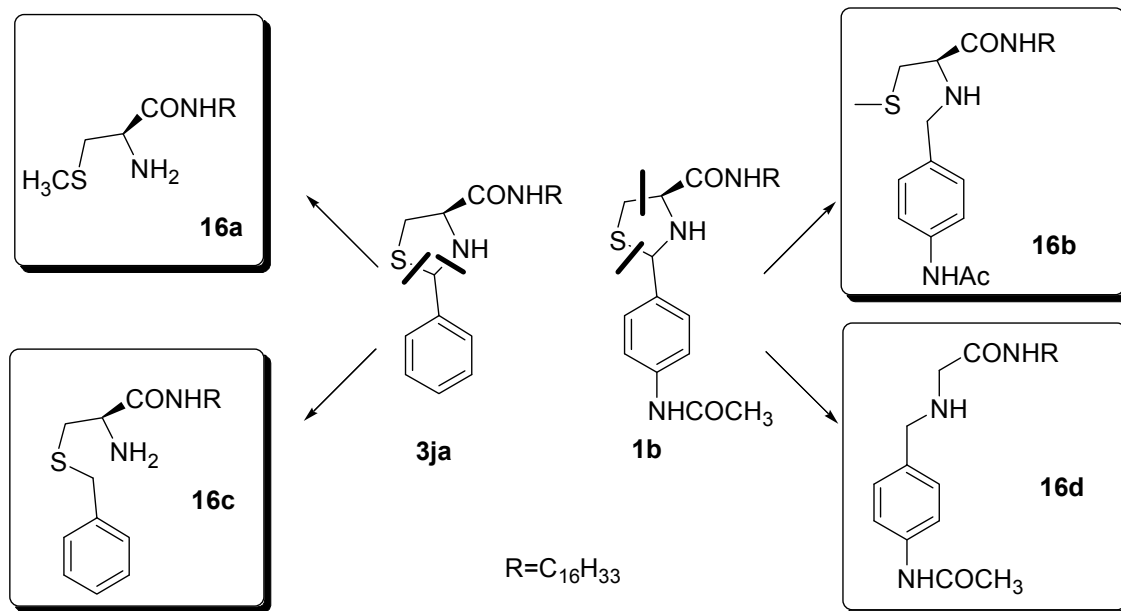
Figure 2-4. Structure relationship of thiazolidine ring-open compounds.

Table 2-4. Cytotoxic activity of thiazolidine ring-open compounds against melanoma.

ID	$IC_{50} \pm SEM$ (µM) (n=3)		
	A375	WM-164	HDFa
16a	13±1	14±1	61±4
16b	109±5	145±5	>100
16c	15±1	13±2	16±1
16d	12±1	11±1	24±1
3ja	ND	1±0	2±0
1b	2±0	1±0	16±3

ND: not determined

2.3.5 SAR Summary of ATCAA for Melanoma

After extensive chemical structure modification and *in vitro* activity studies on melanoma cells, the overall SAR of ATCAA compounds on melanoma cells was summarized in **Figure 2-5**. From the above studies, we generalized several important SAR. Firstly, Thiazolidine ring and the free NH on the ring are very critical for the anti-melanoma activity. The carbon 4 chiral center on the thiazolidine ring is not important for activity because both isomers showed similar potency. Secondly, for the side chain, aliphatic chain with a length of 16 carbons was best for activity. It also can be replaced by 9H-fluoren-2-yl group. Thirdly, the link between the thiazolidine ring and the side chain prefer amide to ester and amine. Lastly, for the substituents on the phenyl ring, electron donating group (EDG) is better than electron withdrawing group (EWG), para- and meta- substitution are the same, ortho-substitution is slightly worse.

2.3.6 SAR of Newly Synthesized Imidazole and Imidazoline Analogs

I found that the chirality at position 4 in thiazolidine ring of ATCAA analogs is not critical for their activity. However, the importance of chirality at position 2 is unknown, because all our previous compounds were tested as diastereomers. Separation of these stereoisomers by chromatographic methods turned out to be extremely difficult. Dr. Li asked for assistance from scientists from Chiralcel Technologies who tried both normal-phase and reverse-phase conditions with their nine chiral columns, but none of the combinations could separate these stereoisomers satisfactorily.

Figure 2-5. SAR summary of ATCAA for melanoma.
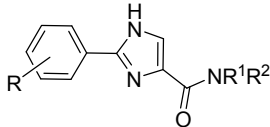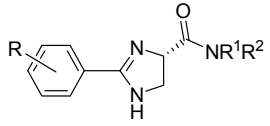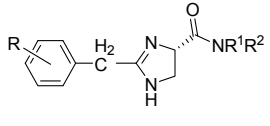
Converting the thiazolidine ring to an imidazoline or imidazole ring represents a very productive approach. First, the nitrogen-containing ring would be very stable. Imidazoline and imidazole rings are important biological building blocks and are present in many existing drugs (103). Second, the imidazoline ring contains only one chiral center, and the imidazole ring contains no chiral center at all. These attributes may alleviate or even eliminate the need for future chiral separations. So Mr. Jianjun Chen made the following modification to ATCAA: a) replacing sulfur with nitrogen or carbon to understand the importance of the heteroatom in the ring, b) introducing one or two double bonds in the ring (imidazoline and imidazole) to understand the importance of the chiral centers, and c) introducing various spacers between the five-member ring and the aromatic ring to understand the relative spatial arrangements for the two rings.

I examined the antiproliferative activity of these imidazoline and imidazole analogs in two melanoma cell lines (human A375 cells and mouse B16 cells) and in a fibroblast cell line. The ability of these new analogs to inhibit the growth of melanoma cancer cell lines and fibroblast cells is summarized in **Table 2-5**.

In summary, none of the new analogs is as active as the lead compound. Although they do not contain any chiral centers, analogs containing an imidazole ring (compounds 5-11) did not have activity at concentrations below 10 μM. Replacing the imidazole ring with an imidazoline ring slightly improved the activity in general (compounds 15-19), with substantial improvement when trimethoxyl or amino acetyl substitutions were added (compounds 20-21). The structure activity for the side chain was similar to that of the thiazolidine analogs, with a saturated C14~C16 chain or an unsaturated C18 chain to be optimal for activity against melanoma cells. Similarly, electronic donating substitutions on the paraposition of the aromatic ring increased activity (compounds 20-21). Replacing sulfur with carbon in the five-member ring produced an inactive compound (compound 30). Collectively, these results indicate that the thiazolidine ring is critical for the activity of this series of compounds.

When a spacer was inserted between the imidazoline/thiazolidine ring and the phenyl ring (compounds 22-29), there is no noticeable improvement in their activity (compound 20 *vs.* compound 22). Increasing the size of the spacer by replacing one hydrogen in the methylene group with a methyl group reduced the activity (compound 23 *vs.* 26, and compound 24 *vs.* 27). Both of these results seemed to indicate detrimental effects of spacers for the activity. Finally, replacing the side chain with a fluorene group resulted in complete loss of activity (compound 23 *vs.* 25). However, with proper parasubstitution on the aromatic ring, the activity dramatically improved (compound 25 *vs.* compound 29) for this series of compounds. On the other hand, with a C16 side chain, the substitution on the phenyl ring had the opposite effect (compound 23 *vs.* 26) in sharp contrast to the non-chain analogs such as 29 and may indicate a different mechanism of action when the long side chain is replaced by a conjugated ring system.

Table 2-5. Cytotoxic activity of imidazolines, imidazoles and comparison with Sorafenib and the lead thiazolidine compounds.

Structure	Compound	R	R^1	R^2	IC$_{50}\pm$SEM (µM) (n=3)		
					A375	B16-F1	HDFa
	5	H	n-C$_{10}$H$_{21}$	H	>30	>30	>30
	6	H	n-C$_{12}$H$_{25}$	H	>30	~30	>30
	7	H	n-C$_{14}$H$_{29}$	H	19±1	38±2	43±2
	8	H	n-C$_{16}$H$_{33}$	H	17±1	40±2	28±1
	9	H	n-C$_{18}$H$_{37}$	H	21±1	>30	47±1
	10	H	(E)-Octadec-8-enyl	H	16±1	32±1	24±1
	11	H	p-Bromophenyl	H	>30	>30	>30
	15	H	n-C$_{14}$H$_{29}$	H	7±0	7±0	17±2
	16	H	n-C$_{16}$H$_{33}$	H	10±0	6±0	60±1
	17	H	n-C$_{18}$H$_{37}$	H	54±1	51±1	111±4
	18	H	(E)-Octadec-8-enyl	H	8±0	12±0	25±3
	19	3,4,5-trimethoxyl	OCH$_3$	CH$_3$	>20	>20	>20
	20	3,4,5-trimethoxyl	n-C$_{16}$H$_{33}$	H	4±1	4±0	13±1
	21	p-NHCOCH$_3$	n-C$_{16}$H$_{33}$	H	5±0	2±0	15±2
	22	3,4,5-trimethoxyl	n-C$_{16}$H$_{33}$	H	4±0	4±0	16±2
	23	H	n-C$_{16}$H$_{33}$	H	8±1	7±0	15±1
	24	H	(E)-Octadec-8-enyl	H	10±1	12±0	16±2
	25	H	2-Fluorene	H	174±11	118±8	>100
	26	H	n-C$_{16}$H$_{33}$	CH$_3$	13±1	12±0	56±7
	27	H	(E)-Octadec-8-enyl	CH$_3$	21±1	17±1	237±39
	28	p-NHCOCH$_3$	n-C$_{16}$H$_{33}$	H	191±14	171±21	>100
	29				14±0	12±0	47±2
	Sorafenib				5±1	5±0	15±1

2.3.7 Flow Cytometry Analysis of Active ATCAA Compounds

Flow cytometry analysis was performed on human melanoma A375 to examine the effect of the new synthetics on cell cycle progression. Analysis of the DNA content of control cells (**Figure 2-6**, top graphs) showed typical distribution of peaks corresponding to cells in G1/G0 phase (65.67~66.97%), S-phase (24.16~28.36%), and G2/M-phase (5.97~8.87%). Upon treatment with compounds 3ad and 1b at 1, 5, 10, and 20 μM concentrations for 48 h, flow cytometric analysis showed that these compounds significantly induced apoptosis (sub-G1 phase) in cancer cells in a dose-dependent manner. The accumulation of cells in sub-G1 phase became apparent at 5 μM.

2.3.8 ATCAA Inhibited Human Melanoma Colony Formation in Soft Agar

Cells grown in 96-well plates do not reflect many properties associated with three-dimensional tumors. Human tumor colony formation assay (*ex vivo* soft agar colony assay) has been suggested as an *in vitro* method to predict the response of an individual patient's tumor to chemotherapeutic agents (104, 105). As a prelude to *in vivo* animal experiments, I investigated the ability of compound 1b and 3ad to inhibit melanoma colony formation by using a well-established method (93, 106, 107). I performed studies with A375 human melanoma cells. Photos and quantified results are shown in **Figure 2-7** and **Figure 2-8**. Compounds 1b and 3ad effectively inhibited A375 colony formation at 2 μM, the lowest tested concentration. At a concentration of 20 μM, compound 3ad almost completely inhibited colony formation, while compound 1b inhibited colony formation by 75%. At the highest tested concentration, 100 μM, melanoma colony formation was completely inhibited by both 1b and 3ad.

2.3.9 Antitumor Efficacy of ATCAA on A375 Xenograft Model

I chose human melanoma A375 cells to test efficacy *in vivo* because ATCAA exhibited potency both *in vitro* assay and colony formation assay against A375 cells. A375 xenograft tumors also exhibited faster tumor growth rate. While compound 3ad was more potent than was 1b in inhibiting melanoma colony formation, it had much poorer selectivity between melanoma cancer cells and fibroblast cells (2.0 fold for 3ad *vs.* 8.9 fold for 1b) as shown in **Table 2-3**. Therefore, I chose 1b for our *in vivo* studies against A375 melanoma tumors. This compound was formulated with 80% Tween 80 and 20% Captex 200 because of its limited water solubility (108). I first determined the maximally tolerated dose (MTD) in ICR (imprinting control region) mice. These mice are less expensive than nude mice and are commonly used for toxicity testing. The MTD for compound 1b was determined to be 42 mg/kg. Two nontoxic dosages (5 mg/kg and 10 mg/kg) were used. I also included DTIC (60 mg/kg) the gold standard for melanoma treatment, as a positive control to assess the efficacy of compound 1b (109). Briefly, male athymic nude mice were injected subcutaneously with 2.5×10^6 A375 cells. Treatment began on day 7 after tumor inoculation, and 1b was injected once a day. Each group had
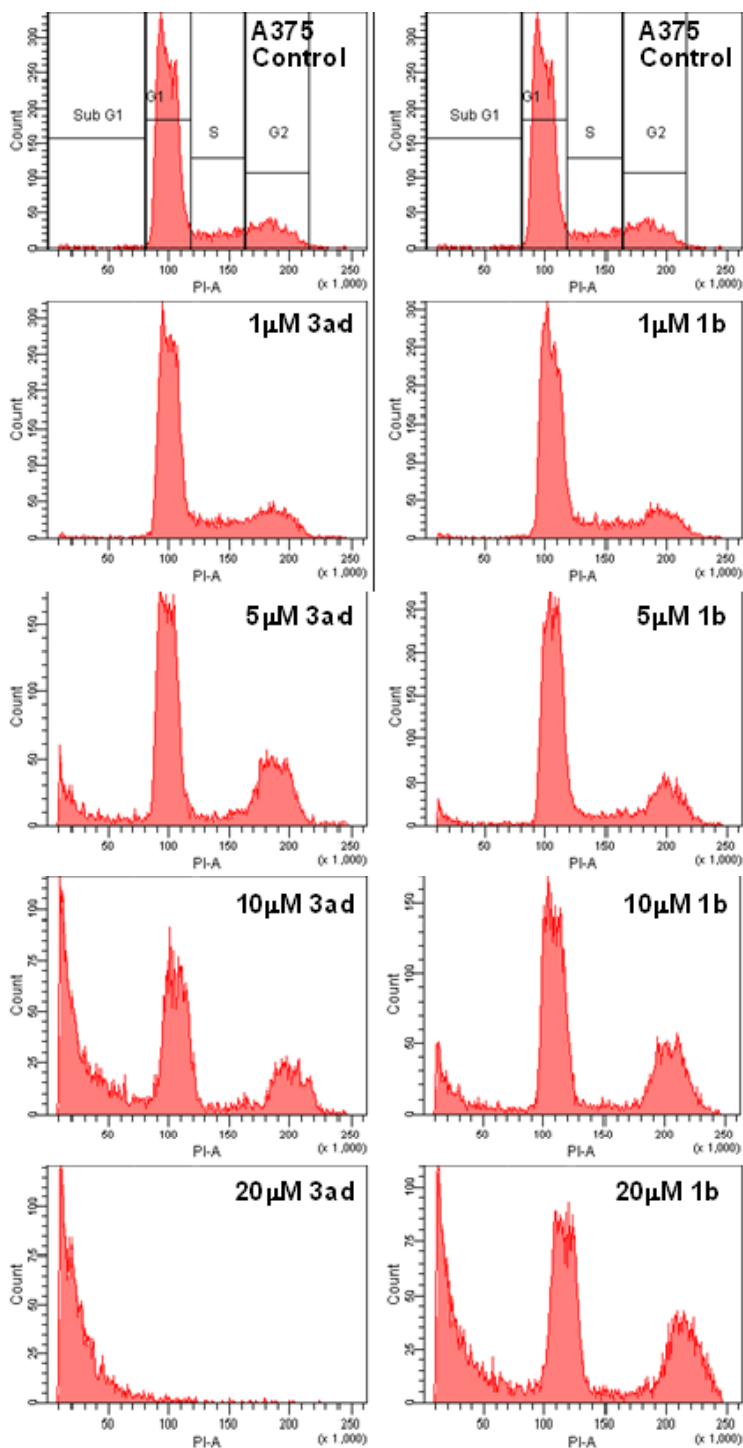
Figure 2-6. Flow cytometry analysis of selected ATCAA compounds.
Sub-G1 phase accumulation was induced by tested compounds on melanoma A375 cells.
(This experiment was done by Mr. Chien-Ming Li, Division of Pharmaceutics, College of Pharmacy, the Ohio State University).

43
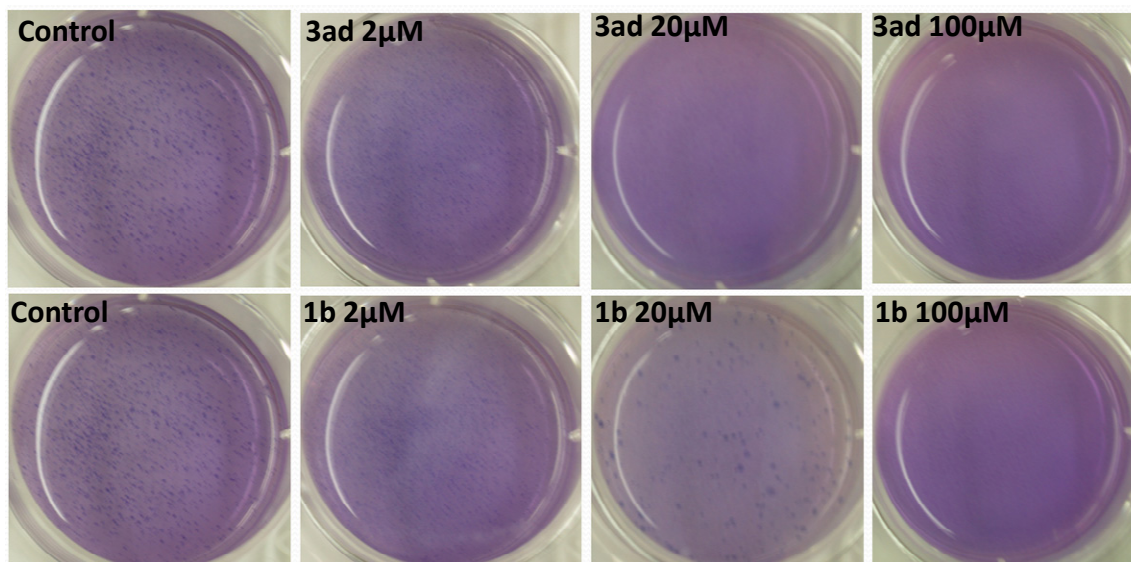
Figure 2-7. Human melanoma A375 cells colony formation in soft agar with ATCAA treatment.
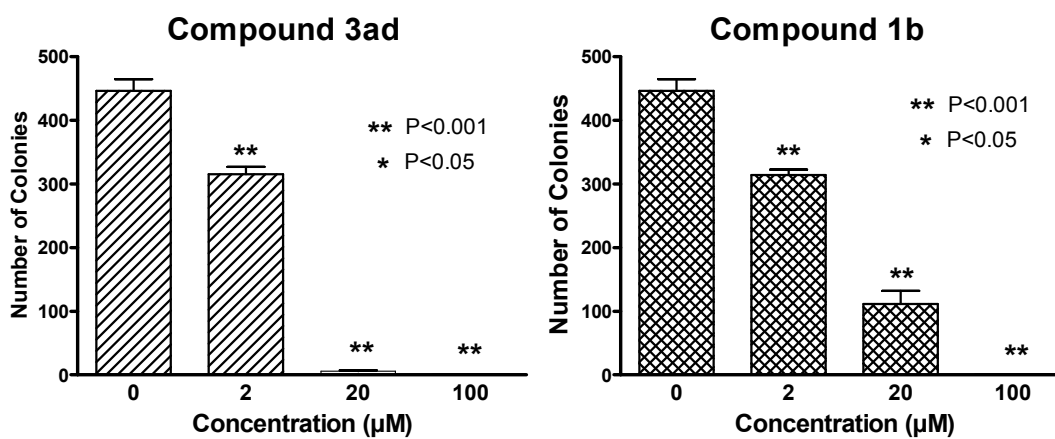
Figure 2-8. Quantified results of colony formation assay with compounds 3ad and 1b treatment.

eight mice. The results are shown in **Figure 2-9**. Compound 1b at 5 mg/kg showed moderate melanoma tumor growth inhibition. After 22 days of treatment, the percentage of tumor reduction was 25%. At a higher dose of 10 mg/kg, compound 1b showed significant melanoma tumor growth inhibition with 62% of tumor reduction. When comparing with DTIC at a dose of 60 mg/kg, which inhibited tumor growth by 42% at the end of treatment, compound 1b clearly showed superior activity in this human melanoma xenograft model. All mice displayed normal activities, and no significant body weight loss was observed during the experiment.

2.4 Conclusions

ATCAA analogs represent a novel class of potent and selective cytotoxic agents for melanoma. Initial analysis indicated that the antineoplastic activity is attributed to their ability to induce DNA break and LDH release in melanoma cells. These SAR studies revealed that the potency of the compounds depends strongly on the chain length and substitutions on the phenyl ring. Our current lead compound is highly potent and moderately selective when compared with Sorafenib, a drug used extensively in clinical trials for melanoma.

Dr. Yan Lu then synthesized a series of ATCAA compounds and thiazolidine ring-opened analogues. Chemical modification and structure-activity relationship of ATCAA compounds were investigated with different substituted 2-phenyl, thiazolidine ring, 4-position linkage, and 4-carboxamide groups based on biological evaluation against melanoma cells. Some compounds are very promising agents against melanoma. Compounds 1b and 3ad effectively inhibited A375 melanoma colony formation. Compound 1b at a dose of 10 mg/kg significantly inhibited melanoma tumor growth *in vivo* and showed higher efficacy than did DTIC at a dose of 60 mg/kg. These compounds did not seem to work via the LPA-GPCR pathway.

Mr. Jianjun Chen also synthesized new imidazole and imidazoline analogs, based on our previous studies, by focusing on the structure activity relationship studies of the central five-member ring. Although the current compounds displayed lower potency when compared with our lead thiazolidine analogs, they may have the distinct advantage of being more stable *in vivo* with the reduced necessity of chiral separations. Some of these new compounds have activity similar to Sorafenib.

45

Figure 2-9. *In vivo* anti-melanoma test of compound 1b on athymic nude mice (n=8 per group) bearing A375 xenograft.
A: Tumor growth curve of control, compound 1b and DTIC treatment. DTIC was used as positive control. B: Average body weight change in control and treatment groups.

46

CHAPTER 3. IDENTIFYING NOVEL MOLECULAR STRUCTURES FOR ADVANCED MELANOMA BY LIGAND-BASED VIRTUAL SCREENING*

3.1 Introduction

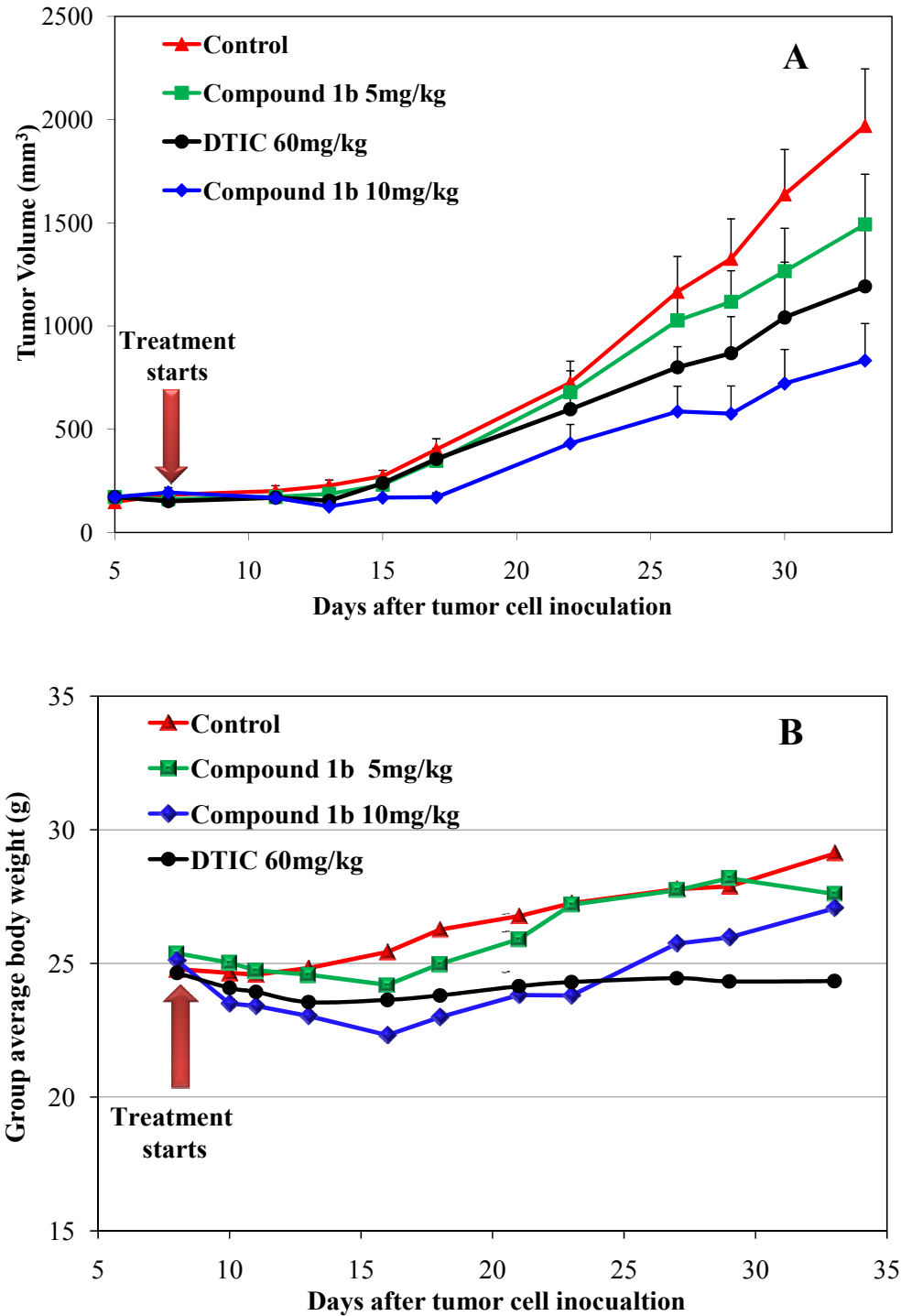In our ongoing efforts to search for small molecules as potential therapeutic agents for advanced melanoma, our team recently discovered a new series of thiazole analogs that showed very potent activity against melanoma cells *in vitro* (110). One of the best compounds in this series has an IC_{50} value below 60 nM. Screening results from the National Cancer Institute (NCI-60 screening) for our lead compound, LY-1-100, indicated nanomolar antiproliferative activity for all the cancer cell lines tested. Preliminary mechanism of action studies on this series of compounds indicated that they may interact with microtubules (110). *In vivo* testing with melanoma tumors showed substantial growth inhibitory activity for this series of compounds. To further expand our understanding of structure-activity relationships and to potentially identify new platforms for active compounds, Dr. Wei Li and Dr. William Seibel explored a compound library from the University of Cincinnati's (UC) Drug Discovery Center, which contains 342,910 small molecules. All compounds are available to us for testing via an established agreement. Usually, compounds are shipped within 2 days of request. Therefore, I can obtain any compound I select easily for biological testing. Although other compound libraries may have more entries than does the UC library, often availability of the compounds is an issue. Therefore, I chose this library for our current studies.

In this chapter, I will discuss two ligand-based virtual screening approaches using the structure of our lead molecule (**Figure 3-1**): 1) similarity search based on atom connectivity using Scitegic Pipeline Pilot software (Accelrys Software, Inc., San Diego, CA) and 2) similarity search based on molecular shape using Schrodinger software (Schrodinger, Inc., New York, NY). Results showed that these two approaches are highly complementary and lead to different active molecular structures. These structures are quite suitable for further structural modification and provide new platforms for our anticancer drug discovery efforts.

3.2 Experimental Methods

3.2.1 Validation of Connectivity Similarity Search

To validate the connectivity similarity search approach, Dr. Wei Li first established a relatively small testing compound library. This library contains 22 known compounds similar to LY-1-100, 10 known dissimilar compounds, and a diverse set of 2000 compounds pulled from the University of Cincinnati Drug Discovery Center
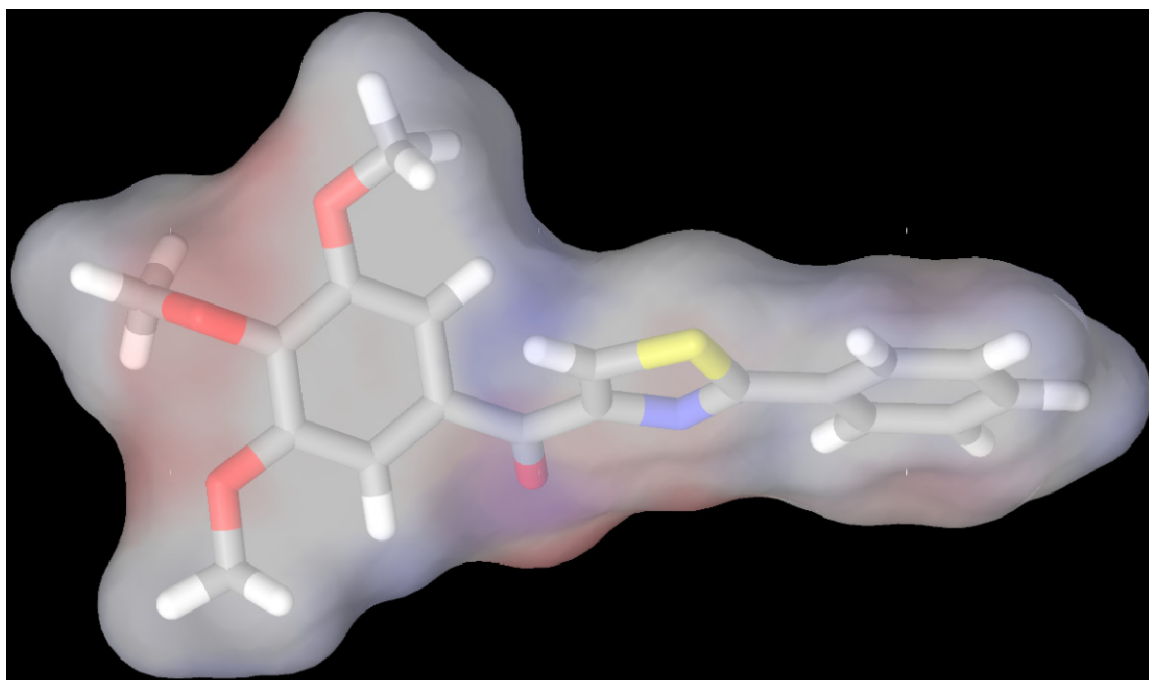
Figure 3-1. Structure and molecular surface of lead compound, LY-1-100.
This figure was prepared by Dr. Wei Li, Department of Pharmaceutical Sciences,
University of Tennessee Health Science Center.

Compound Library (totally 342,910 compounds). These 2000 compounds were selected to be "druglike" in that they adhered to Lipinski rules and were filtered from a wide variety of functional groups. Dr. Wei Li seeded the known 32 compounds in the small testing library so they could be evenly distributed through the database file. Then Dr. Seibel conducted a connectivity similarity search for lead compound LY-1-100 against the 2032 testing compound library. The small compound library was subjected to five similarity filters in parallel using the ECFP2, ECFP4, ECFC6, FCFP4, and FCFP6 property sets and Tanimoto distances using LY-1-100 as the lead structure (111-113). The top 400 compounds most similar to LY-1-100 from each of these operations were ranked by calculated similarity; then an average rank for each compound across the methods was calculated. The detailed algorithm of the search is shown in **Figure 3-2**.

3.2.2 Atom Connectivity-Based Virtual Screening

A protocol was designed within Accelrys's Pipeline Pilot in the UC Drug Discovery Center. The entire compound library was subjected to the same five similarity filters in parallel as described in the validation process. Then an average rank for each compound was also calculated. Our experience suggests that each of the property sets has some inherent strengths and weaknesses with respect to any given structure, so we used the above multiple, parallel similarity analysis to ensure that the optimal compounds by any method were not missed. The detailed algorithm of the search is shown in **Figure 3-2**.

3.2.3 Validation of Shape Similarity Search

Dr. Wei Li also tested our shape-based virtual screening using the same test database. The lead compound, LY-1-100, has a relatively rigid structure. So it has less conformer than other molecules. Therefore, Dr Li chose its lowest energy conformer at an environment of pH 7.4 as an active conformation, which is consistent with our recently reported crystal structure of LY-1-100 (110).

All structures in this database were first prepared with the Ligprep software model (Schrodinger, Inc., New York, NY). During this preparation step, hydrogen atoms were explicitly added, all possible ionization states were generated between pH 5.0 and pH 9.0 using the Ionizer module, and the 3D molecular structures were minimized with OPLS_2005 forcefield. Tautomers were also generated in this step. All structures were then subjected to shape similarity search using the Phase software module. Each structure was allowed to sample up to 100 conformers for which molecular shapes were calculated and compared with that of LY-100. Similarity scores were ranked from most similar to least similar.
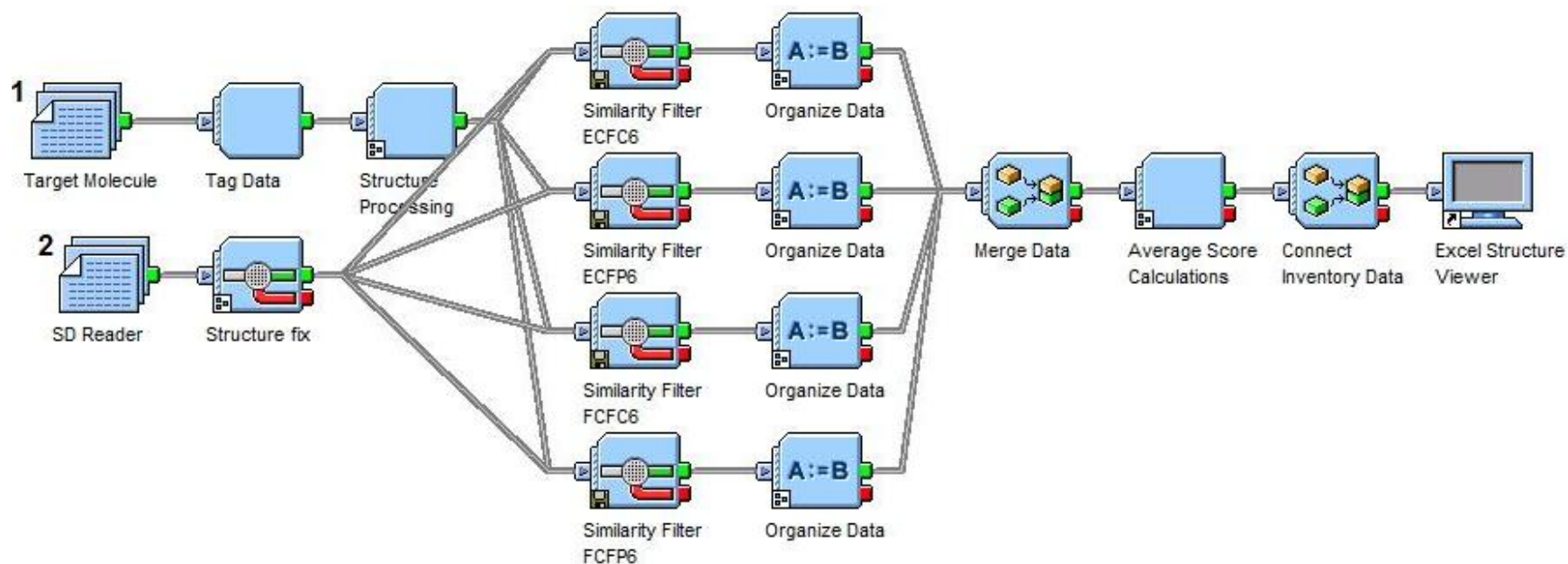
Figure 3-2. General protocol flowchart for virtual screening validation and virtual screening.
This figure was prepared by Dr. William Seibel, University of Cincinnati Drug Discovery Center, University of Cincinnati.

3.2.4 Molecular Shape-Based Virtual Screening

To make the intensive computation of shape-based virtual screening manageable for these 342,910 compounds, the database was first broken down into 17 smaller databases. Each small database contained about 20,000 molecules and was subsequently prefiltered to remove molecules containing reactive groups. Molecules in each small database were then prepared by the Ligprep software module to generate proper 3D structures with all possible ionization states between pH 5.0 and pH 9.0. Typically 30,000 to 50,000 structures were produced from this step for each database. Subsequently, 100 conformations were generated for each of the structures in the database, and the shape of each conformation was then compared to that of LY-1-100. A normalized shape similarity value was computed for each molecular conformation relative to that of LY-1-100, with 0 the most dissimilar and 1 the exact same shape. Dr. Li set the threshold for a hit as a shape similarity greater than 0.7 regardless of surface property to keep the maximum hits. All hits were ranked down from the most similar hit. These calculations were repeated for each small database for all the molecules in the original database.

3.2.5 Biological Assay and Data Processing

Hits from the two similarity searches were analyzed and their structures examined. The top hits were requested from the UC Drug Discovery Center for a subsequent two-step *in vitro* assay. The first step was a fixed drug concentration screening assay on two melanoma cell lines. Compounds that killed at least 50% of both cancer cells at 10 µM were selected for the second step, and their IC_{50} values on two melanoma cell lines and one control cell line were determined. Human malignant melanoma cells A375 and mouse melanoma cells B16-F1 were used to evaluate the compounds' *in vitro* anticancer activity. Both A375 cells and B16-F1 cells were obtained from American Type Culture Collection (Manassas, VA). All cell lines were cultured in DMEM media (Cellgro Mediatech, Inc., Herndon, VA), supplemented with 10% FBS (Cellgro Mediatech, Inc.), 1% antibiotic/antimycotic mixture (Sigma-Aldrich, Inc., St. Louis, MO), and bovine insulin (5 µg/mL; Sigma-Aldrich). Cultures were maintained at 37°C in a humidified atmosphere containing 5% CO_2.

For the initial screening step, A375 and B16-F1 cells were seeded to 96-well plates at a density of 4000~5000 cells/well, respectively. After cells adhered to the plate, media were changed and test compounds were added together with media at a fixed concentration of 10 µM in duplicate. After 48-h incubation, cell viability was evaluated by using the CellTiter 96® AQueous One Solution Cell Proliferation Assay (114). This assay is based on the bioreduction of MTS [3-(4, 5-dimethylthiazol-2-yl)-5-(3-carboxymethoxyphenyl)-2-(4-sulfophenyl)-2H-tetrazolium]. This tetrazolium dye can be converted by living cells into a colored formazan product that is soluble in tissue culture medium and, therefore, provides a sensitive readout of cell life or death that can be monitored spectroscopically. After incubating cells with compounds for 48 h, 20 µL of CellTiter 96 AQueous One Solution Reagent was pipetted into each well, which contained the samples in 100 µL of culture medium. Plates were incubated for another

1.5 h at 37°C in a humidified, 5% CO_2 atmosphere. Absorbance was recorded at 490 nm in a BioTek EL800 96-well plate reader (BioTek Instruments, Inc., Winooski, VT). Each compound's cell killing rate was normalized against a no-treatment control.

The second step was to further measure the IC_{50}s of active compounds selected from the initial step. I used the activity on fibroblast cells as a control to determine the selectivity of these compounds between cancer cells and normal cells. Human dermal fibroblast cells were purchased from Cascade Biologics, Inc., (Portland, OR) and cultured in the same condition as the two melanoma cell lines. After cells were seeded on 96-well plates, they were exposed to a wide range of eight concentrations of each compound in quadruplicate to determine the IC_{50} values. Then the CellTiter 96 AQueous One Solution Cell Proliferation Assay was used to measure cell viability. IC_{50} values were calculated by nonlinear regression analysis using GraphPad Prism (GraphPad Software, San Diego, CA) (115, 116). Each assay was repeated three times on different occasions.

3.3 Results and Discussion

3.3.1 Validation of Connectivity Similarity Search

Results from the connectivity search using the test database showed that the first 19 most similar compounds were from the 22 seeded similar compounds according to the consensus score (average rank). The lowest rank of all seeded similar compounds was 31st in the search results. The highest ranking "dissimilar" compound was ranked at 131st. This is approximately 6.5% of the way through the small 2032 compound database, making it analogous to the 22,106[th] ranked compound from the original search of the 342,910 compounds library. This validation exercise clearly showed that similar compounds are easily ranked higher than dissimilar compounds by the connectivity indices-based methods we used.

3.3.2 Connectivity Similarity Search

The connectivity searches produced a combined total of 1292 compounds. To illustrate that each property set identified somewhat different similar structures, only 13 compounds were in common among all five searches, 49 in common among four searches, and 160 in common among three searches. Results were consistent with a limited number of highly similar compounds and a fairly rapid digression to relatively low-similarity compounds. Out of these 1292 compounds, I selected the top-ranked 110 compounds, middle-ranked 110 compounds, and bottom-ranked 110 compounds to screen their activity on the two cancer cell lines: A375 and B16-F1. Our decision to select compounds from the top-, middle-, and bottom-ranked compounds was not only to ensure testing of any highly similar (and therefore likely to be active) compounds (top-ranked) but also to search for active compounds of more divergent structure (middle- and low-ranked compounds). Each of the 330 compounds was incubated with cells at a

52

concentration of 10 µM for 48 h in duplicate. Percentages of cell death induced by these compounds are shown in **Figure 3-3**. Three active compounds were identified from the 110 top-ranked compounds (UC-297549, UC-791794, and UC-791475), one active compound from the 110 middle-ranked compounds (UC-406551), and four active compounds from the 110 bottom-ranked compounds (UC-791814, UC-791792, UC-792257, and UC-193691). IC_{50} values for these active compounds were subsequently measured on A375, B16-F1, and fibroblast cells (**Table 3-1**). The best compound identified, UC-297549, had an IC_{50} value less than 1 µM on A375 cells and good selectivity between cancer cells and normal cells. Very interestingly, almost all of these compounds contained a basic terminal amine group close to an aromatic ring. This feature is different from the lead compound structure (LY-1-100), suggesting that adding a properly positioned amine group may enhance the activity of LY-1-100. Another important feature revealed from **Table 3-1** is that a basic terminal amine group may help increase selectivity. Among the identified eight active compounds, only one did not have the basic terminal amine group (UC-406551). The selectivity of this compound was worse than that of the lead compound. All other seven active compounds, which have the basic terminal amine group, had better selectivity than our lead compound. Finally, a basic terminal amine group is also expected to have the added benefit of a reduced logP value and improved water solubility.

With this in mind, Dr. Yan Lu synthesized a new analog of LY-1-100 in which an amino group was added to the para-position of the phenyl ring (compound LY-2-183H). To our great satisfaction, LY-2-183H was more active and selective than LY-1-100 was (**Table 3-1**). As expected, LY-2-183H had much better water solubility, which is an important factor for future *in vivo* animal testing. Further optimization of this structure is currently in progress.

3.3.3 Additional Analog Screening Based on Active Compounds Identified from Connectivity-Based Screening

Encouraged by the structure of the initial connectivity screening and using the same protocol as described above in combination with substructural analysis, I selected an additional 40 compounds whose structures were close to the 8 active compounds. When I tested the activity for these 40 compounds on A375 and B16-F1 cells, 4 active compounds (10% hit rate, **Figure 3-4**) were identified (UC-792247, UC-792341, UC-98514, and UC-831104). Their IC_{50} values against all three cell lines are shown in **Table 3-2**. While these four compounds were not as active as was UC-297549, they contained more structural features than LY-1-100 and may provide more opportunities for further structural modifications.

3.3.4 Validation of Shape Similarity Search

During the testing compound library preparation step, the Ligprep process generated 6767 distinct structures from the original 2032 entries. Thirty-five ionization

53

Figure 3-3. *In vitro* screening results for compounds identified from atom connectivity-based virtual screening.
Percentage of cell death resulted from compound treatment was normalized by non-treatment control. Each bar represents the average of two replications.

Cytotoxicity of Compounds in Plate 624 on A375
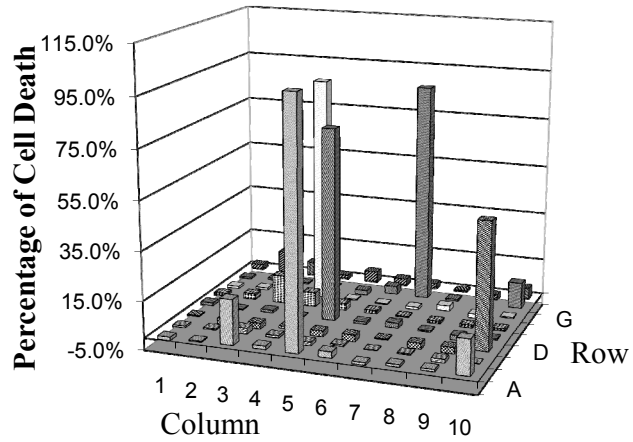
Cytotoxicity of Compounds in Plate 624 on B16-F1
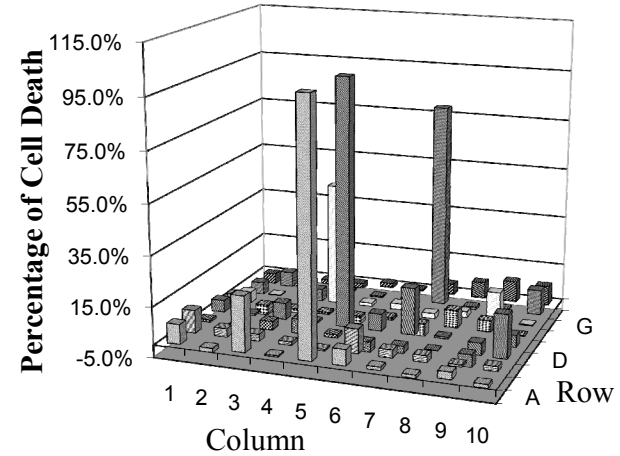
Cytotoxicity of Compounds in Plate 820 on A375
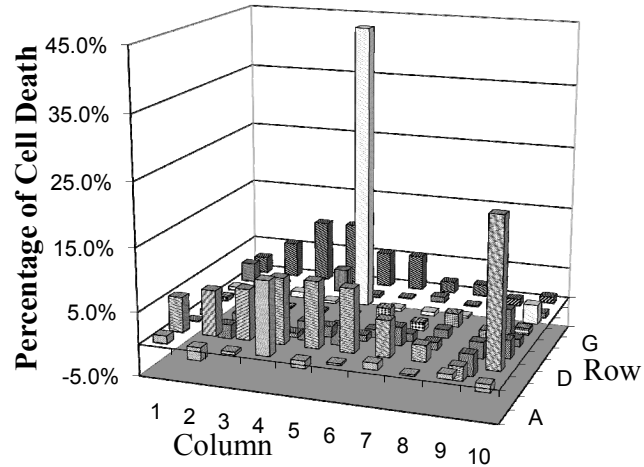
Cytotoxicity of Compounds in Plate 820 on B16-F1

55
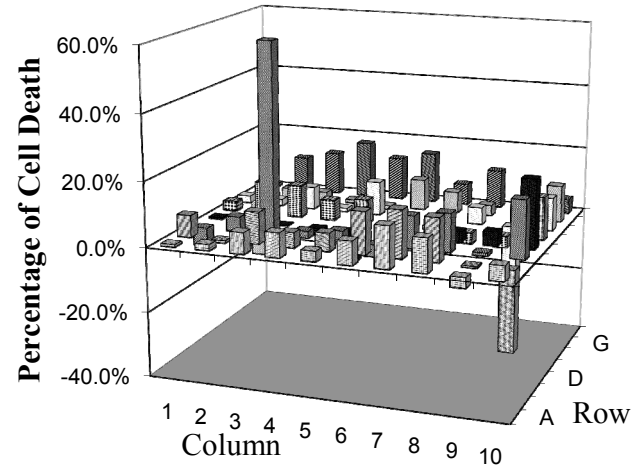
Cytotoxicity of Compounds in Plate 821 on A375
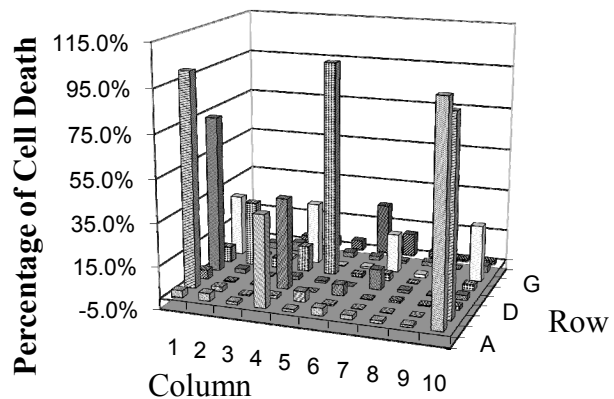
Cytotoxicity of Compounds in Plate 821 on B16-F1
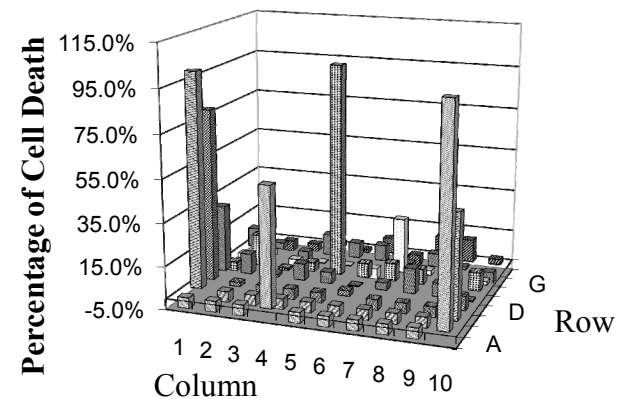
Cytotoxicity of Compounds in Plate 822 on A375
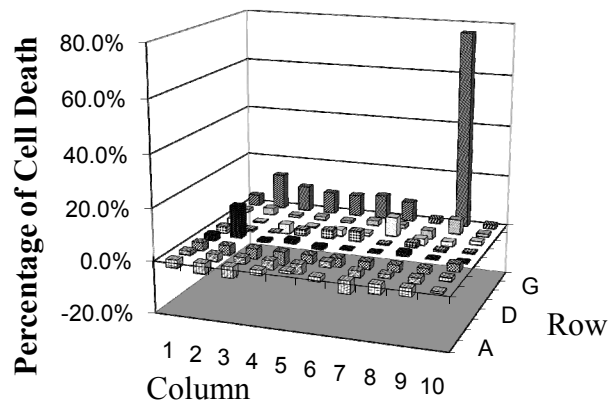
Cytotoxicity of Compounds in Plate 822 on B16-F1
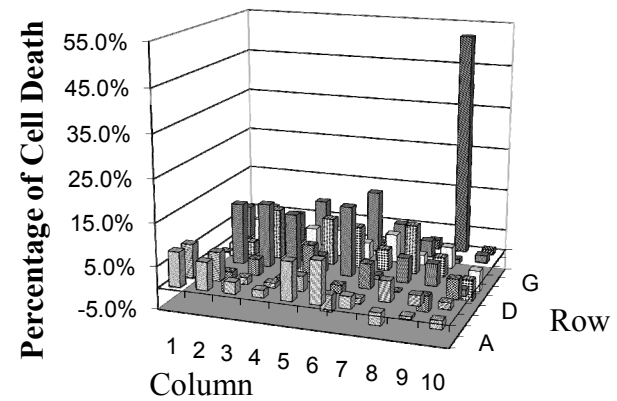
Figure 3-3. (continued)

Table 3-1. IC$_{50}$ of lead compound, eight active compounds identified from atom connectivity-based virtual screening, and newly synthesized compounds.

UC number	Structure	IC$_{50}\pm$SEM (μM) (n=3)			Selectivity*
		B16-F1	A375	HDFa	
LY-1-100 (Lead structure)		55±5 nM	28±5 nM	35±4 nM	1
297549		12±2	500±100 nM	>20	>3
791814		8±1	4±1	8±1	1
791792		9±1	6±1	10±1	1
791794		9±1	8±1	9±1	1
792257		10±1	10±1	>20	>2
791475		11±1	9±1	18±2	2
406551		11±1	14±1	4±0	0.3
193691		7±1	8±0	21±3	3
LY-2-183H		14±4 nM	11±3 nM	18±2 nM	2

*Selectivity is defined as the ratio of IC$_{50}$ on fibroblast over the IC$_{50}$ average in the two cancer cell lines.

57

Cytotoxicity of Compounds in Plate 848 on A375
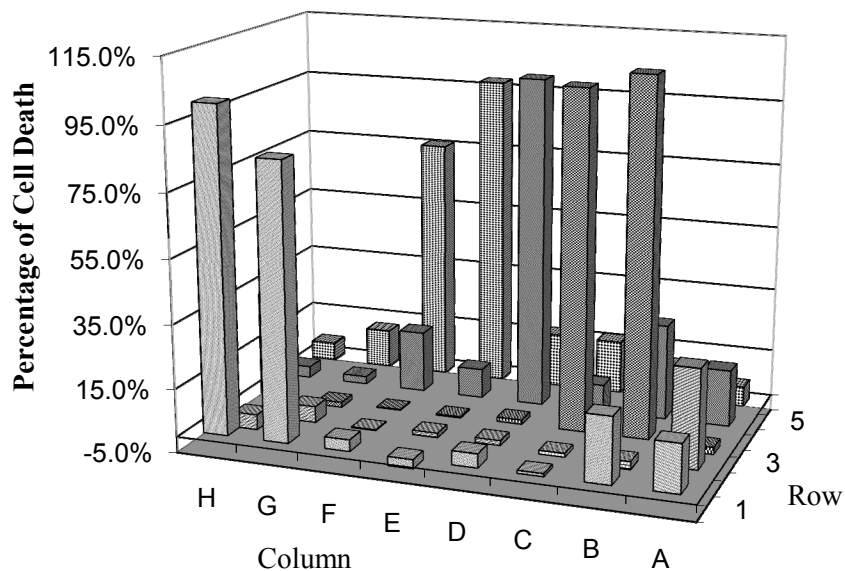
Cytotoxicity of Compounds in Plate 848 on B16-F1
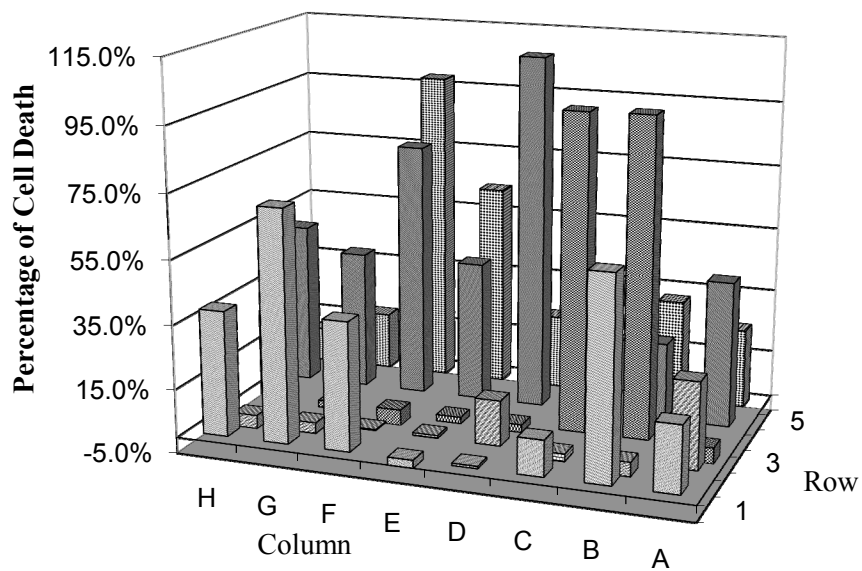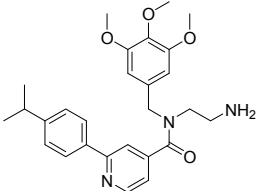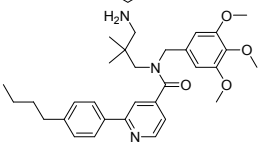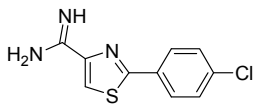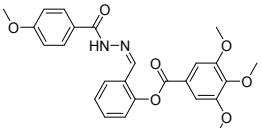
Figure 3-4. *In vitro* screening results for compounds identified from further atom connectivity similarity search based on previously identified active compounds. All compounds were tested at 10 μM concentration on A375 and B16-F1 melanoma cells. Each bar represents the average of two replications.

58

Table 3-2. IC$_{50}$ of active compounds identified from further atom connectivity similarity search based on previously identified active compounds.

UC number	Structure	IC$_{50}\pm$SEM (μM) (n=3)			Selectivity*
		B16-F1	A375	HDFa	
792247		6±1	4±0	11±1	2
792341		6±1	3±0	10±2	2
98514		3±0	300±100 nM	6±0	4
831104		3±0	3±1	6±1	2

*Selectivity is defined as the ratio of IC$_{50}$ on fibroblast over the IC$_{50}$ average in the two cancer cell lines.

59

states were generated for the 32 seeded molecules, including 24 similar structures (protonated and unprotonated forms for both LY-2-103 and LY-2-84), and 11 dissimilar structures (**Figure 3-5**, seeded similar structures are highlighted in yellow, and dissimilar structures are highlighted in red). Validation search results for the seeded structures are listed in **Figure 3-5**. From these results, I can see that the top 26 entries from this search contained 20 of the 24 seeded similar structures (86% similar structures from 0.35% of total database). The four remaining similar structures ranked at 107, 255, 281, and 1508. Twenty-three out of 24 (96%) similar structures were found within the 4.2% of the total structures in this sample database. The saturated thiazole ring and the amide bond in LY-2-74 are responsible for its low similarity ranking of 1508, when compared with the molecular shape of LY-100 (**Figure 3-1**). This structure also showed the worst similarity rank in the connectivity-based similarity search (rank 31st). In contrast, the ranks for the 10 dissimilar structures spanned from 332 to 6712 out of the 6767 structures. In summary, I found that this shape similarity search approach could identify similar compounds, which provides reasonable validation for screening the entire database.

3.3.5 Shape Similarity Search

The classical concept of lock and key interaction between a receptor and its ligand indicates that molecular shape is a critical factor for high binding affinity. Similarities in connectivity and molecular shape have overlap but also have their own individual spaces. To explore potentially new platforms based on the molecular shape of LY-1-100, Dr. Li performed shape similarity searches against this database. These searches produced a little over 5000 structures that had a similarity score larger than 0.7 and did not contain any reactive groups. I selected the 88 top-ranked compounds and performed an initial single concentration screening (**Figure 3-6**). Two active compounds (UC-521092 and UC-398535), which are very close analogs, were identified, and their IC_{50}s are shown in **Table 3-3**. The tight criterion (similarity score must be at least 0.7) was likely responsible for limiting greater variations for identified structures.

Although still not as active as LY-1-100, these two compounds were more potent than compounds identified from connectivity-based virtual screening, with IC_{50} values in the nanomolar range. One important hint revealed from this search was that a properly constructed amide linkage between the five-member ring and the trimethoxyphenyl ring may be very beneficial to anticancer activity. Previously, Dr. Lu made one compound (LY-2-30) containing an amide bond that was not active. Based on results of this screening, Dr. Lu prepared another analog in which the direction of the amide bond was reversed to directly connect the carbonyl group to the trimethoxyphenyl ring (LY-2-173b-OTs). The activity of this compound was greatly improved (**Table 3-3**).

The high activity of compounds identified from this shape similarity search likely resulted from the very close structural features to LY-1-100. Obviously, this similarity also limited their structural variations; therefore, a dramatically different scaffold from LY-1-100 will be difficult to obtain. Hence, at least for this database, shape similarity search will not provide completely new molecular structures. On the other hand,

60

Figure 3-5. Seeded structures in validation testing library with shape similarity ranks. Seeded similar structures are highlighted in yellow. Dissimilar structures are highlighted in red.
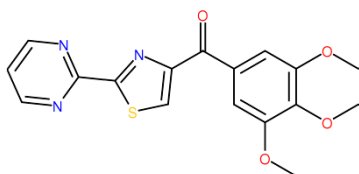
TN Name: LY-2-122
title: 855555
Shape Sim: 0.956346823882
entry id: 8910
Similarity Rank: 1
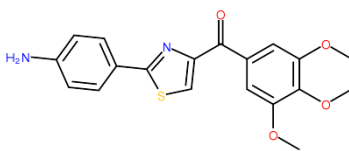
TN Name: LY-2-183
title: 735555
Shape Sim: 0.95250193819
entry id: 8911
Similarity Rank: 2
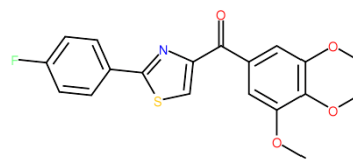
TN Name: LY-2-45
title: 615555
Shape Sim: 0.952469090673
entry id: 8912
Similarity Rank: 3
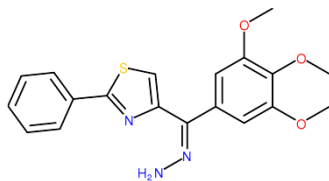
TN Name: LY-2-176A
title: 525555
Shape Sim: 0.942492900121
entry id: 8913
Similarity Rank: 4
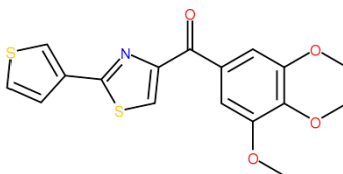
TN Name: LY-2-105
title: 795555
Shape Sim: 0.940105637529
entry id: 8914
Similarity Rank: 5
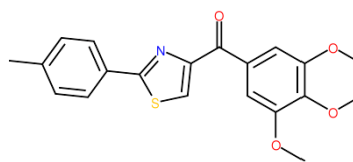
TN Name: LY-2-104
title: 645555
Shape Sim: 0.937374050216
entry id: 8915
Similarity Rank: 6
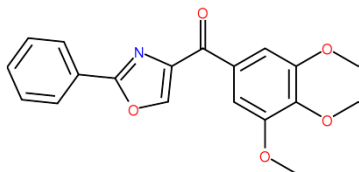
TN Name: LY-2-163
title: 885555
Shape Sim: 0.93486642428
entry id: 8916
Similarity Rank: 7
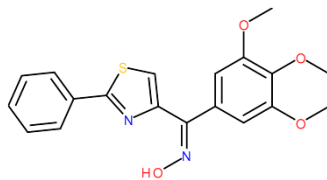
TN Name: LY-2-173A
title: 495555
Shape Sim: 0.897033632287
entry id: 8917
Similarity Rank: 8
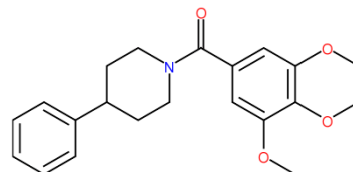
TN Name: LY-2-194
title: 945555
Shape Sim: 0.891212697874
entry id: 8918
Similarity Rank: 9
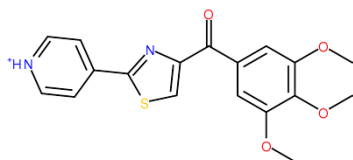
TN Name: LY-2-84
title: 825555
Shape Sim: 0.967433373886
entry id: 8909
Similarity Rank: 10
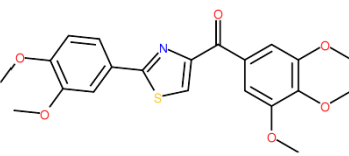
TN Name: LY-2-52
title: 765555
Shape Sim: 0.885174367947
entry id: 8919
Similarity Rank: 11
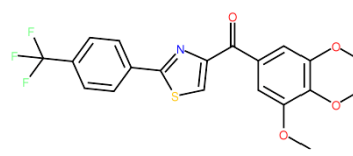
TN Name: LY-2-170
title: 675555
Shape Sim: 0.875733013519
entry id: 8920
Similarity Rank: 12
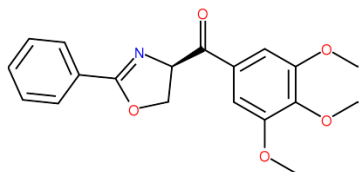
TN Name: LY-2-165
title: 915555
Shape Sim: 0.87418013741
entry id: 8921
Similarity Rank: 13
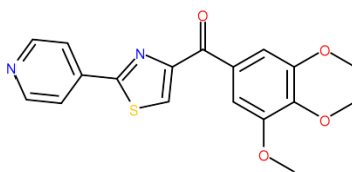
TN Name: LY-2-84
title: 825555
Shape Sim: 0.874107443087
entry id: 8922
Similarity Rank: 14
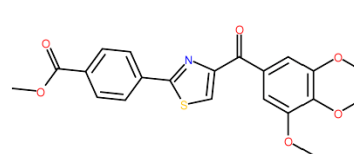
TN Name: LY-2-149
title: 705555
Shape Sim: 0.858375632951
entry id: 8923
Similarity Rank: 15
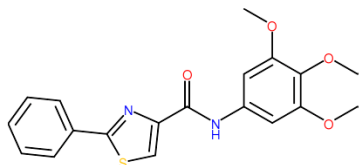
TN Name: LY-2-30
title: 555555
Shape Sim: 0.835902713766
entry id: 8925
Similarity Rank: 17
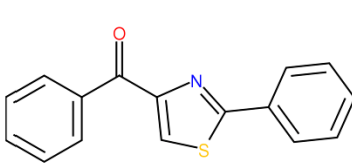
TN Name: LY-2-97
title: 975555
Shape Sim: 0.823240844522
entry id: 8927
Similarity Rank: 19
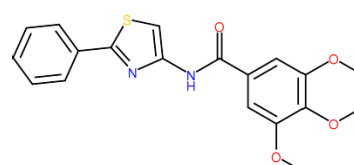
TN Name: LY-2-173b-OTs
title: 585555
Shape Sim: 0.820563760383
entry id: 8928
Similarity Rank: 20
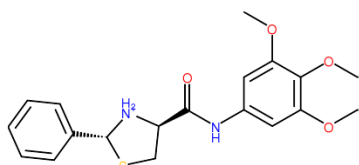
TN Name: LY-2-72
title: 435555
Shape Sim: 0.819756876003
entry id: 8929
Similarity Rank: 21
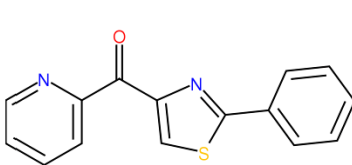
TN Name: LY-2-103
title: 1005555
Shape Sim: 0.813796386954
entry id: 8934
Similarity Rank: 26
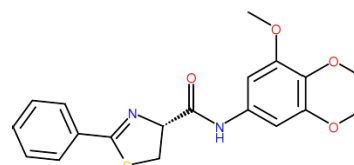
TN Name: LY-2-28
title: 1035555
Shape Sim: 0.770542448596
entry id: 9015
Similarity Rank: 107
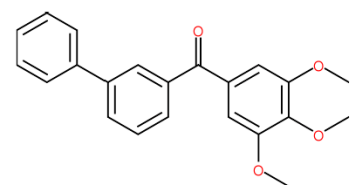
TN Name: LY-2-127
title: 405555
Shape Sim: 0.748903854875
entry id: 9163
Similarity Rank: 255
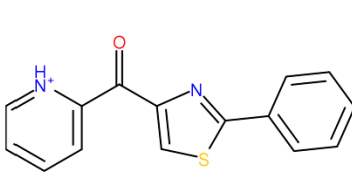
TN Name: LY-2-103
title: 1005555
Shape Sim: 0.746101642039
entry id: 9189
Similarity Rank: 281
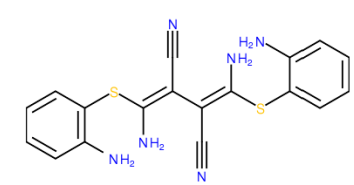
TN Name: 10 other 9
title: 345555
Shape Sim: 0.74109407726
entry id: 9240
Similarity Rank: 332

Figure 3-5. (continued)
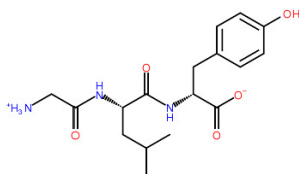
TN Name: 10 other 4
title: 195555
Shape Sim: 0.700579174062
entry id: 9820
Similarity Rank: 912
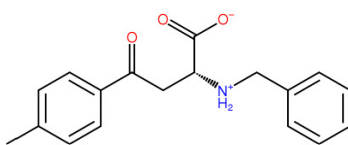
TN Name: 10 other 5
title: 225555
Shape Sim: 0.698131477844
entry id: 9874
Similarity Rank: 966
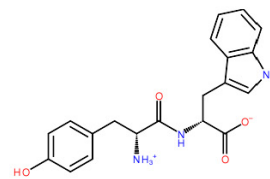
TN Name: 10 other 3
title: 165555
Shape Sim: 0.684318135541
entry id: 10152
Similarity Rank: 1244
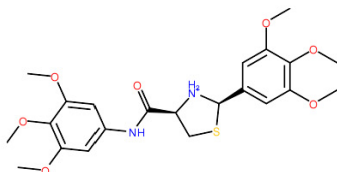
TN Name: LY-2-74
title: 465555
Shape Sim: 0.671585257095
entry id: 10416
Similarity Rank: 1508
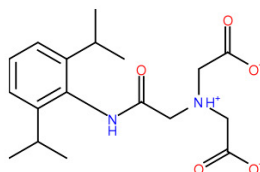
TN Name: 10 other 1
title: 105555
Shape Sim: 0.669602313836
entry id: 10458
Similarity Rank: 1550
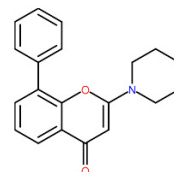
TN Name: 10 other 8
title: 315555
Shape Sim: 0.660778872054
entry id: 10673
Similarity Rank: 1765
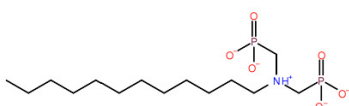
TN Name: 10 other 2
title: 135555
Shape Sim: 0.608588254613
entry id: 12307
Similarity Rank: 3399
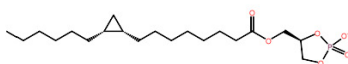
TN Name: 10 other 6
title: 255555
Shape Sim: 0.603004968174
entry id: 12507
Similarity Rank: 3599
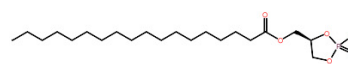
TN Name: 10 other 7
title: 285555
Shape Sim: 0.581513223034
entry id: 13258
Similarity Rank: 4350
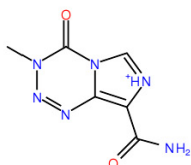
TN Name: 10 other 10
title: 375555
Shape Sim: 0.432871122727
entry id: 15613
Similarity Rank: 6705
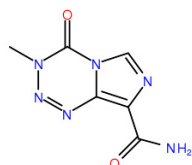
TN Name: 10 other 10
title: 375555
Shape Sim: 0.4287030282
entry id: 15620
Similarity Rank: 6712

Figure 3-5. (continued)

64

Cytotoxicity of Compounds in Plate 561 on A375
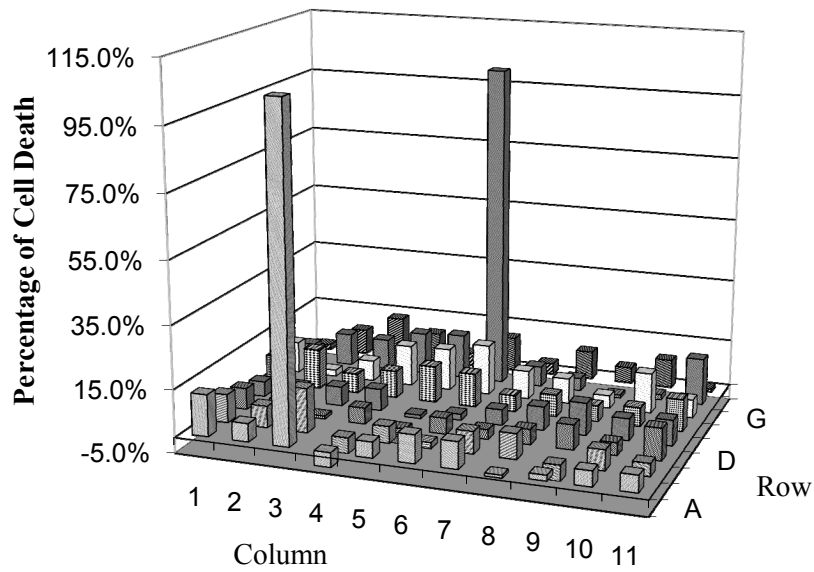
Cytotoxicity of Compounds in Plate 561 on B16-F1
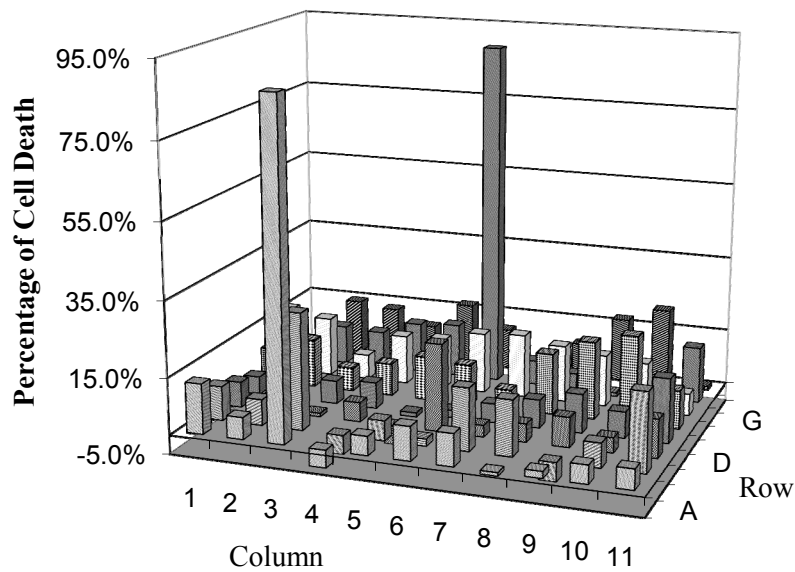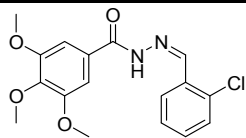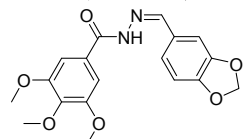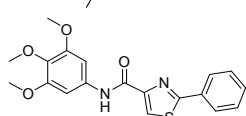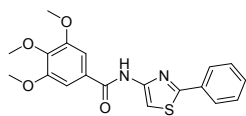
Figure 3-6. *In vitro* screening results for compounds identified from molecular shape-based virtual screening.

65

Table 3-3. IC$_{50}$ of active compounds identified from a shape similarity search, one inactive compound, and one newly synthesized compound based on the information get from shape similarity search.

UC number	Structure	IC$_{50} \pm$SEM (μM) (n=3)			Selectivity*
		B16-F1	A375	HDFa	
521092		800±200 nM	200±100 nM	300±100 nM	1
398535		2±1	400±100 nM	400±200 nM	0.3
LY-2-30		>100	>100	>100	N/A
LY-2-173b-OTs		19±2	7±1	53±4	4

*Selectivity is defined as the ratio of IC$_{50}$ on fibroblast over the IC$_{50}$ average in the two cancer cell lines.

depending on the criteria of the connectivity search, completely novel structural features and new molecular platforms could be identified, but loss of activity may be expected. These two approaches are therefore highly complementary.

3.3.6 Comparison of Two Similarity Search Methods

Generally speaking, the connectivity similarity search gave us more diverse structure scaffolds that are bioactive than did the shape similarity search. For example, I got eight bioactive compounds in the first round of whole-library connectivity similarity search and four bioactive compounds in the further search. I obtained highly varied scaffolds such as compound UC193691, in which I found the lead compound trimethoxyphenyl ring replaced by an isothiourea group; in compound UC98514, I found the lead compound phenyl right replaced by the amidine group. But in the shape similarity search, I only got two bioactive compounds, and they both shared very close features with the lead compound. On the other hand, the shape similarity search gave us more bioactive compounds than did the connectivity search. The two hits from the shape similarity search had IC_{50} values on melanoma cell lines in the nanomolar range, while hits from the connectivity search were mostly in the micromolar range. The reason for this difference was largely to the result of the inherent algorithm difference of these two screening approaches.

We did not choose receptor-based virtual screening because we did not confirm the target for this new class compounds at the initial stage. Later mechanism of action studies revealed that the target is the tubulin colchicine binding site.

3.4 Conclusions

Using both connectivity- and shape similarity-based virtual screening against a large database, I identified 14 new molecules from the UC compound library that are active against melanoma cells. These molecules provide several new functional groups and structure features compared with the lead structure. In summary, the novel pharmacophoric elements identified through these virtual screening exercises include a) a terminal basic amine group can improve activity and selectivity; b) a properly constructed amide linker between the five-member ring and the trimethoxyphenyl ring is beneficial to bioactivity; c) the thiazole ring in the lead compound is not necessary for bioactivity, and it can be replaced with an N-methylene hydrazine linker; d) an isothiourea group can replace the lead compound trimethoxyphenyl ring; and e) an amidine group can replace the phenyl ring of the lead compound.

This information is helpful for understanding the structure-activity relationship and for further improving compound activity. While the shape similarity search did not provide diverse active structures, the active compounds identified were generally much more active than those identified by the connectivity search. Combining both connectivity and shape similarity search techniques was complementary for our ligand-

based drug discovery efforts. Further modification of the lead compound is in progress based on the information obtained from these virtual screenings.

CHAPTER 4. DISCOVERY AND BIO-EVALUATION OF 4-SUBSTITUTED METHOXYBENZOYL-ARYL-THIAZOLE AS NOVEL ANTI-MELANOMA AGENTS*

4.1 Introduction

Microtubule is composed of α- and β-tubulin dimmer, which plays an important role in cell mitosis, motility and organelle distribution (117). The formation of microtubule from tubulin is a dynamic process that involves the polymerization and depolymerization of α- and β-heterodimer. These dynamic behaviors are crucial to cell mitosis, which is the process of chromosomal division to form new cells (118). Interference with tubulin-microtubule dynamics may be one of the attractive potential strategies in developing an anticancer drug (119, 120). There are some antitubulin agents developed with great potency, which may achieve low nano-molar range in the inhibition of cell proliferation by inducing cell cycle to be arrested in G2/M phase and subsequently the inhibition of cell division (121, 122).

Tubulin heterodimer has three major known pharmacologic sites, including taxane, vinca, and colchicine site. Vinca and colchicine domain ligands destabilize and inhibit microtubule formation. Taxane–site agents stabilize and promote the formation of microtubules, having the opposite effects of vinca and colchicine domain ligands. Some of the antitubulin agents have been successfully developed for clinical use, such as paclitaxel on taxane domain, and vincristine, vinorelbine, vinblastine on vinca domain. However, they are substrates of P-glycoprotein and have drug resistance issues (123, 124). Although no clinical application colchicine-domain binding drugs yet, there are some agents which are on the phase I or II stage of development (125, 126). To address the drug resistance of antitubulin agents for each binding-domain, many new generation antitubulin agents are developed to overcome the issue caused by over expression of P-glycoprotein and/or the MDR1 (127-130).

I have been actively engaged in searching novel anticancer agents that target on tubulin. More recently, a series of 4-Substituted Methoxylbenzoyl-Aryl-Thiazole (SMART) has been developed in our laboratory (100). This series compounds was developed from 2-aryl-thiazolidine-4-carboxylic acid amides (ATCAA) which I discussed in chapter 2. SAR studies of ATCAA indicated that replacement of the lipid chain with a bulky aromatic ring in the 4-amide position of ATCAA attached to the thiazolidine ring still kept the anti-proliferative activity. This finding afforded us a new point to replace the fatty amide chain with a number of aromatic groups, which would maintain the cytotoxicity. With further investigation of ATCAA analogues, structure modifications were made on thiazolidine ring and 4-carboxylic amide linker. Thus, substituted methoxylbenzoyl-aryl-thiazole (SMART) compounds were discovered.

The general structure of SMART agents with as showed in **Figure 4-1**. The SMART agents have a structure containing three conjugated aromatic rings (A, B and C rings, respectively) with a ketone linkage between B and C rings. Thiazole was introduced in B ring instead of thiazolidine ring in ATCAA. The linker between B and C rings was modified from an amide to carbonyl group. The C ring was characterized by the presence of differently-substituted phenyl groups, in particular, the 3, 4, 5-trimethoxy substituted phenyl at C ring played an important role of antiproliferative activity against melanoma.

According to the study, I characterized the biologic effect using three representative SMART compounds: SMART-100, SMART-45, and SMART-211. SMART-100 and SMART-45 are the most potent SMART compounds in our laboratory; however, they exhibit poor solubility. SMART-211 was synthesized to increase solubility by adding a hydroxyl- group on the A-ring, and it still remained potent cytotoxicity with IC_{50} value of 120 nM on several melanoma cell lines. I examined these SMARTs on cell proliferation in a variety of cancer cell lines including MDR-positive cell lines and summarized the SAR. I determined the binding site to tubulin, the ability of inhibition on tubulin polymerization. Together with Mr. Chien-ming Li, I determined pharmacokinetic parameters on mice, and developed a formulation for the improvement of the poor solubility of SMARTs. I also examined the anticancer efficacy using nude mice bearing human melanoma A375 xenograft.

4.2 Materials and Methods

4.2.1 Compounds and Reagents

All the SMART compounds were synthesized by Dr. Yan Lu. Paclitaxel, vinblast-ine, and colchicine were obtained from Sigma-Aldrich. Ethanol was obtained from Decon labs, Inc. Cremophor ELP was obtained from BASF, Inc. CellTiter 96® AQueous One Solution Reagent was obtained from Promega.

4.2.2 Cell Culture and Cytotoxicity Assay

The A375 and B16-F1 melanoma cancer cells were obtained from American Type Culture Collection (Manassas, VA). WM-164 cells were derived from patient metastatic melanoma tumors and were a gift from Dr. Meenhar Herlyn (Wistar Institute, Philadelphia, PA). Human Dermal Fibroblast (adult) cells (HDFa) were obtained from Cascade Biologics. This cell line was used as control to determine selectivity. The P-gp overexpressing multi-drug resistant cell line MDA-MB-435/LCC6MDRI and matching sensitive parent cell line were kindly provided by Dr. Robert Clarke (Georgetown University, Washington, DC). Cells were grown as monolayers by using standard cell culture conditions. All cells were cultured in DMEM (Mediatech, Inc., Manassas, VA), supplemented with 10% FBS (Atlanta Biologicals, Lawrenceville, GA), 1%

LPA
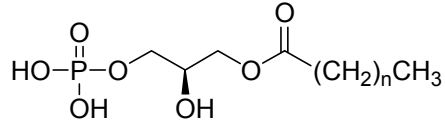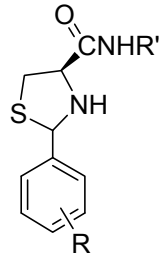
ATCAA
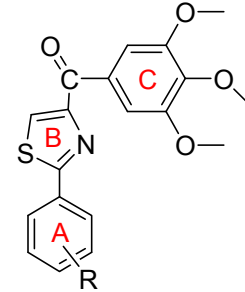
Fatty chain series, ATCAA-1:
R= 4-NHCOCH$_3$, R'=n-C$_{16}$H$_{33}$

Aromatic ring series, ATCAA-2:
R= 4-NHCOCH$_3$, R'=
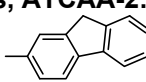
SMART

R = 4-H, SMART-100

R= 4-F, SMART-45

R= 4-OH, SMART-211

Figure 4-1. Structures of LPA, ATCAA and SMART.

71

antibiotic/antimycotic mixture (Sigma-Aldrich, St. Louis, MO), and bovine insulin (5 µg/mL) (Sigma-Aldrich, St. Louis, MO).

Cultures were maintained at 37°C in a humidified atmosphere containing 5% CO_2. 1000 to 5000 cells were plated into each well of 96-well plates depending on growth rate and exposed to different concentrations of a test compound for 48 h in three to five replicates. Cell numbers at the end of the drug treatment were measured by the MTS assay. Absorbance was recorded at 490 nm in a BioTek EL800 96-well plate reader (BioTek Instruments, Inc., Winooski, VT). Percentages of cell survival versus drug concentrations were plotted and the IC_{50} (concentration that inhibited cell growth by 50% of untreated control) values were obtained by nonlinear regression analysis using GraphPad Prism (GraphPad Software, San Diego, CA).

4.2.3 Cell Cycle Analysis

Flow cytometry was performed to study cell cycle phase distribution. A375 cells were cultured in growth media until the confluence was about 70%, and then cells were starved in 0.5% charcoal-stripped serum (CS-FBS) for 48 h before the experiment. A375 then were treated with 0, 10, 50, 200, and 1000 nM of SMART-100, -45, and -211 for 24 h in growth media. The cellular DNA was stained with PBS containing 100 µg/mL propidium iodide, and 100 µg/mL RNase A. Flow cytometry assay was used to determine the distribution of a population of cells to different stages of cell cycle.

4.2.4 *In Vitro* Microtubule Polymerization Assay

Bovine brain tubulin (0.4 mg) (Cytoskeleton, Denver, CO) was mixed with 10 µM of test compound and incubated in 120 µL of general tubulin buffer (80 mM PIPES, 2.0 mM $MgCl_2$, 0.5 mM EGTA, pH 6.9 and 1 mM GTP). The absorbance of wavelength at 340 nm was monitored every 60s for 20 min by the SYNERGY 4 Microplate Reader (Bio-Tek Instruments, Winooski, VT). The spectrophotometer was set at 37°C for tubulin polymerization.

4.2.5 Tubulin Colchicine Competition Assay

[3H]colchicine competition-binding scintillation proximity assay (SPA) (Cytoskeleton Inc, Denver, CO) was used to evaluate SMART compounds that bind to the colchicine binding site on tubulin. Biotin-labeled tubulin (0.5 µg) was mixed with [3H]colchicine (0.08 µM) (Perkinelmer LLC., Shelton, CT) and varies concentrations of SMARTs. Streptavidin-labeled SPA beads (80 µg) (GE-healthcare Bio-Sciences Corp., Piscataway, NJ) are added, and co-incubated in 200 µL binding buffer [80 mM PIPES (pH 6.8), 1 mM EGTA, 10% glycerol, 1 mM $MgCl_2$, and 1 mM GTP] for 45 min at 37°C. IC_{50} values (concentrations that inhibited 50% of tritiated colchicine binding) were

determined by nonlinear regression analysis with GraphPad Prism (GraphPad Software, San Diego,CA).

4.2.6 Microtubule Imaging Using Fluorescence Microscope

In order to get a visually appreciable proof of SMART compounds interacting with tubulin inside the cells, I examined microtubule arrangement in human melanoma WM-164 cells upon treatment with different compounds. I selected the Cellomics Cytoskeleton rearrangement kit (Thermo Scientific, Rockford, IL) which is widely used for such studies and followed the instructions from the manufacturer. WM-164 Melanoma cells were treated with each compound for 18 h in duplicate using a collagen-coated 96-well plate (Becton Dickinson Labware, Bedford, MA). Then cells were fixed with 4% paraformaldehyde (Thermo Scientific, Rockford, IL) and permeabillized using permeabilization buffer supply from the kit. Primary antibody for tubulin and fluorescence labeled secondary antibody were subsequently added to the cells. Cell nuclei were stained by DAPI. Whole Cell Stain Green was also applied to all cells. All images were acquired with an Olympus IX71 inverted fluorescence microscope (Olympus Corporation, Tokyo, Japan) with overlays from separate images of tubulin (red), nuclei (blue) and whole cells (green). For comparison, I also included paclitaxel, colchicine along with SMART compound.

4.2.7 Pharmacokinetic Studies in Mice

Male ICR mice 6 to 8 weeks of age were used to perform pharmacokinetic study. Drug solutions were dissolved in DMSO/PEG300 (80/20) and administrated by a single i.v. injection into the tail vein. For SMART-100, 5 and 15 mg/kg of body weight were administrated. For SMART-45, 15 mg/kg of body weight was administrated. Blood samples were obtained via cardiac puncture under isoflurane anesthesia at 2, 5, 15, and 30 min, 1, 2, 4, 8, 16, and 24 h after administration, using 3-4 animals per group. Sodium heparin (5 µL of 1,000 USP units/mL per sample) was used as an anticoagulant. Blood samples were collected on ice, and separated by centrifuging at 3000g for 10 min to obtain plasma. All samples were stored at -20ºC until analysis.

Protein precipitation method was used for sample preparation. Plasma samples were thawed at room temperature.150 µL of acetonitrile (ACN) containing an internal standard, a SMART analog, was added to 100 µL of plasma sample, and then was thoroughly vortexed for 15 s. After centrifugation at 14,000 RPM for 10 min at 4°C, the supernatant was transferred into high-performance liquid chromatography vials and directly used for LC-MS/MS analysis.

Plasma concentration-time data were analyzed by non-compartmental analysis using WinNonlin 5.2 (Pharsight Corporation, Mountain View, CA). The area under the plasma concentration-time curve from time 0 to infinity (AUC_{inf}) was calculated by the trapezoidal rule with extrapolation to time infinity. The terminal half-life ($t_{1/2}$) was

73

calculated as $0.693/\lambda_z$, where λ_z is the terminal phase rate constant. The plasma clearance (CL) was calculated using the equation $CL=Dose_{iv}/AUC_{inf,\ iv}$, where $Dose_{iv}$ and $AUC_{inf,\ iv}$ are the IV dose and corresponding area under the plasma concentration-time curve from time 0 to infinity, respectively. Volume of distribution based on terminal phase (V_z) was calculated using $V_z=Dose_{iv}/(\lambda_z*AUC_{inf,\ iv})$. The peak plasma concentration (C_{max}) and the time when it occurred (t_{max}) in the IP group were obtained by visual inspection of the plasma concentration-time curves. Clearance after IP (CL/F) was calculated as $Dose_{ip}/AUC_{inf,\ ip}$. Volume of distribution after IP (V_z/F) was calculated as $Dose_{ip}/(\lambda_z*AUC_{inf,\ ip})$. IP bioavailability (F) was calculated using $F=(AUC_{inf,ip}*Dose_{iv})/(AUC_{inf,\ iv}*Dose_{ip})$, where $Dose_{ip}$, $Dose_{iv}$, $AUC_{inf,\ iv}$, and $AUC_{inf,\ ip}$ are the IP and IV dose and the corresponding areas under the plasma concentration-time curves from time 0 to infinity, respectively.

4.2.8 LC-MS/MS Method for Measuring SMART Compounds

Sample solution (10 µL) was injected into an Agilent series HPLC system (Agilent 1100 Series Agilent 1100 Chemstation, Agilent Technology Co, Ltd). SMART-100 and SMART-45 were separated on a narrow-bore C4 column (Varian Inc, 2.1×150 mm, 5 µm, Palo Alto, CA). Gradient mode was used to achieve the separation of analytes using mixtures of mobile phase A (5% acetonitrile containing 0.1% formic acid) and mobile phase B (95% acetonitrile containing 0.1% formic acid) at a flow rate of 300 µL/min. Mobile phase A was used at 100% from 0 to 1 min followed by a linearly programmed gradient to 100% of mobile phase B within 3 min, 100% of mobile phase B was maintained for 1 min before a quick ramp to 100% mobile phase A. Mobile phase A was continued for another 8 min towards the end of analysis.

A triple-quadruple mass spectrometer, API Qtrap[TM] (Applied Biosystems/MDS SCIEX, Concord, Ontario, Canada), operating with a TurboIonSpray source was used. SMART-100 and SMART-45 were infused into the mass spectrometer at 1 mg/L and 10 µL/min to optimize the instrument parameters used for LC-MS/MS. The Q1 full scan spectrums of SMART-100 and SMART-45 were first obtained to identify $[M+H]^+$ ion as the precursor ion to generate product ion scans for selecting the most distinctive precursor-product ion pair. For the most sensitive quantitative analysis, the mass spectrometer was operated in the multiple reaction monitoring (MRM) mode, which includes m/z 356.2→ 188.2 for SMART-100, 374.2→ 206.2 for SMART-45, and m/z 434.0 → 266.0 for an internal standard, which is analog of SMART compound. Dwelling time was set to 100 ms for each analyst, and 50 ms for the internal standard. Detection limit is 0.2 ng/mL for SMART-45, -100, and -211.

The spraying needle voltage was set at 5000 V for positive mode. Curtain gas was set at 10; Gas 1 and gas 2 were set at 50. Collision-Assisted-Dissociation (CAD) gas at medium, and the source heater probe temperature at 500°C. DP, EP, CXE were set at 16, 10, and 15 V, respectively. Data acquisition and quantitative processing were accomplished using Analyst[TM] software, Ver. 4.0 (Applied Biosystems).

4.2.9 Antitumor Efficacy on A375 Xenografted Athymic Nude Mice

A375 cells (5×10^7/mL) were prepared in phenyl red free DMEM media containing 10% FBS, and mixed with 1:1 of Matrigel (BD Biosciences, San Jose, CA). Tumors were established by injection 100 μL of mixture (2.5×10^6 cells per animal, s.c. into low flank of mice) to 6-8-week-old male athymic nude mice. Treatments were initiated when tumor reached a mean group size of 150 mm^3. Tumor volume (mm^3) was measured with calipers and determined by the formula, $\pi/6 \times L \times W^2$, where length (L) and width (W) are in mm. The formulation of Tween80/Captex200 (80/20) were used to prepare SMART-100 (20 mg/kg), and SMART-45 (15 mg/kg). Mice were administrated by i.p. daily for 34 days (10 mice per group).

4.3 Results and Discussion

I studied the structure-activity relationship (SAR) in our laboratory and selected three potent SMARTs to perform the mechanism of action. SMART-100 has no substitution on the A-ring. SMART-45 and SMART-211 have fluorine (-F) and hydroxy (-OH) on the A-ring, respectively. SMART-45 and -100 have poor solubility; however, SMART-211 is a water-soluble compound. The effects of SMART-100, -45, and -211 on the proliferation of melanoma cancer cells (B16-F1, A375, and WM-164) and normal fibroblast cells are summarized in **Table 4-1**. SMARTs inhibit the proliferation of prostate and melanoma cancer cells with IC$_{50}$ values in the low nano-molar range. Overall, the potency of SMART-45 is similar to SMART-100, and greater than SMART-211.

4.3.1 SAR Studies
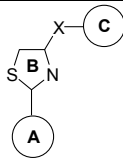
4.3.1.1 SAR of the B Ring

Please see **Figure 4-1** for the designation of A, B, and C ring of SMART compounds. In the previous ATCAA compounds, I found the thiazolidine ring, which contained a free NH at its 3-position, was important for cytotoxicity. Once the B ring thiazolidine moiety was replaced by a thiazoline ring, the antiproliferative activity decreased sharply from 600 nM to over 50 μM on WM-164 cell lines (83). The ATCAA-1 fatty amide derivatives that were most effective against melanoma cell lines were examined and shown to have an IC$_{50}$ 2 μM (**Table 4-2**). Replacement of the long fatty chain with a certain aromatic bulky subsistent such as fluorene (ATCAA-2) showed inhibitory activity on both cancer cell lines (IC$_{50}$=2~4 μM). The fluorene group in 4-carboxylic amide position was also replaced by 3, 4, 5-trimethoxylphenyl group (2a and 2b), but the potency against both cancer cell lines was lost. The subsequent B ring modification from saturated thiazolidine compound 2a to unsaturated thiazole 5 did not show any cytotoxicity against either cancer cell line tested. But thiazoline enantiomers 4a and 4b (*R*-isomer and *S*-isomer, showed similar antiproliferative activities) showed

75

Table 4-1. Cytotoxic activity comparison of representative SMART compounds with other anticancer drugs.

Compound name	IC$_{50}$±SEM (nM) (n=3)			
	A375	B16-F1	WM-164	HDFa
SMART-100	28±5	55±5	64±6	40±5
SMART-45	29±11	43±21	41±6	40±7
SMART-211	93±11	113±6	99±10	289±92
Paclitaxel	12±3	17±2	18±3	12±3
Vinblastine	1±0	5±1	1±0	3±1
Colchicine	20±3	29±5	10±2	18±2
Bortezomib	8±1	24±2	8±1	26±2

Table 4-2. *In vitro* cytotoxic activity of modified ATCAA compounds.

	A ring	B ring[a]	C ring[b]	X	IC$_{50}$±SEM (μM) (n=3)	
					B16-F1	A375
ATCAA-1	*p*-NHAc-Ph	TZD	C$_{16}$H$_{33}$	CONH	2±0	2±0
ATCAA-2	*p*-NHAc-Ph	TZD	9H-fluoren-1-yl	CONH	4±0	2±0
2a	Ph	TZD	3,4,5-trimethoxyl-Ph	CONH	>100	>100
2b	3,4,5-trimethoxyPh	TZD	3,4,5-trimethoxyl-Ph	CONH	>100	>100
4a*(4R)*	Ph	TZL	3,4,5-trimethoxyl-Ph	CONH	38±3	23±2
4b*(4S)*	Ph	TZL	3,4,5-trimethoxyl-Ph	CONH	30±3	14±1
5	Ph	TZ	3,4,5-trimethoxyl-Ph	CONH	>100	>100
8f	Ph	TZ	3,4,5-trimethoxyl-Ph	CO	55±5 nM	28±5 nM
Colchicine					29±5 nM	20±3 nM

[a]TZD=thiazolidine, TZL=thiazoline, TZ=thiazole
[b]For ATCAA-1, C position contains a lipid chain.

improved activity (IC$_{50}$=14~38 μM) compared with 2a, 2b and 5. When the amide CONH linkage between B ring and C ring was replaced by a carbonyl linker, the mixtures of thiazoline/thiazole ketone 8f were obtained instead of desired thiazoline ketone, because the auto-dehydrogenation between thiazoline and thiazole occurred. Surprisingly, introduction of the carbonyl group linker and thiazole led to a significant enhancement of growth inhibition of examined cancer cell lines with a low nanomolar level (8f, IC$_{50}$=21~71 nM), which is comparable to the natural anticancer agent colchicine. Thus a series of the SMART compounds with B as a thiazole ring were designed and synthesized based on the discovery of 8f and their anticancer activity was evaluated against melanoma.

4.3.1.2 SAR of the C Ring
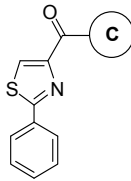
We started our investigation of the C position of the SMART by introducing different substituted phenyls or alkyl chain. Variation of the phenyl substituents has a remarkable change in effect on potency. The *in vitro* assay as shown in **Table 4-3** gave us an interesting result but only 3, 4, 5-trimethoxylphenyl in C ring (8f) showed excellent inhibition against all cancer cells (IC$_{50}$=28~55 nM). Compound 8g, with a 3, 5-dimethoxyphenyl group, showed 6-fold average cytotoxicity lower than 8f. Modifications of 8f by removal of one methoxy at *meta*-position (8e) or two methoxy groups (8b, 8c and 8d) from 8f led to a dramatic loss in activity (IC$_{50}$>20 μM). Although *ortho*-substituted monomethoxy compound 8d exhibited weak activity against a certain cell lines compared with *meta*-/*para*-MeO substituted 8c/8b and dimethoxyphenyl compound 8e, none of them showed significant potency in inhibition compared with 8f. Similar trends were also seen in 8h and 8j with 2-fluorophenyl and hexadecyl in C ring modifications.

4.3.1.3 SAR of the A Ring

In SAR studies of the ATCAA compounds, I found that the electronic properties of substituents of the phenyl ring in the 2-positioin of the thiazolidine ring strongly affected the anticancer activity in ATCAA compounds — electron-withdrawing groups (EWG) on 2-phenyl gave higher activities than those with electron-donating groups (EDG). Dr. Lu also introduced different *para*-substituted EWG and EDG on A phenyl ring of the SMART molecules. From the IC$_{50}$ value against these cancer cell lines, electronic effects of A ring phenyl substituents did not show clear influence on antiproliferative activity. Introduction of a weak EWG (4-F in 8n, IC$_{50}$s: 33~43 nM) or weak EDG (4-CH$_3$ in 8k, IC$_{50}$s: 11~21 nM), both increased the potency compared with 8f (see **Table 4-4**). The replacement of *para*- position with strong EWG such as NO$_2$ (8p), CN (8q), CF$_3$ (8t) or introducing strong EDG (3, 4-dimethoxy) to A phenyl ring (8o) exhibited comparable antiproliferative activity.
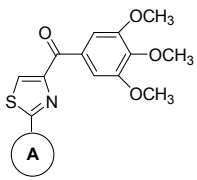
To compare the effects of *ortho*-, *meta*- and *para*- substitutions, a fluoro atom was introduced to different positions of A phenyl ring (8l, 8m and 8n). The various *o*-, *m*-, *p*-

Table 4-3. *In vitro* cytotoxic activity of SMART compounds with C rings modification.

| Compounds | C Ring | IC$_{50}$±SEM (µM) (n=3) | |
		B16-F1	A375
8a	Ph	>100	>100
8b	4-Methoxy-Ph	>100	>100
8c	3-Methoxy-Ph	>100	>100
8d	2-Methoxy-Ph	59±21	70±33
8e	3, 4-Dimethoxy-Ph	>100	>100
8f	3,4,5-Trimethoxy-Ph	55±5 nM	28±5 nM
8g	3, 5-Dimethoxy-Ph	350±20 nM	170±10 nM
8h	2-Fluoro-Ph	>100	>100
8j	Hexadecyl[a]	19±18	16 ± 15

[a]Compound 8j has a lipid chain at C ring position.

Table 4-4. *In vitro* cytotoxic activity of SMART compounds with A rings modification.

| Compounds | A Ring | IC$_{50}$±SEM (nM) (n=3) | |
		B16-F1	A375
8f	Ph	55±5	28±5
8k	4-Methyl-Ph	21±10	11±5
8l	2-Fluoro-Ph	27±11	30±9
8m	3-Fluoro-Ph	287±36	304±25
8n	4-Fluoro-Ph	43±21	33±14
8o	3, 4-Dimethoxy-Ph	161±29	34±10
8p	4-Nitro-Ph	56±12	38±9
8q	4-Cyano-Ph	53±16	59±24
8t	4-Trifluoromethyl-Ph	92±16	23±5
8u	4-Bromo-Ph	32±5	13±2
8v	4-Ethyl-Ph	70±8	17±2
8x	4-Pyridine	>100000	>100000
8y	2-Pyrimidine	2300±860	4100±740
8z	2-Thienyl	38±15	20±7
10	H[a]	>100000	>100000

[a]Compound 10 has a proton at A ring position.

substituents did not exhibit equal activities. *o*-fluoro substituted 8l showed the lowest IC_{50}s (27~30 nM) against melanoma cells. 8n has similar average IC_{50}s (33~43 nM) against melanoma compared with 8l. *Meta*-substituted compound 8m showed lowest activity on melanoma cells (IC_{50}s: 287~304 nM).

Turning to the effects of steric hindrance group on the A phenyl ring substituents, I found that *p*-bromo (8u, IC_{50}s: 13~32 nM) caused a slightly decrease in antiproliferative activity relative to *p*-fluoro position (8n, IC_{50}s: 6~12 nM). Reduced activity against both cancer cell lines is obvious when *p*-methyl (8k, IC_{50}s: 11~21 nM) was replaced with a *p*-ethyl group (8v, IC_{50}s: 17~70 nM).

To investigate if phenyl played an essential role at A ring in cytotoxicity, Dr. Lu also removed phenyl at 2-thiazole position and compound 10 was obtained. This modification caused a total loss of activity compared with 8f. The replacement of the A ring by pyridine (compound 8x) had the same effect. Moreover, substituting 2-pyrimidine in A ring (compound 8y) also caused a significant loss of activity (IC_{50}s: 2~4 μM). However, introducing the thiophene replacement of phenyl (8z) into A position slightly improved the potency (IC_{50}s: 20~38 nM) compared to 8f (IC_{50}s: 28~55 nM).

4.3.1.4 SAR of Pharmaceutically Acceptable Salt Groups to the SMARTs

Most of the SMART compounds have good solubility in organic solvents such as $CHCl_3$, CH_2Cl_2 and DMSO. But they show poor water-solubility. Dr. Lu designed and synthesized water-soluble salts of the SMART by introducing a hydrophilic group such as NH_2 (8w) and COOH (8r) into A ring and generated the HCl or sodium salt. Another modification is replacing A/C rings in 8a with pyridine (8i, 8x, 8y) or pyrimidine rings, which could also be converted into HCl salts. These modifications reduced the calculated LogP values (LogP=3~4) compared with 8a and 8f (LogP=4, See **Table 4-5**). Introducing *p*-amino to A phenyl (8w) is the only case to increase the antiproliferative activity (HCl salt, IC_{50}s: 11~29 nM) compared with 8f against all cell lines. Although replacing phenyl with pyrimidine (8y) kept partial activity against both cancer cells, the potency range was markedly reduced from nano-molar to micromolar compared with 8f. Unfortunately introducing COOH to *para*- phenyl A ring and pyridine to A or C rings (8i, 8r, 8x) all resulted in the total loss of the anticancer activity. A total loss of potency was seen in the methyl ester 8s of acid 8r against both cancer cell lines. Demethylation of compound 8f afforded water soluble 3, 4, 5-trihydroxyphenyl at C ring compound 11, but this demethylation results in complete loss of antiproliferative activity against all tested cancer cells, which also points out the importance of 3, 4, 5-trimethoxyphenyl at C position.

4.3.1.5 SAR Summary

The general SAR of SMART compounds on melanoma cells was summarized in **Figure 4-2**. Present SAR studies revealed that 3, 4, 5- trimethoxyphenyl was the essential

Table 4-5. *In vitro* cytotoxic activity of SMART compounds containing hydrophilic group.
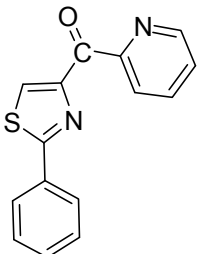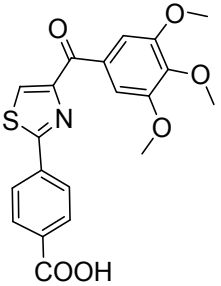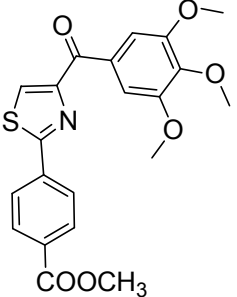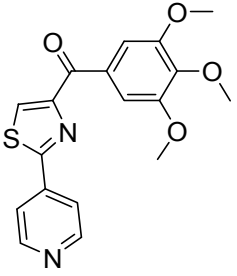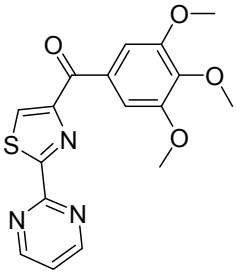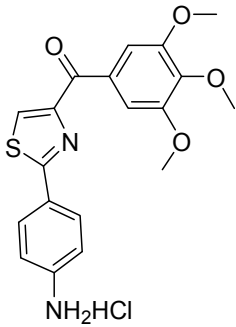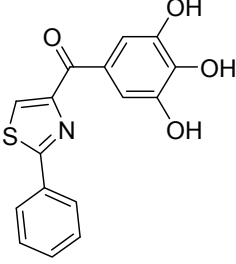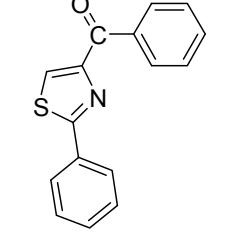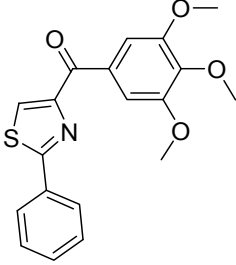
Compounds	Structure	IC$_{50}$±SEM (nM) (n=3)		CLogP[a]
		B16-F1	A375	
8i		>100000	>100000	4
8i·HCl		>100000	>100000	-
8r		>100000	>100000	4
8s		>100000	>100000	4
8x		>100000	>100000	3
8x·HCl		>100000	>100000	-

Table 4-5. (continued)

| Compounds | Structure | IC$_{50}$±SEM (nM) (n=3) | | CLogP^a |
		B16-F1	A375	
8y		2300±860	4100±740	3
8w·HCl		29±10	11±2	-
11		>100000	>100000	3
8a		>100000	>100000	5
8f		55±5	28±5	4

^{a} Calculated LogP data using Chemoffice 2005, Chemdraw Ultra 9.0 software.
^{b} LogP value were calculated based on free base.

(d). Ketone C=O linkage significantly improved the potency compared with CONH linker.

(c). C ring is specific for 3, 4, 5-trimethoxyl substituted phenyl

(b). Thiazole ring kept potency, thiazoline and thiazolidine ring lost potecy

(a). A ring: No obvious electronic effect. *p*-F-Ph, *p*-CH$_3$, p-NH$_2$-Ph is helpful for potency.
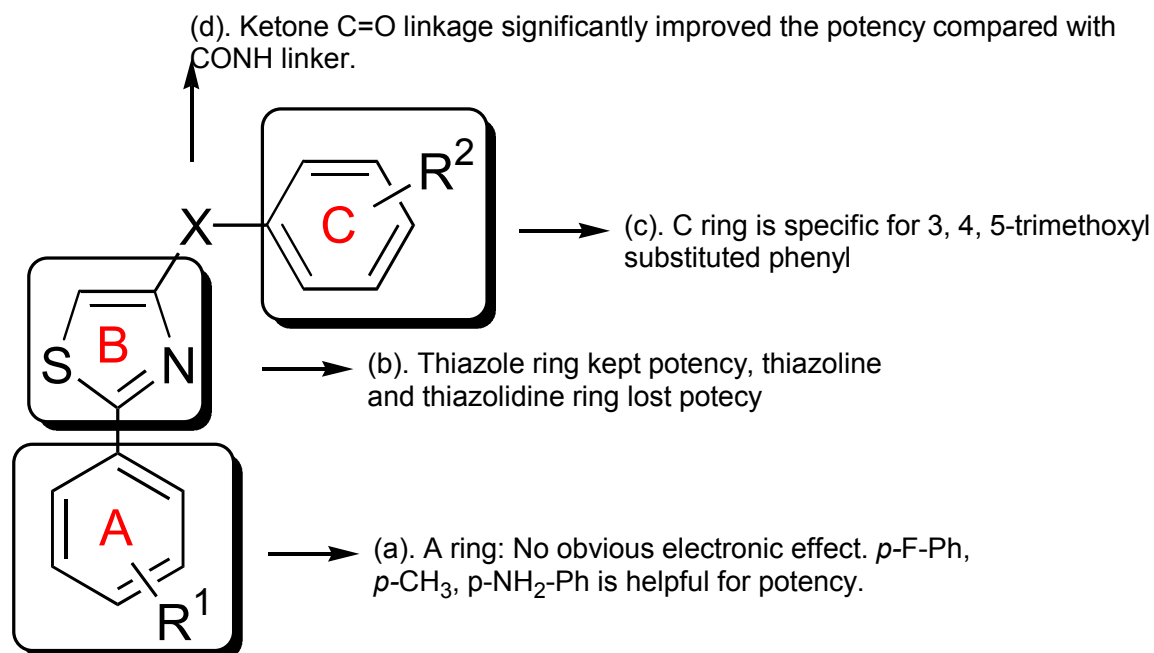
Figure 4-2. SAR summary of the SMART compounds.

group in the C ring to keep excellent antitumor potency. p-Fluoro, p-NH$_2$ and p-CH$_3$ substituents in A ring will increase the activity, with no clear difference in effect on activity between EWG and EDG when A are substituted phenyl rings. The carbonyl linkage between B ring and C ring played an important role for the high potency.

4.3.2 SMARTs Overcome Multi-Drug Resistance on Drug Resistant Melanoma Cells

MDA-MB-435/LCC6MDRI cells over-express P-gp, and were used to test whether SMARTs were substrates of P-glycoprotein comparing to its parental cell line, MDA-MB-435. I demonstrated that paclitaxel, vinblastine, and colchicine were more resistant against MDR-positive cells than those with the parent sensitive cells. Please see **Figure 4-3** for selected dose-response curves and **Table 4-6** for summary of results. The resistance indexes were 69.3, 27.5, and 65.8 respectively. In the meantime, SMARTs did not show significantly difference on those two cell lines. The resistance indexes were around 1. This strongly suggested that SMARTs were not substrates for P-glycoprotein.

4.3.3 SMARTs Target Tubulin on Colchicine Binding Site

The strategy I used here to find out the cellular target of SMART compounds is the same as I described for ABI compounds in Chapter 5. I first did a cell cycle analysis for A375 cells after treatment with SMART-100, -45, and -211 (0, 10, 50, 200, and 1000 nM) for 24 h prior to staining with propidium iodide and cell cycle analysis. The proportion of cells in G2/M phase increased when treated with 50 nM of SMART-100 and -45, and SMART-211 showed the effect until the concentration was 200 nM. Some representative cell cycle distribution graphs were shown in **Figure 4-4**. Quantified representation of all results was shown in **Figure 4-5**. SMART-100 and SMART-45 had no effect on cell cycle distribution below 50 nM. About 16% of untreated cells were observed in G2/M phase, whereas the cells treated with more than 50 nM of colchicine or SMART compounds showed a greater proportion of cells in G2/M phase. The increase in G2/M phase cells was accompanied by a decrease in G1 populations, relative to control.

In vitro tubulin polymerization assay was used to identify the target of SMART compound on tubulin. This experiment was performed by my colleague Mr. Chien-Ming Li. He demonstrated that SMART-100 inhibited tubulin polymerization in a dose-response manner in the previous study (15). In the current study, 10 μM of SMARTs were used to examine the inhibition of tubulin polymerization. In **Figure 4-6**, all three SMART compounds inhibited tubulin polymerization, indicating that SMARTs did target on tubulin. SMART-100 showed similar inhibitory ability as SMART-45, and greater than SMART-211. *In vitro* tubulin polymerization could be blocked by SMARTs, and the ability of inhibition on tubulin polymerization was also related to their IC$_{50}$ values on cell anti-proliferation. 10 μM of substrates were examined in this study because high concentration of tubulin (4 mg/mL) was used to form microtubule.
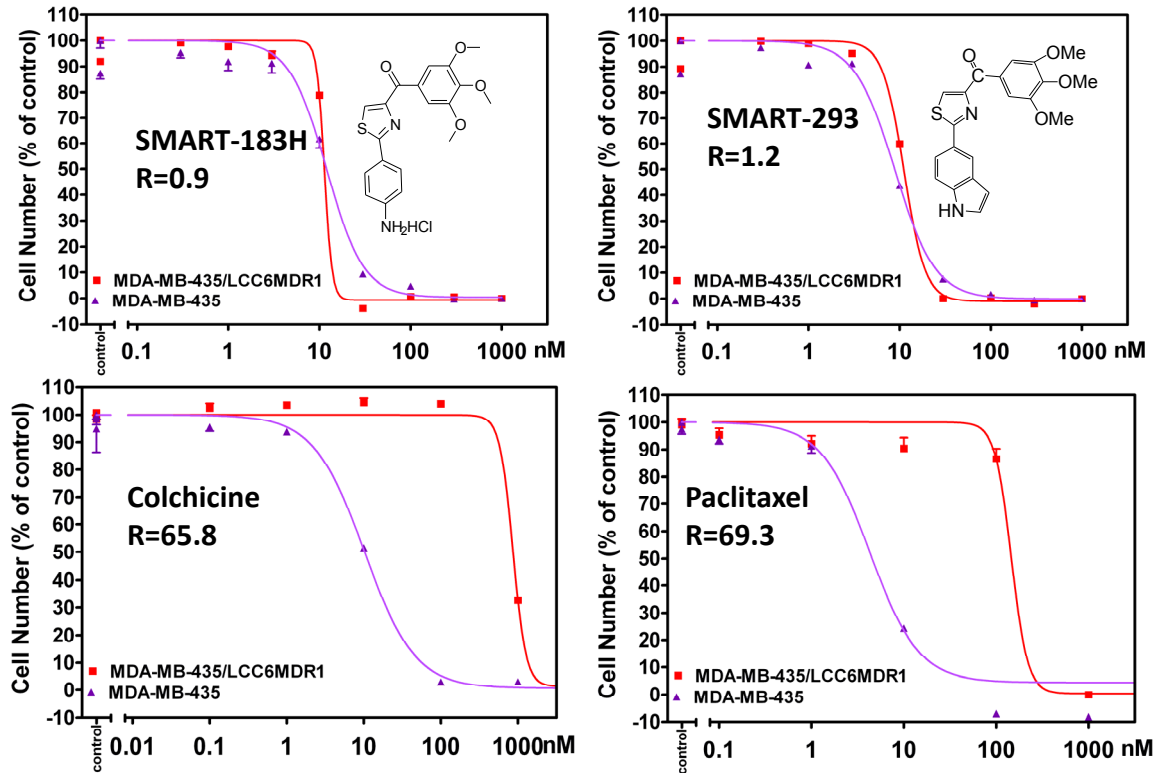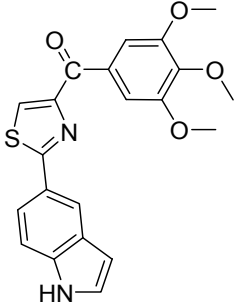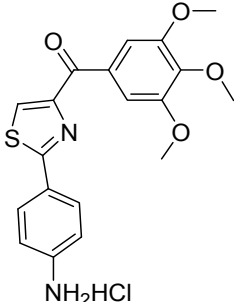
Figure 4-3. Dose response curves showed SMART compounds overcome multi-drug resistant for melanoma compared with colchicine and paclitaxel.
R: resistance index, this value were calculated by dividing IC_{50} values on multi-drug resistant cell line MDA-MB-435/LCC6MDR1 by IC_{50} values on the matching sensitive parent cell line MDA-MB-435.

Table 4-6. SMART compounds showed equal potency against multi-drug resistant melanoma cells and parent sensitive cells.

Compounds	Structure	$IC_{50} \pm SEM$ (nM) (n=3)		Resistance index (R) *
		MDA-MB-435	MDA-MB-435 /LCC6MDRI	
SMART-293		9±1	11±2	1
SMART-183H		12±2	11±1	1
Colchicine		10±1	658±50	66
Paclitaxel		4±1	277±41	69
Vinblastine		400±100 pM	11±1	28

*Resistance indexes were calculated by dividing IC_{50} values on multi-drug resistant cell line MDA-MB-435/LCC6MDR1 by IC_{50} values on the matching sensitive parent cell line MDA-MB-435.

85

www.manaraa.com
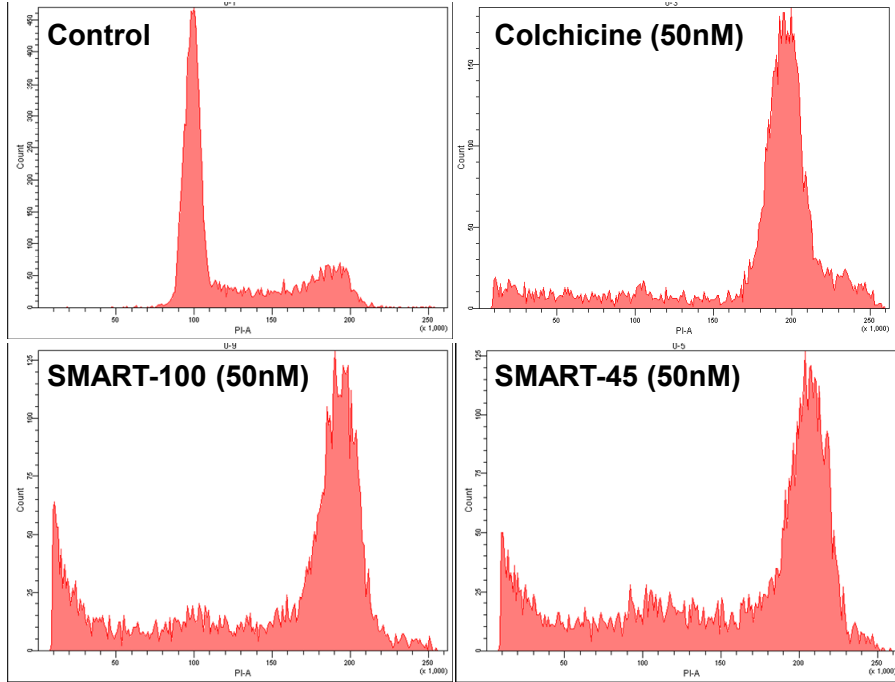
Figure 4-4. Cell cycle analysis showed SMART compounds and colchicine arrested A375 cells in G2/M phase after incubation for 24 h.
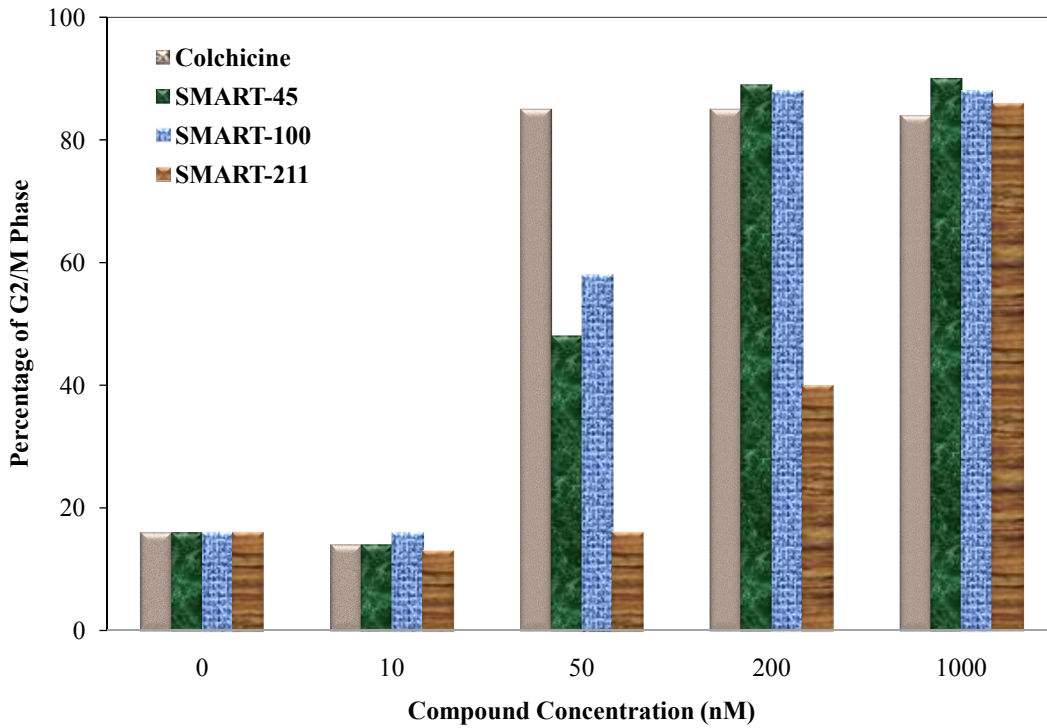
Figure 4-5. Quantified cell cycle analysis results showed SMART compounds and colchicine arrested A375 cells into G2/M phase in a dose dependent manner.
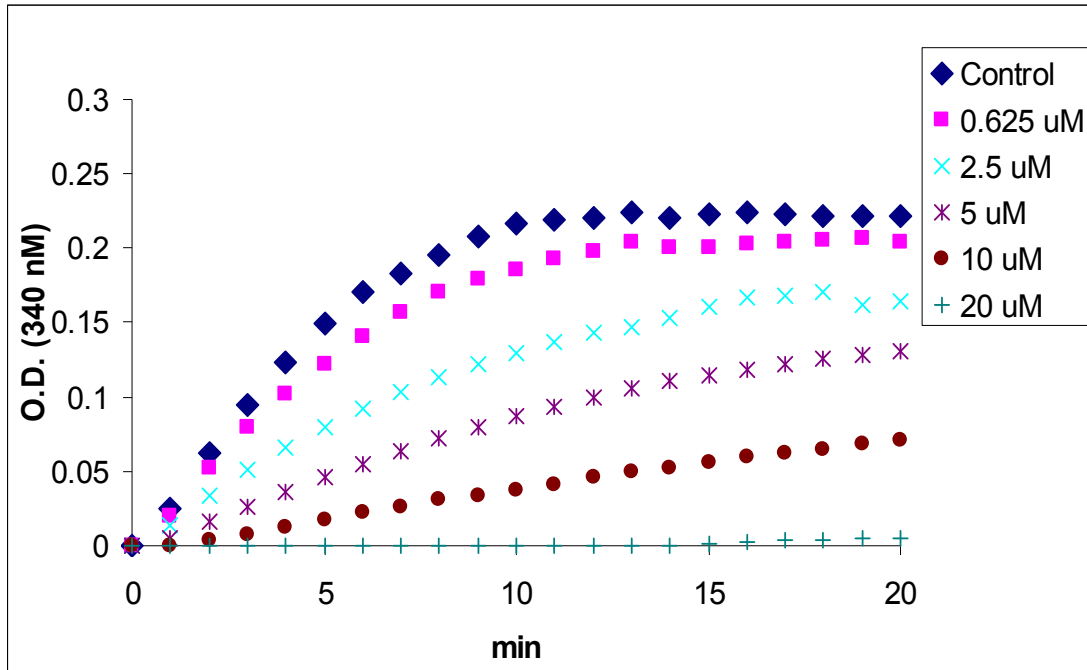
Figure 4-6. SMART-100 inhibited *in vitro* tubulin polymerization in a dose dependent manner.
This experiment was done by Mr. Chien-Ming Li, Division of Pharmaceutics, College of Pharmacy, the Ohio State University.

[3H]colchicine competition-binding assay was used to confirm that SMART bind to tubulin at the colchicine binding site. In the meantime, I also measured the relative binding affinity. Binding graph (**Figure 4-7)** showed that: 1), SMART compounds can competitively bind to tubulin colchicine binding site. As concentration of these three testing compounds increased from 0.1 μM to 100μM, more and more tritiated colchicine were competitively stripped away from tubulin. Thus gave out lower and lower SPA counts. 2), SMART compounds have relatively high binding affinity to the tubulin colchicine binding site. **Table 4-7** Showed that software calculated IC_{50} value for binding. SMART-100 has the highest binding affinity among the three tested compounds. Its value is close to colchicine, although a little bit higher than that. 3), the binding affinity was positively correlated with *in vitro* anti-melanoma activity. The higher of the binding affinity, the higher is the anti-melanoma activity. In our experiment, the D value is 0.08 μM, the Kd value is around 1 μM according to literature (131). So the IC_{50} is very close to Ki value. Our result is quite comparable with literature reported Ki value for colchicine binding to tubulin. On the binding graph, some data point is a little bit below 0. That is caused by experimental variation. Theoretically, the maximum inhibition is 0.

Microtubule images (**Figure 4-8**) showed that all four tested compounds results in cytoskeleton rearrangements. There is a significant difference between paclitaxel and other two compounds (Colchicine and SMART-100). Treatment with paclitaxel resulted in condensation of microtubules nice surrounding the nuclei compared with control, consistent with its mechanisms of action for stabilizing microtubules. On the contrary, treatment with colchicine or SMART-100 all has similar effect on microtubules, and result in some degree of microtubule fragmentations, consistent with their common mechanism of action for destabilize microtubules.

In summary, our data clearly showed that SMARTs triggered several molecular events, which include binding to colchicine site of tubulin, inhibiting on tubulin polymerization, arresting cells in G2/M phase and resulting microtubule fragmentation.

4.3.4 Pharmacokinetic Properties of SMART-100, SMART-45 and SMART-211

I first examined SMART-100 at a dose level of 5 mg/kg (**Figure 4-9**). The plasma concentration-time profiles of SMART-100 after single IV and IP administration are shown in panel A and B of **Figure 4-9**. The derived pharmacokinetic parameters are shown in **Table 4-8**. The formulation I used for both injections were DMSO/PEG300 (80/20). SMART-100 appeared rapidly in plasma after IP injection with peak level (C_{max}) observed in less than 2 min after administration. This suggested a rapid absorption of the compound from the injection site. The compound was distributed extensively in the body with a volume of distribution of 112 L/kg. A very high clearance of 223 mL/min/kg indicates extensive metabolism and rapid elimination. The high clearance resulted in a relative short terminal half-life of 349 min after IV and 358 min after IP administration despite of the huge volume of distribution. The IP bioavailability is only 31%. I thought the poor bioavailability was largely due to the poor water solubility of the compound and too simple formulation.
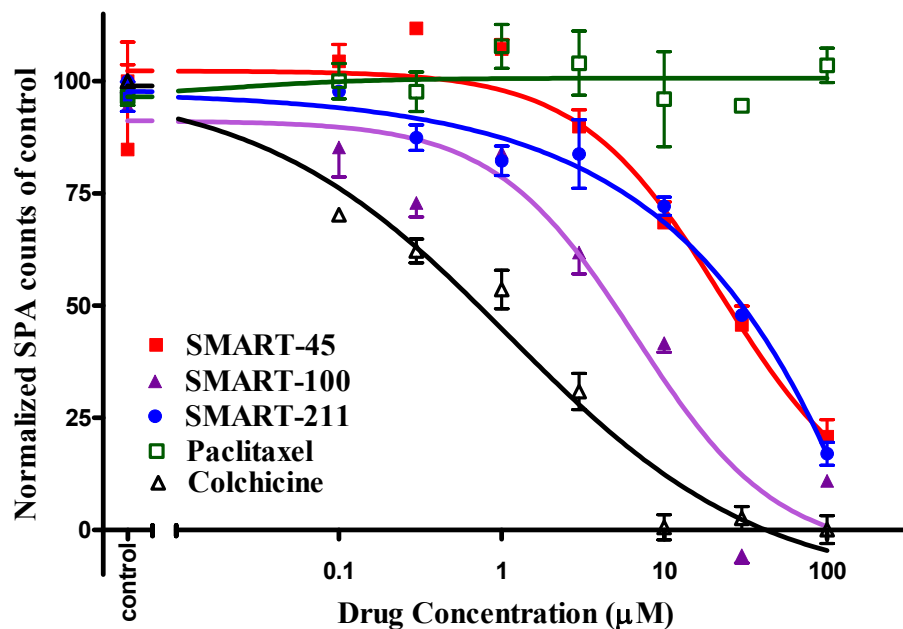
Figure 4-7. Tubulin binding assay showed SMART compounds competitively bound to tubulin colchicine binding site in a concentration dependant manner.
As concentration of these compounds increased from 0.1 μM to 100μM, more and more tritiated colchicine were competitively stripped away from tubulin. Thus gave out lower and lower SPA counts. The negative control paclitaxel just gave out a flat line because it didn't bind to the colchicine binding site on tubulin. Each data point represents an average of three replicates.

Table 4-7. Comparison of tubulin binding affinity and *in vitro* cytotoxic activity between SMART compounds and known tubulin interacting drugs.

Compounds	$IC_{50} \pm SEM$ (n=3)	
	For tubulin binding (μM)	On A375 (nM)
SMART-100	7±3	28±5
SMART-45	22±4	29±11
SMART-211	38±2	93±11
Colchicine	1±0	20±3
Paclitaxel	N/A	12±3
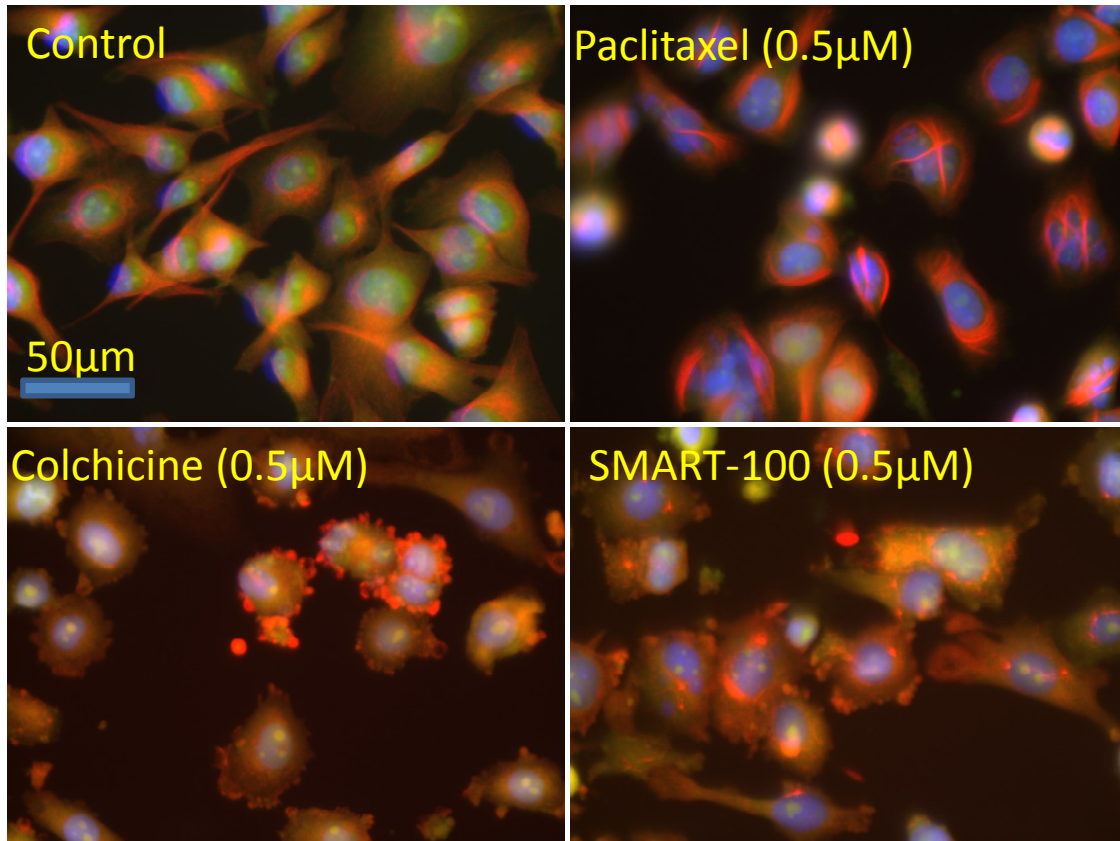
Figure 4-8. Microscopic images of immunofluorescence labeled microtubules inside WM-164 melanoma cells showed microtubule modality was dramatically changed after compounds treatment for 18 h.
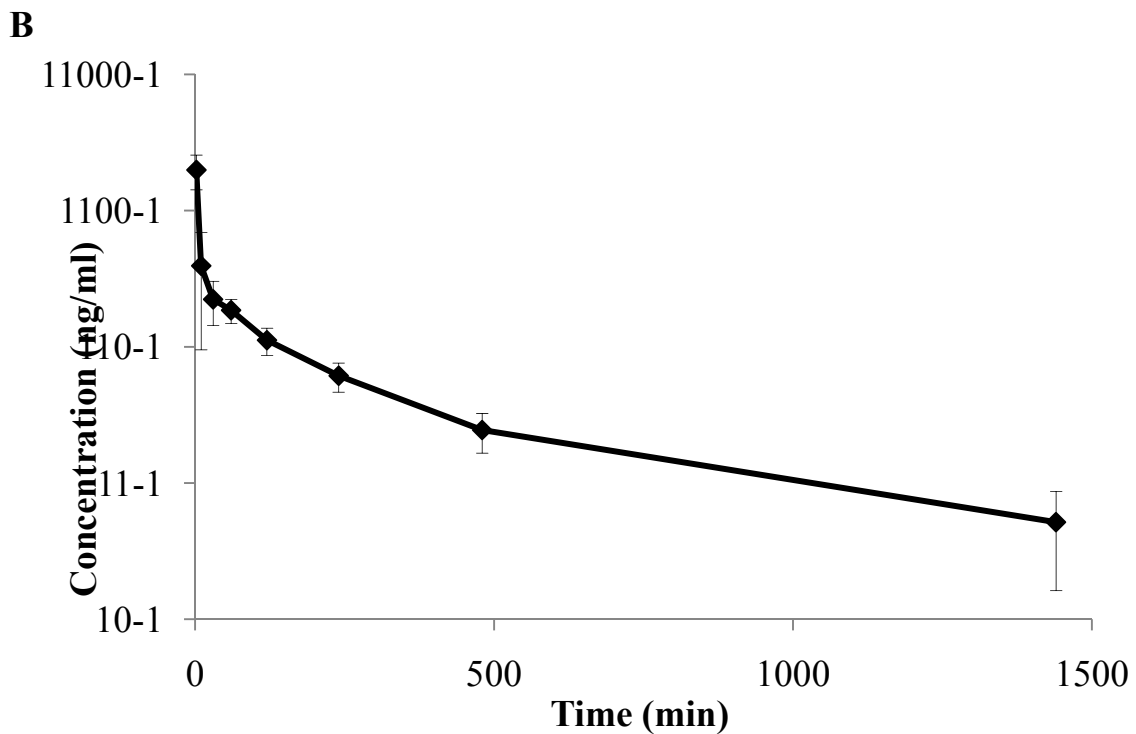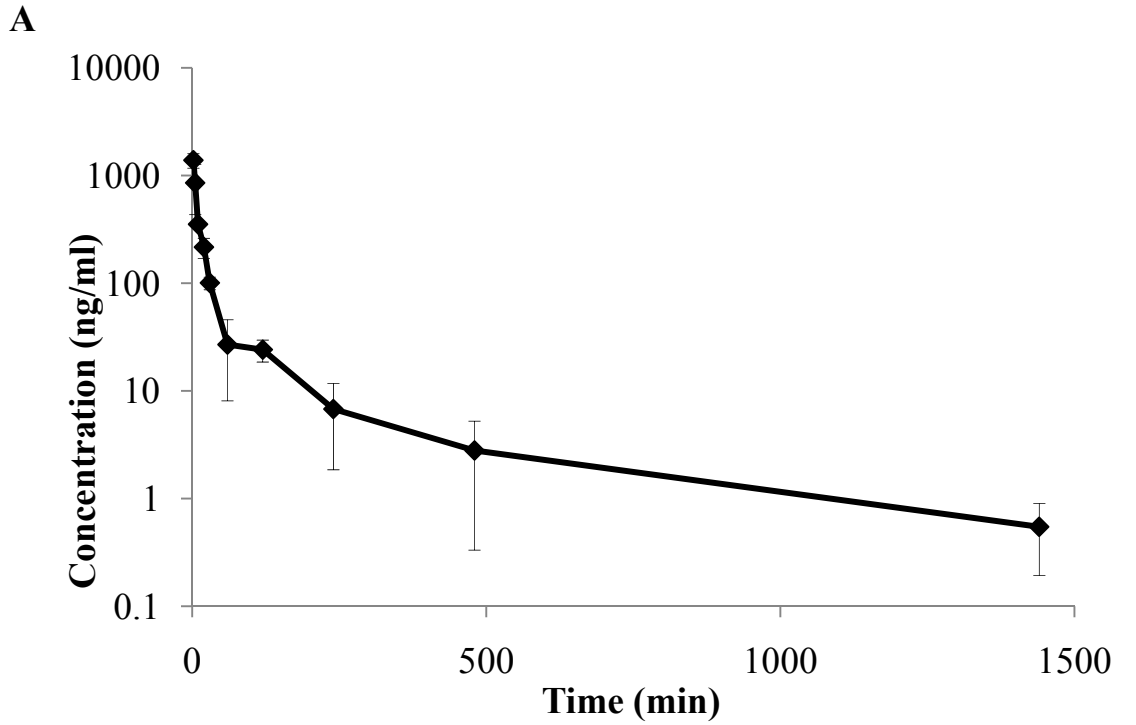
Figure 4-9. Measured plasma concentration-time profiles (mean±SD) after bolus administration of 5 mg/kg SMART-100 to ICR mice (n=3 per group).
A: i.v. injection, formulation, DMSO:PEG300=80:20 (v/v). B: i.p. injection, formulation, DMSO:PEG300=80:20 (v/v).

Table 4-8. Pharmacokinetic parameters of SMART-100, SMART-45, and SMART-211.

Route	Compound and dose	$t_{1/2}$ (min)	AUC_{inf} (ng·min/mL)	AUC_{last} (ng·min/mL)	Clearance (mL/min/kg)	V_z (mL/kg)	V_{ss} (mL/kg)	Bioavailability (%)
IV	SMART-100 5 mg/kg[a]	349	22434	22159	223	112311	24803	
	SMART-100 15 mg/kg[a]	140	115336	115221	130	26274	4926	
	SMART-45 15 mg/kg[a]	141	134340	134051	112	22643	6588	
	SMART-211 15 mg/kg[a]	334	168759	151526	95	45954	5420	
IP	SMART-100 5 mg/kg[a]	358	7038	6771	710	366859		31
	SMART-100 15 mg/kg[a]	308	17645	17189	850	378339		15
	SMART-100 15 mg/kg[b]	123	55842	55760	269	47507		48
	SMART-45 15 mg/kg[b]	182	72001	71719	208	54674		54
	SMART-211 15 mg/kg[b]	208	122578	122440	122	36700		73

[a]Compound was formulated with DMSO:PEG300=80:20 (v/v).
[b]Compound was formulated with Tween80:Captex200=80:20 (v/v).

92

I then examined SMART-100 at a dose level of 15 mg/kg and compared two different formulations for IP injection. One is DMSO/PEG300 (80/20), one is Tween80/captex200 (80/20). The later formulation was one of the self-emulsifying drug delivery systems (SEDDS), which contained a mixture of oil (captex200) and surfactant (Tween80), and improved the solubility of our lipophilic SMARTs (132). The plasma concentration-time profiles of SMART-100 after single IV and IP administration are shown in panel A, B, and C of **Figure 4-10**. The derived pharmacokinetic parameters are shown in **Table 4-8**. Compared different dose of SMART-100 with the same DMSO/PEG300 (80/20) formulation, higher dose (15 mg/kg) gave lower bioavailability (15% *vs*. 31%). This may be due to higher concentrated SMART-100 in DMSO/PEG300 (80/20) precipitated out more after IP injection. Thus more compounds became unavailable for absorption. Absorption of SMART-100 after IP injection with Tween80/captex200 (80/20) formulation was slower than DMSO/PEG300 (80/20). The former one had a t_{max} of 15 min *vs*. the later one of 1 min. That's because the former formulation delayed the release of compound. With the help of this new formulation, the bioavailability was increased from 15% to 48%. 15 mg/kg of SMART-100 had 5.1-fold area on under the curve (AUC) than the dose with 5 mg/kg. The other parameters like $t_{1/2}$, volume of distribution, and clearance also changed dramatically along with dose change. This suggested that SMART-100 may have non-linear kinetics.

I next examined SMART-45 and SMART-211 at a dose level of 15 mg/kg with the new formulation for IP injection. The plasma concentration-time profiles of SMART-100 after single IV and IP administration are shown in panel A and B of **Figure 4-11** and **Figure 4-12**. The derived pharmacokinetic parameters are shown in **Table 4-8**. The IP bioavailability of SMART-45 and –SMART-211 were 54% and 73% respectively. This confirmed the new formulation's ability to increase bioavailability. I then used this formulation for our further *in vivo* xenograft studies, and no toxic effects were found in the vehicle group of A375 xenograft models, suggesting that this formulation was safe to use for long-term (more than one month) xenograft studies.

With the same dose of 15 mg/kg of SMART-45 and SMART-100, the parameters of AUC (min·ng/mL), $t_{1/2}$ (min), V_z (L/kg), and CL (mL/min/kg) were very close to each other. That can be understood by their similarity of chemical structure and lipiphilicty. SMART-211 has relative lower clearance and thus its terminal half life was relatively longer. But overall SMART compounds exhibited high clearances and short half-life. Once-daily regimen was designed to improve compounds exposure and treatment efficacy for our xenograft studies.

The calculated clearances of SMART compounds are much higher than the mouse hepatic blood flow rate. There maybe three reasons account for this. First, this may be due to expetimental error. Especially when drug concentration is close to detection limit, the measurement error is relatively large. Second, this may be due to incomplete tail vein injection. The drug amount actually got into the vein may be is less then what we planned. Third, SMART compounds may have extra-hepatic metabolism. For example, the enzyme in the blood, speen, heart or other organs may be can metablize these compounds.
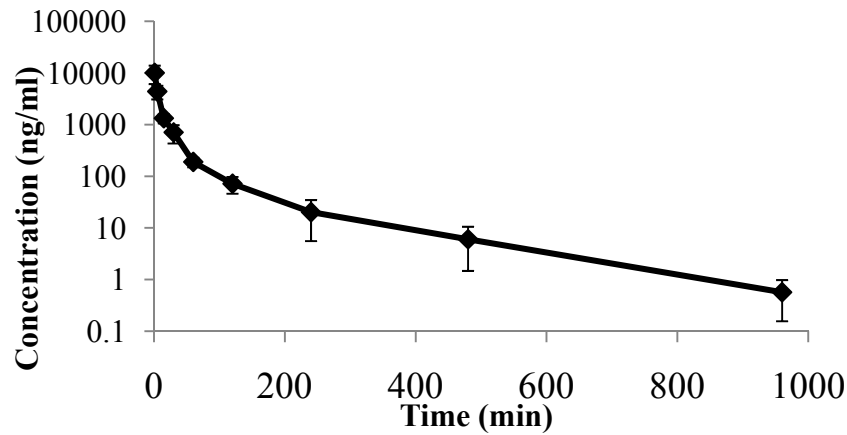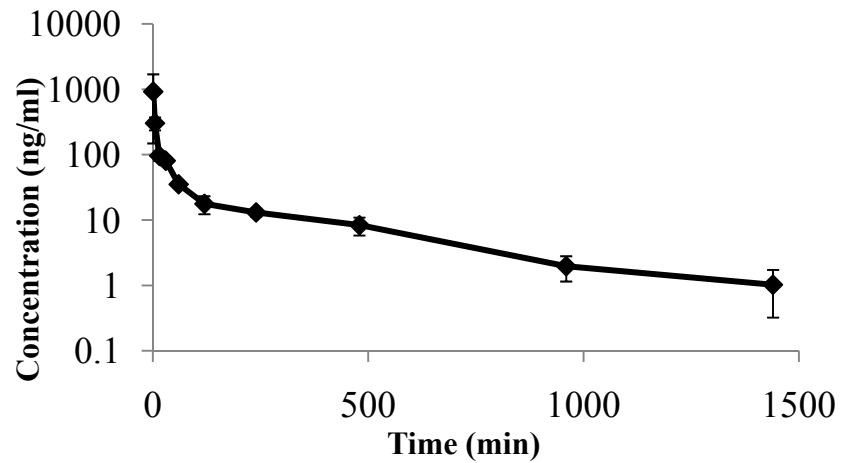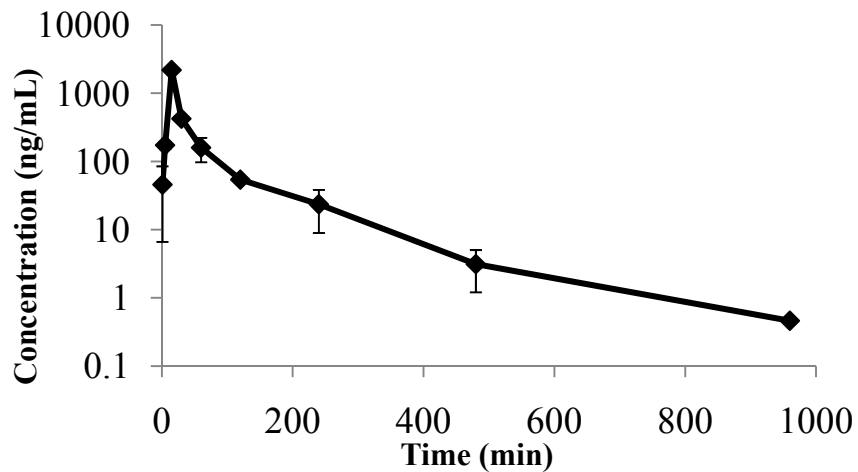
Figure 4-10. Measured plasma concentration-time profiles (mean±SD) after bolus administration of 15 mg/kg SMART-100 to ICR mice (n=3 per group).
A: i.v. injection, formulation, DMSO:PEG300=80:20 (v/v). B: i.p. injection, formulation, DMSO:PEG300=80:20 (v/v). C: i.p. injection, formulation, Tween80:Captex200=80:20 (v/v).

94
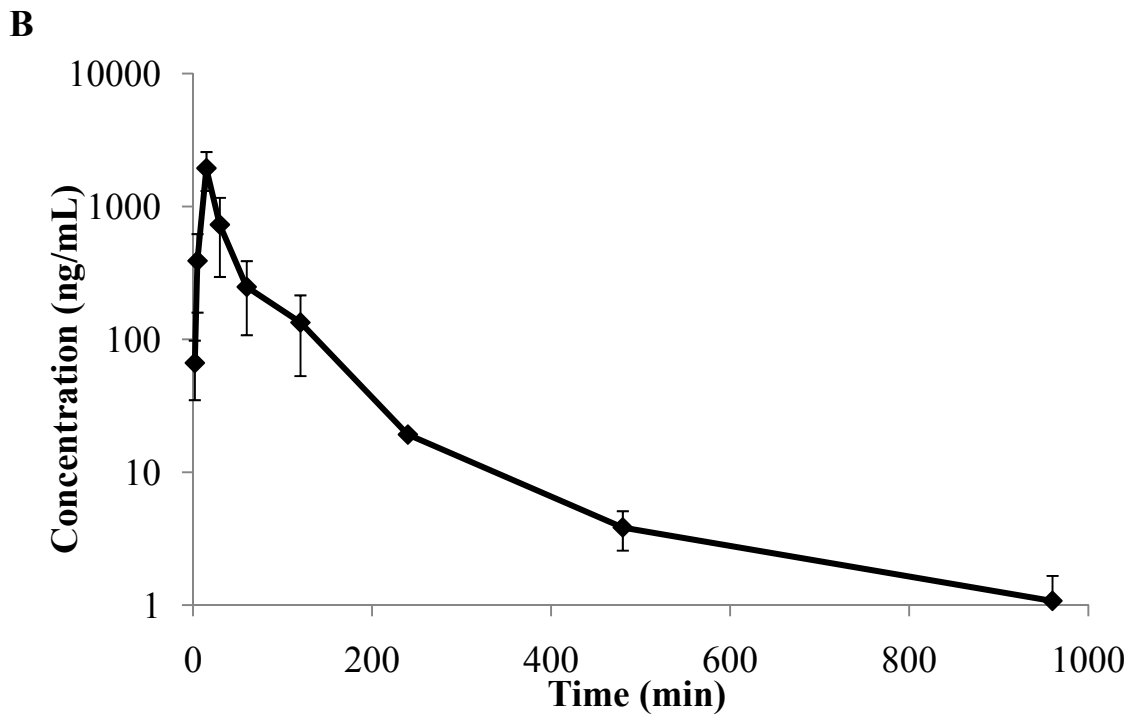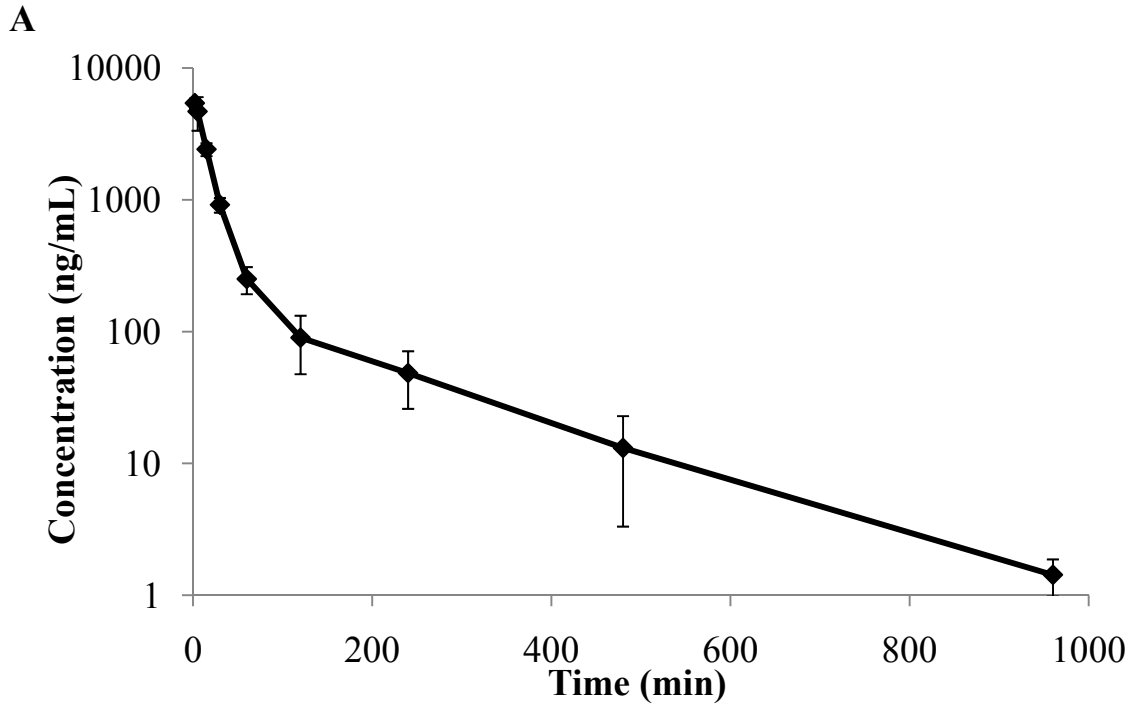
Figure 4-11. Measured plasma concentration-time profiles (mean±SD) after bolus administration of 15 mg/kg SMART-45 to ICR mice (n=3 per group).
A: i.v. injection, formulation, DMSO:PEG300=80:20 (v/v). B: i.p. injection, formulation, Tween80:Captex200=80:20 (v/v).
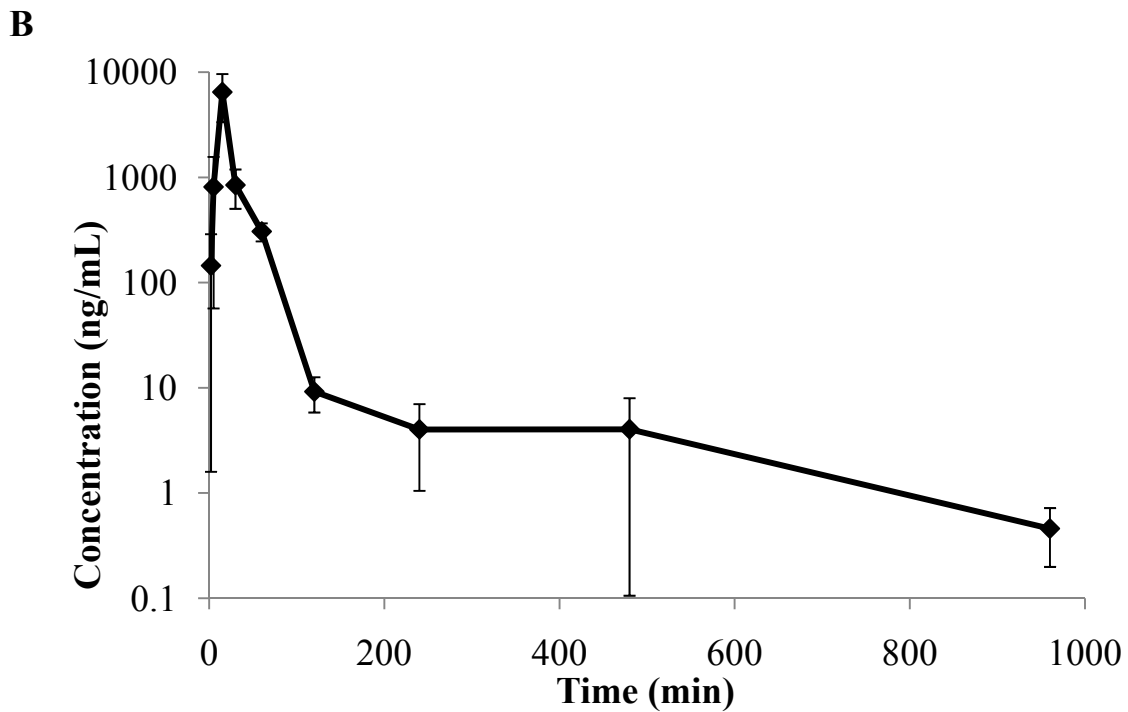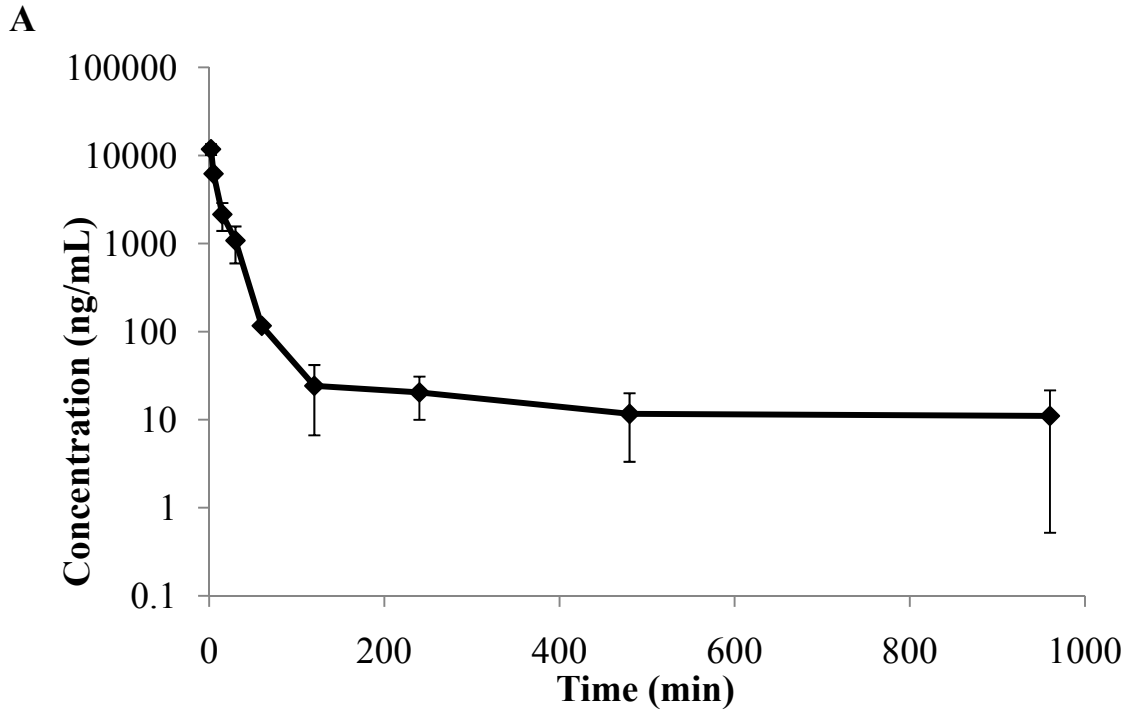
Figure 4-12. Measured plasma concentration-time profiles (mean±SD) after bolus administration of 15 mg/kg SMART-211 to ICR mice (n=3 per group).
A: i.v. injection, formulation, DMSO:PEG300=80:20 (v/v). B: i.p. injection, formulation, Tween80:Captex200=80:20 (v/v).

4.3.5 Antitumor Efficacy of SMARTs on A375 Xenograft Model

I examined 20 mg/kg of SMART-100 and 15 mg/kg of SMART-45 treatments on A375 human melanoma xenograft model. Nude mice were administrated i.p. every day for consecutive 32 days when the tumor size was ~150 mm^3. As shown in **Figure 4-13**, SMART-100 and SMART-45 exhibited significant inhibition of tumor growth. Summary of the data was presented in **Table 4-9**. The average tumor size in control group increased by about 13 folds. I obtained 4.8-fold and 4.2-fold tumor increases in SMART-100 treated (20 mg/kg) and SMART-45 treated (15 mg/kg) groups, respectively. SMART-100 reduced tumor growth rate with a %TGI of 70% (20 mg/kg treatment), and SMART-45 inhibited 72% (15 mg/kg treatment). I also calculated %T/C for our efficacy study. With 20 mg/kg treatment of SMART-100 and 15 mg/kg treatment of SMART-45 on A375 xenograft, I observed %T/C values of 36% and 33%, respectively. The data indicated that SMART-100 and -45 were pretty active in inhibiting A375 xenografts growth on athymic nude mice.

In the mean time, the general activities of mice in all groups were normal during the treatment period. At the conclusion of the experiment, the group average body weight increased by 3.1g for control group, 2.2g for SMART-45 treated group, and 2.4g for SMART-100 treated group. Corrected by group average tumor weight, which were 1.3g for control group, 0.6g for SMART-45 treated group, and 0.6g for SMART-100 treated group, the net group body weight gain were 1.8g for control group, 1.6g for SMART-45 treated group, and 1.8g for SMART-100 treated group. One mouse in control group, one mouse in SMART-100 treated group, and two mice in SMART-45 treated group died during the experiment period. I also observed big hard lumps in the injection sites of dead mice. So I guess the death of the mice was due to injection, not the toxicity of compounds treatment. No any other acute toxicity phenomenon was observed.

4.4 Conclusions

We have discovered a new class of simple synthetic compounds based on a 2-aryl-4-(3, 4, 5-trimethoxylbenzoyl)-thiazole molecular skeleton, which was derived from thiazolidine ring modification of ATCAA structures. Chemical modification of different substituted aryl in A and C rings and structure-activity relationship of the SMART were investigated based on biological evaluation against melanoma cells *in vitro*. I have demonstrated that SMARTs are very potent in inhibiting melanoma cell proliferation *in vitro*. In the meantime, our data also showed SMARTs overcame multi-drug resistance in drug resistant melanoma cell line, suggesting they are not substrates for P-gp. Mechanism of action studies showed these compounds bound tubulin at the colchicine binding site thus inhibit tubulin polymerization. The *in vivo* efficacy studies showed that SMARTs significantly inhibited A375 melanoma tumor growth on nude mice xenograft models. The dramatic biologic effect of SMARTs suggested that it has great potential for melanoma chemotherapy.
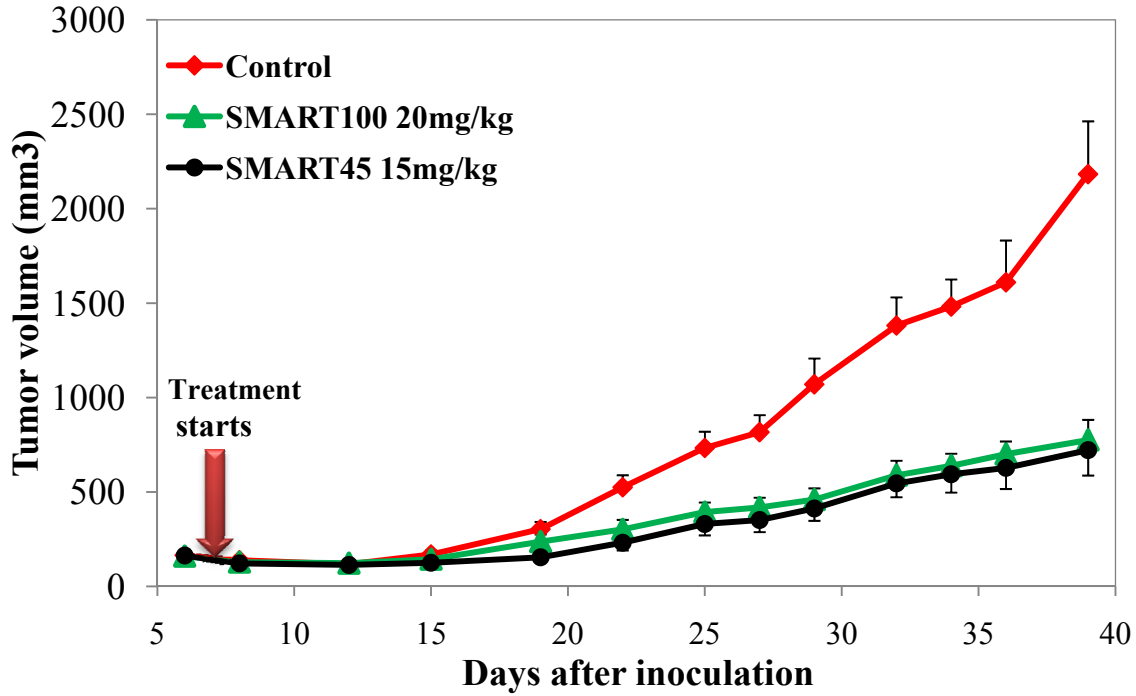
Figure 4-13. *In vivo* efficacy of SMARTs on nude mice bearing A375 melanoma xenograft tumor (n=10 per group).
A375 cells (2.5×10^6) were injected s.c. on the right flank. The compounds were given by i.p. daily when tumor size was 150 mm^3.

Table 4-9. Summary of mice number, mice body weight change, and tumor size change during *in vivo* efficacy experiment.

Groups	Number of animals		Body weight (g) Mean±SEM		Tumor size (mm^3) Mean±SEM		TGI[a]	T/C[b]
	Start	End	Start	End	Start	End		
Vehicle control	10	9	19±2	22±3	165±11	2183±279	N/A	N/A
SMART-100, 20 mg/kg	10	9	19±2	21±2	160±15	775±107	70%	36%
SMART-45, 15 mg/kg	10	8	19±2	21±3	164±12	722±135	72%	33%

[a]TGI (tumor growth inhibition) were measured on the final day for drug-treated compared with vehicle-treated mice and calculated as 100× {1-[(Treated, final - Treated,day1)/(Control, final - Control, day1)]}.
[b]T/C were generated from the mean-treated tumor volume on the final day divided by the mean control tumor volume on the final day times 100.

CHAPTER 5. NOVEL IMIDAZOLES TARGET TUBULIN POLYMERIZATION AND OVERCOME MULTI-DRUG RESISTANCE IN METASTATIC MELANOMA

5.1 Introduction

I have previously dicussed the discovery of substituted methoxylbenzoyl-aryl-thiazole (SMART) compounds that showed good anti-melanoma activity both *in vitro* and *in vivo* (100). But poor solubility and fast metabolism were two major problems associated with these compounds. After a thorough structure-activity relationship (SAR) study and extensive lead compound modification, we discovered a new class of compounds: 2-aryl-4-benzoyl-imidazoles (ABIs). The general structure of this class of compounds is shown in **Figure 5-1**. Mr. Jianjun Chen used an imidazole ring to replace a thiazole ring for the following two reasons: (a) To increase water solubility. The imidazole ring has a lower LogP value and a higher pKa value compared with the thiazole ring. Thus, imidazole compounds are more hydrophilic and more basic. It is also easier to make them into salt, thereby further increasing water solubility. (b) To increase metabolic stability. The thiazole ring is liable to oxidation, so it can make the whole molecule unstable to cytochrome enzymes (133).

To our great satisfaction, I have identified experimentally two advantages of ABIs over SMART compounds: (a) slightly increased *in vitro* activity. The IC$_{50}$s of some ABIs were in the low nanomolar range on several melanoma cell lines. (b) I have discovered that the trimethoxyphenyl substituent can be replaced by a metabolically more stable p-fluorophenyl ring and retain good anticancer activity. In this chapter, I will summarize more findinga about ABIs such as their effect on MDR melanoma cells, effect on melanoma colony formation, and *in vivo* anti-melanoma efficacy. I also will explain how we identify the cellular target of ABIs.

5.2 Materials and Methods

5.2.1 Compounds and Reagents

Compound ABI-270 {IUPAC name: (4-Fluoro-phenyl)-[2-(4-methoxy-phenyl)-1H-imidazol-4-yl]-methanone}, compound ABI-274 [IUPAC name: (2-p-Tolyl-1H-imidazol-4-yl)-(3,4,5-trimethoxy-phenyl)-methanone], and compound ABI-288 {IUPAC name: [2-(4-Chloro-phenyl)-1H-imidazol-4-yl]-(4-fluoro-phenyl)-methanone} were synthesized by Mr. Jianjun Chen in our lab. Bortezomib was obtained from Millennium Pharmaceuticals, Inc. (Kansas City, MO) through a material transfer agreement. Compound ABT-751 was synthesized by Dr. Yan Lu. Paclitaxel, vinblastine, colchicine, dimethyl sulphoxide (DMSO), and Tween 80 were obtained from Sigma-Aldrich (St. Louis, MO). Captex 200 was obtained from ABITEC Corporation (Paris, IL). CellTiter 96® AQueous One Solution Reagent was obtained from Promega Corporation (Madison,

Substituted methoxybenzoyl-aryl-thiazole (SMART)

2-aryl-4-benzoyl-imidazoles (ABI)

ABI-270

ABI-274

ABI-288
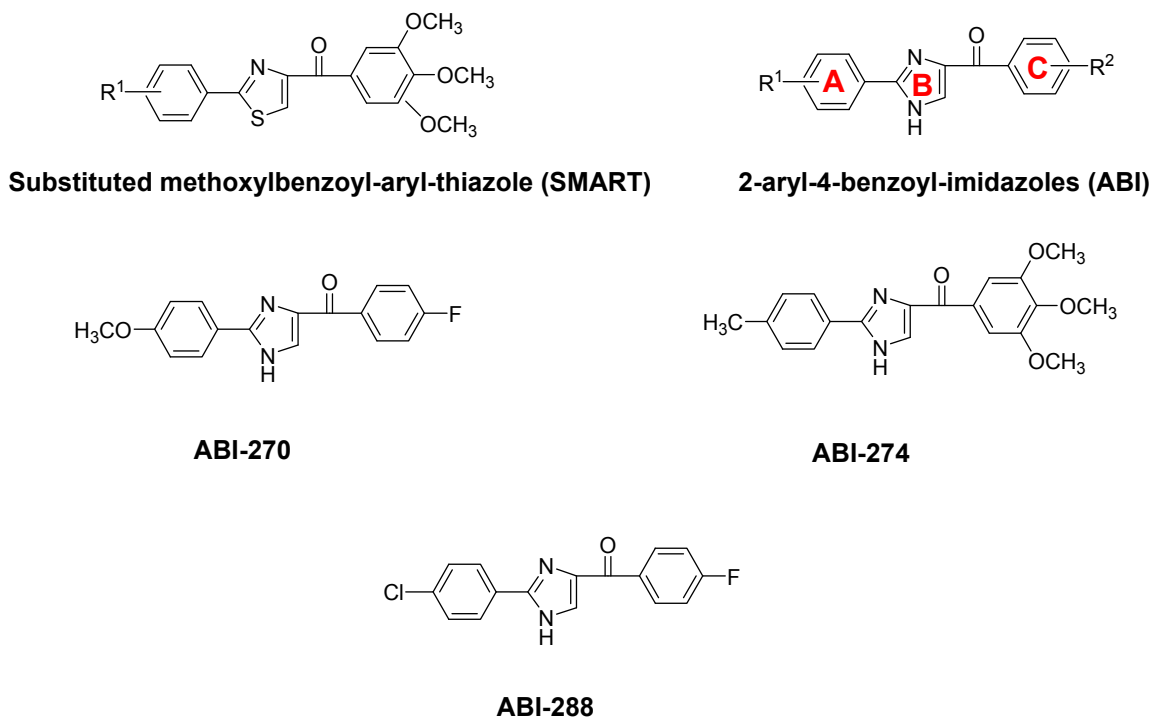
Figure 5-1. Structures of SMART, ABI, and three representative ABI compounds: ABI-270, 274, and 288.

WI). DTIC for injection, USP (a formulation for human use), was obtained from APP Pharmaceuticals, LLC (Schaumburg, IL).

5.2.2 Cell Culture

The A375 and B16-F1 melanoma cancer cells were obtained from American Type Culture Collection. WM-164 cells were derived from patient metastatic melanoma tumors and were a gift from Dr. Meenhar Herlyn (Wistar Institute, Philadelphia, PA). The P-gp overexpressing multi-drug resistant cell line MDA-MB-435/LCC6MDRI and matching sensitive parent cell line were kindly provided by Dr. Robert Clarke (Georgetown University, Washington, DC). Cells were grown as monolayers by using standard cell culture conditions. All cells were cultured in DMEM (Mediatech, Inc., Manassas, VA), supplemented with 10% FBS (Atlanta Biologicals, Lawrenceville, GA), 1% antibiotic/antimycotic mixture (Sigma-Aldrich, St. Louis, MO), and bovine insulin (5 µg/mL) (Sigma-Aldrich, St. Louis, MO).

5.2.3 *In Vitro* Antiproliferative Activity Assay

The CellTiter 96® AQueous One Solution Cell Proliferation Assay was used to determine the activity of each compound (please see reference Chapter 3 Section 3.2.5 Biological Assay and Data Processing, for details).

5.2.4 Colony Formation Assay in Soft Agar

B16-F1 melanoma cells were plated at a colony-forming density (2000 cells per well on six-well plates) on top of 0.8% base agar. Cells were grown in 0.4% agar together with DMEM medium supplemented with fetal bovine serum and an antibiotic-antimycotic solution at 37°C in an atmosphere of 95% air and 5% CO_2 (93). Cells were treated with compounds ABI-270, -274, and -288 at different concentrations (20, 100, and 500 nM). Compounds were added to the media from 1-mM DMSO stock solutions, and a corresponding dilution of DMSO was used as control. Cells were grown for 14 days. Plates were photographed, and the number of colonies was measured by Artek 880 Automated Colony Counter (Artek Systems Corporation, Farmingdale, NY).

5.2.5 Animals

Female C57BL/6NHsd mice, age 7-8 weeks, were obtained from Harlan Laboratories, Inc. (Indianapolis, IN). Male double homozygous SCID hairless outbred (SHO) mice, age 6-8 weeks, were obtained from Charles River Laboratories International, Inc. (Wilmington, MA). The laboratory housing the animals met all Association for Assessment and Accreditation and Laboratory Animal Care specifications. All of the

102

procedures were conducted in accordance with the guidelines of our Institutional Animal Care and Use Committee.

5.2.6 *In Vivo* Antitumor Study

For C57BL/6 mice, logarithmic growth phase B16-F1 (5×10^5) cells were injected subcutaneously (s.c.) in the right dorsal flank. For SHO mice, logarithmic growth phase A375 (5×10^7/mL) cells were prepared in phenyl red-free, FBS-free DMEM media and mixed at 1:1 ratio with Matrigel (BD Biosciences, San Jose, CA). Tumors were established by injecting 100 μL of this mixture subcutaneously in the right dorsal flank of each mouse (2.5×10^6 cells per mouse). When the tumor reached a mean size of 100~150 mm^3, mice were randomized into 4 groups for C57BL/6 mice and 3 groups for SHO mice and treatments were started. The formulation of Tween80/Captex200 (80/20) was used to prepare the compound solution. ABI-288 at 15 and 45 mg/kg was used for C57BL/6 mice with intraperitoneal (i.p.) injection once daily for 13 days. ABI-288 at 25 mg/kg was used for SHO mice with i.p. injection once daily for 31 days. Injection volume was 30 μL. The control group was given only a vehicle solution injection at the same frequency. DTIC was reconstituted with sterile water according to drug usage instructions, and 100 μL of this solution was given i.p. to each mouse.

Tumor volume was measured three times a week with a Traceable® electronic digital caliper (Fisher Scientific, Inc.) and calculated by using the formula $a\times b^2\times0.5$, where a and b represented the larger and smaller diameters, respectively (94). Tumor volume was expressed as cubic millimeters. Data were expressed as mean±SD for each group and plotted as a function of time. Tumor growth inhibition (TGI) at the conclusion of the experiments was calculated from the formula 100-100*[(T-T0)/(C-C0)] where T represented mean tumor volume of a treated group on a specific day, T0 represented mean tumor volume of the same group on the first day of treatment, C represented mean tumor volume of a control on a specific day, and C0 represented mean tumor volume of the same group on the first day of treatment (95, 134). Animal general activity and average body weight of each group were monitored during the entire experiment period to assess compound acute toxicity. The statistical significance of observed differences between growth curves was evaluated by Student's t test. At the end of treatment, all mice were euthanized by CO_2, and tumors were harvested for further study.

5.2.7 Cell Cycle Analysis

Flow cytometry analysis was performed as described elsewhere to study cell cycle phase distribution (95). A375 cells were cultured in 10 cm tissue culture dishes until the confluence was about 80%, and then cells were treated with 0, 10, 50, 200, and 1000 nM of colchicine, ABI-270, -278, and -288 for 24 h in growth media. Cellular DNA was stained with PBS containing 50 μg/mL propidium iodide and 100 μg/mL RNase A. The cell cycle was determined using a BD LSR-II cytometer (BD Biosciences, San Jose,

103

CA) with 10,000 cells scored. Data were analyzed and graphs were prepared using the Modfit 2.0 program (Verity Software House, Topsham, ME).

5.2.8 *In Vitro* Tubulin Polymerization Assay

Bovine brain tubulin (0.4 mg) (Cytoskeleton, Denver, CO) was mixed with 10 µM of tested compounds and incubated in 120 µL of general tubulin buffer (80 mM PIPES, 2.0 mM $MgCl_2$, 0.5 mM EGTA, pH 6.9, and 1 mM GTP). The absorbance of wavelength at 340 nm was monitored every 60 s for 15 min by the SYNERGY 4 Microplate Reader (Bio-Tek Instruments, Winooski, VT). The spectrophotometer was set at 37°C for tubulin polymerization.

5.2.9 Molecular Modeling

Dr. Li selected the crystal structure of N-deacetyl-N-(2-mercaptoacetyl)-colchicine (DAMA-colchicine) in tubulin complex (PDB code: 1SA0) which has been most widely used for modeling approaches (135-137). He used Schrodinger Molecular Modeling Suite 2009 (Schrodinger LLC, New York, NY) for the docking practice. ABIs were built and prepared using the Ligprep module, and they were docked into the colchicine binding site using the Glide module in Schrodinger Suite. The best docking complexes were subject to restricted molecular dynamics to release any strains by using Macromodel module with OPLS-2005 force field. The ligand and its surrounding residues within 15 Å were allowed to move freely, while residues outside the 15-Å radius were kept rigid.

5.2.10 Tubulin Colchicine Site Binding Assay

Biotin-labeled tubulin (0.5 µg/well) (Cytoskeleton, Inc., Denver, CO) was mixed with [3H]colchicine (0.08 µM) (PerkinElmer LLC., Shelton, CT) and various concentrations of tested compounds in 96-well plates. The mixture was incubated at 37°C in binding buffer [80 mM PIPES (pH 6.8), 1 mM EGTA, 10% glycerol, 1 mM $MgCl_2$, and 1 mM GTP] for 45 min with gentle shaking. At the end of incubation, Streptavidin-labeled SPA beads (80 µg/well) (GE-healthcare Bio-Sciences Corp., Piscataway, NJ) were added. Signals were read using a TopCount NXT scintillation counter (PerkinElmer LLC, Shelton, CT). IC_{50} values (concentrations that inhibited 50% of tritiated colchicine binding) were determined by nonlinear regression analysis with GraphPad Prism (GraphPad Software, San Diego,CA).

5.2.11 Microtubule Imaging Using Immunofluorescence Microscope

Cellomics Cytoskeleton rearrangement kit (Thermo Scientific, Rockford, IL) was used to get a visually appreciable proof of ABIs interacting with tubulin inside the cells.

104

WM-164 melanoma cells were treated with each compound for 18 h in duplicate using a collagen-coated 96-well plate (Becton Dickinson Labware, Bedford, MA). Then cells were fixed with 4% paraformaldehyde (Thermo Scientific, Rockford, IL) and permeabilized using permeabilization buffer supply from the kit. Primary antibody for tubulin and fluorescence-labeled secondary antibody were subsequently added to the cells. Cell nuclei were stained by DAPI. Whole Cell Stain Green was also applied to all cells. All images were acquired with an Olympus IX71 inverted fluorescence microscope (Olympus Corp., Tokyo, Japan) with overlays from separate images of tubulin (red), nuclei (blue), and whole cells (green). For comparison, I also included paclitaxel, colchicine and ABT-751, along with ABIs.

5.3 Results and Discussion

5.3.1 ABIs Have Great Potency on Melanoma Cell Lines

I tested ABI antiproliferative activity on three melanoma cell lines: A375, B16-F1, and WM-164. A375 and WM-164 are malignant human melanoma cell lines. B16-F1 is a pigment-producing mouse melanoma cell line. In order to thoroughly study the SAR for ABIs and look for the most efficacious compounds in this set, Mr. Jianjun Chen extensively modified the structure and synthesized 55 imidazole analogs. In this compound pool, I identified 29 active compounds that have IC_{50} values less than 10 μM on the three selected melanoma cell lines. (The synthesis and SAR of ABIs will be published in another chemistry-oriented article). Twelve very active compounds had IC_{50} values less than 100 nM. The most active one had IC_{50}s less than 10 nM on A375 and WM-164 cells. The structure of three representative compounds is shown in **Figure 5-1**. I compared our ABIs' activity with other anticancer drugs such as paclitaxel, vinblastine, colchicine, bortezomib, and ABT-751 (**Table 5-1**). Paclitaxel and vinblastine are clinically used anticancer drugs known to target cell tubulin (138, 139). Although colchicine is not an FDA-approved drug for cancer treatment, its prodrug, ZD6126, is in clinical trial for solid tumors (140). Bortezomib is the first therapeutic proteasome inhibitor and was approved in 2003 by the FDA for use in multiple myeloma (141). ABT-751 is known to target the tubulin colchicine binding site. It is a promising drug candidate in clinical trial for children with relapsed or refractory neuroblastoma(142).

From our results, the three representative ABIs showed great potency on all three tested melanoma cell lines with IC_{50}s all less than 80 nM. The best compound, ABI-274, was even more active than paclitaxel and colchicine on A375 and WM-164 cells. Its potency was very close to that of bortezomib. Compared with ABT-751, ABI-274 was about 60 times more potent (calculated by IC_{50} average of three melanoma cell lines). The great *in vitro* potency of the ABIs suggests that they are very good candidates for melanoma treatment.

Besides their great *in vitro* potency, another important improvement is that ABI-270 and ABI-288 do not have a trimethoxy group in their structure but retain good

Table 5-1. *In vitro* cytotoxic activity of representative ABI compounds and comparison with other anticancer drugs.

Compound name	$IC_{50} \pm SEM$ (nM) (n=3)		
	A375	B16-F1	WM-164
ABI-270	31±5	63±7	28±3
ABI-274	9±2	46±5	8±2
ABI-288	52±4	73±6	74±9
Paclitaxel	12±3	17±2	18±3
Vinblastine	1±0	5±1	1±0
Colchicine	20±3	29±5	10±2
Bortezomib	8±1	24±2	8±1
ABT-751	1111±108	2127±351	661±56

activity. The lack of a trimethoxy group differentiated them chemically from previous SMART compounds and colchicine, thereby overcoming the metabolic instability drawback of the trimethoxy group.
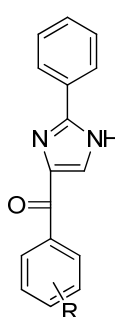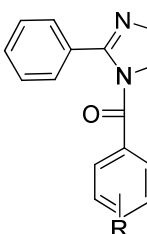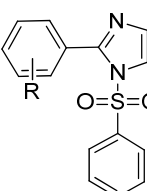
5.3.2 SAR Studies

5.3.2.1 SAR of Substitutions on the C Ring

Please see **Figure 5-1** for the designation of A, B, and C ring in ABI compounds. A variety of compounds (5aa-5ai) with an un-substituted A-ring and different C ring substituents generally showed moderate activity (**Table 5-2**), with IC_{50} values in the micromolar range (unless specified, the IC_{50} value for a specific compound discussed in the text is referred to as an average of all three cell lines). The most potent compound of this series was 5aa with an average IC_{50} value of 160 nM. The removal of one of the methoxy groups from the 3, 4, 5-trimethoxy on the C ring (5ad, 5ae) led to a significant loss of activity (IC_{50}>10 μM for 5ae and an IC_{50} of 3 μM for 5ad). This finding is consistent with results from SMART compounds in which the 3, 4, 5-trimethoxy substituted compound was most potent. It should be noted that the compound with 4-fluoro on the C ring (5af) also showed relatively good activity (IC_{50}=1 μM), a finding that has an important implication, because replacing the trimethoxy moiety with a 4-fluoro group may provide good activity and improved metabolic stability. Interestingly, the position of the fluorine on the C ring was critical for activity because a shift from 4-fluoro to 3-fluoro resulted in a total loss of activity (IC_{50}>10 μM for 5ag compared with 1 μM for 5af). This result suggested that a potential hydrogen bond donor is present close to the 4-position of this ring. As shown in the molecular modeling studies below, this hydrogen bond donor is likely to be the thiol group in Cys-241 in loop 7 of the β-subunit in α/β-tubulin dimer.

Other substituents such as methoxy and methyl at the 3 or 4 position on the C ring (5ab, 5ac, 5ah, 5ai) were also evaluated, but none showed good activity (IC_{50}>10 μM). As clearly indicated in **Table 5-2**, the positions of the A and C rings were critical. A simple shift of the C ring moiety from position 4 to position 1 in the imidazole ring (B ring resulted in total loss of activity (IC_{50}>10 μM for 5aba, 5aaa, 3a, 3x, 3j). This result is consistent with recent reports in which the position of the aryl group was found to be important for antiproliferative activity (143, 144). Bellina and co-workers reported potent antitumor activity for a series of 1, 5- and 1, 2-diaryl-1*H*-imidazole analogs. While the 1, 5-diaryl-imidazole analogs have nanomolar activity, a simple shift of the diaryl substitution from the 1, 5-position to 1, 2-position resulted in significantly lower activity down to the micromolar range (143). Similarly, Wang and co-workers reported that 4, 5-disubstituted and 1, 5-disubstituted imidazoles are much more active than the corresponding 1, 2-disubstituted imidazoles (144).

107

Table 5-2. *In vitro* cytotoxic activity of ABI compounds with B and C ring modification.

Structure	ID	R	IC$_{50}$±SEM (μM) (n=3)		
			A375	B16-F1	WM-164
	5aa	3,4,5-(OMe)$_3$	200±80 nM	100±12 nM	100±25 nM
	5ab	4-OMe	>10	>10	>10
	5ac	3- OMe	>10	>10	>10
	5ad	3, 5-(OMe)$_2$	3±1	5±1	2±0
	5ae	3, 4-(OMe)$_2$	>10	>10	>10
	5af	4-F	1±0	1±0	1±0
	5ag	3-F	>10	>10	>10
	5ah	4-Me	>10	>10	>10
	5ai	3-Me	>10	>10	>10
	5aba	4-OMe	>10	>10	>10
	5aaa	3,4,5-(OMe)$_3$	>10	>10	>10
	3a	H	>10	>10	>10
	3x	4-NO$_2$	>10	>10	>10
	3j	4-OBn	>10	>10	>10

108

5.3.2.2 SAR of Substitutions on the A Ring

Because compounds with 3, 4, 5-trimethoxy and 4-fluoro substitutions on the C ring showed good activity, a series of compounds was synthesized with fixed substitutions on the C ring (4-fluoro or 3, 4, 5-trimethoxy) and different substitutions on the A ring (**Table 5-3**). These compounds demonstrated excellent antiproliferative activity with IC_{50} values as low as 8 nM on WM-164 cell line (5da). In general, compounds incorporating a single substituent on the para-position of the A ring were more potent as can be seen from the activities of 5ca, 5cb, 5da, 5db, 5fa, 5fb, 5ga, and 5gb (IC_{50}=8~110 nM). 5db-HCl salt (IC_{50}=172 nM) showed slightly diminished activity compared with the corresponding free base 5db (IC_{50}=109 nM). Compound 5fb (IC_{50}=64 nM), with a single halogen substituent in the para-position of the A and C rings, demonstrated potent and was devoid of a methoxy moiety. Compounds with 3, 4, 5-trimethoxy substituents on the A ring lost activity completely (IC_{50}>10 μM for 5ea, 5eb), suggesting very different binding environments near the A ring and C ring. Removal of the 5-methoxy substituent from the A-ring improved activity significantly (IC_{50}=330 nM and >10 μM for 5ha, 5ea respectively). Demethylation of the 3, 4, 5-trimethoxy decreased activity sharply from 43 nM (5fa) to 4 μM (6fa). Similar results were observed for 6ea, 5ka, 5kb, and 6ha due to the demethylation of subsituents on either the A or C ring. Electron-donating groups (4-methoxy, 4-dimethylamino, 4-methyl) and electron-withdrawing groups (4-chloro, 2-trifluoromethyl) on the A ring did not show substantial differences in activity. The introduction of a trifluoromethyl group at the ortho position of the A ring caused complete loss of activity (IC_{50}>10 μM for 5ia, 5ib). The presence of a benzoloxy group at the para position of A ring (IC_{50}=75 nM for 5jb) resulted in a 440-fold increase in activity when compared with the para-hydroxy compound 5kb (IC_{50}=33 μM). It is worthwhile to note that compound 5jb, with the 4-fluoro in the C ring, has better activity than does its counterpart 5ja, which has a 3, 4, 5-trimethoxy group in the C ring (IC_{50} is 75 nM for 5jb, and 7 μM for 5ja).
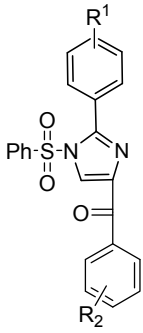
5.3.2.3 SAR of Additional Substitutions on the B Ring

To our surprise, some of the compounds with a phenylsulfonyl protection group attached to the nitrogen of the imidazole ring (4cb, 4db, 4fb, 4ga, 4gb, 4ha, 4jb) were also very active with IC_{50} in the nanomolar range (**Table 5-4**).Generally the activities of these compounds are comparable to their corresponding unprotected counterparts as exemplified by comparing the activities of 4cb (43 nM), 4db (111 nM), 4fb (72 nM), 4ga (285 nM), 4gb (87 nM), 4ha (268 nM), and 4jb (61 nM) with their corresponding unprotected counterparts 5cb (36 nM), 5db (109 nM), 5fb (64 nM), 5ga (131 nM), 5gb (72 nM), 5ha (330 nM), and 5jb (75 nM). Other compounds (4ab-4ag, 4ea, 4eb, 4hb, 4ia, and 4ib, 1-50 μM) were generally much less active, also in line with their counterparts (5ab-5ag, 5ea, 5eb, 5hb, 5ia, and 5ib, 1-50 μM).

109

Table 5-3. *In vitro* cytotoxic activity of ABI compounds with A ring modification.

Structure	ID	R^1	R^2	$IC_{50}\pm SEM$ (nM) (n=3)		
				A375	B16-F1	WM-164
	5ba	4-F	3,4,5-$(OMe)_3$	205±19	320±41	73±8
	5ca	4-OMe	3,4,5-$(OMe)_3$	30±5	108±12	31±4
	5cb	4-OMe	4-F	31±5	63±7	28±3
	5da	4-Me	3,4,5-$(OMe)_3$	9±2	46±5	8±2
	5db	4-Me	4-F	142±13	222±10	156±19
	5db-HCl			108±11	297±23	112±9
	5ea	3,4,5-$(OMe)_3$	3,4,5-$(OMe)_3$	4800	>10000	>10000
	5eb	3,4,5-$(OMe)_3$	4-F	>10000	>10000	>10000
	5fa	4-Cl	3,4,5-$(OMe)_3$	43±5	168±14	26±3
	5fb	4-Cl	4-F	52±4	73±6	74±9
	6fa	4-Cl	3,4,5-$(OH)_3$	3900	1810	2100
	5ga	4-$N(Me)_2$	3,4,5-$(OMe)_3$	82±9	361±29	80±11
	5gb	4-$N(Me)_2$	4-F	56±7	129±11	62±8
	5ha	3,4-$(OMe)_2$	3,4,5-$(OMe)_3$	113±14	1400±200	191±18
	5hb	3,4-$(OMe)_2$	4-F	10000	4210	1400
	5ia	2-CF_3	3,4,5-$(OMe)_3$	>10000	>10000	>10000
	5ib	2-CF_3	4-F	>10000	>10000	>10000
	6ea	3,4,5-$(OH)_3$	3,4,5-$(OH)_3$	>10000	>10000	>10000
	5ja	4-OBn	3,4,5-$(OMe)_3$	5200	10000	5500
	5jb	4-OBn	4-F	93±8	117±16	90±12
	5ka	4-OH	3,4,5-$(OMe)_3$	1600	2400	1800
	5kb	4-OH	4-F	10000	>10000	>10000
	6ha	3,4-$(OH)_2$	3,4,5-$(OH)_3$	>10000	>10000	>10000
	Colchicine			20±3	29±5	10±2

Table 5-4. *In vitro* cytotoxic activity of ABI compounds with protection on B ring.

Structure	ID	R^1	R^2	IC$_{50}\pm$SEM (nM) (n=3)		
				A375	B16-F1	WM-164
	4ab	H	4-OMe	>10000	>10000	>10000
	4ac	H	3-OMe	>10000	>10000	>10000
	4ah	H	4-Me	>10000	>10000	>10000
	4af	H	4-F	630±72	946±86	596±61
	4ag	H	3-F	>10000	>10000	>10000
	4cb	4-OMe	4-F	36±5	71±8	43±6
	4db	4-Me	4-F	113±14	287±31	107±14
	4ea	3,4,5-(OMe)$_3$	3,4,5-(OMe)$_3$	>10000	>10000	>10000
	4eb	3,4,5-(OMe)$_3$	4-F	3840	>10000	>10000
	4fb	4-Cl	4-F	88±9	107±12	70±6
	4ga	4-N(Me)$_2$	3,4,5-(OMe)$_3$	162±13	1200±90	308±32
	4gb	4-N(Me)$_2$	4-F	55±7	242±26	56±4
	4ha	3,4-(OMe)$_2$	3,4,5-(OMe)$_3$	192±15	970±68	139±15
	4hb	3,4-(OMe)$_2$	4-F	960±59	2000±400	1400±30
	4ia	2-CF$_3$	3,4,5-(OMe)$_3$	>10000	>10000	>10000
	4ib	2-CF$_3$	4-F	>10000	>10000	>10000
	4jb	4-OBn	4-F	64±7	110±15	48±5

111

5.3.3 ABIs Overcome Multi-Drug Resistance on Drug Resistant Melanoma Cells

Drug resistance is the major cause of cancer chemotherapy failure. One major contributor to multi-drug resistance is overexpression of P-glycoprotein (P-gp). This protein is a clinically important transporter protein belonging to the ATP-binding cassette family of cell membrane transporters. It can pump substrates including anticancer drugs out of tumor cells through an ATP-dependent mechanism (145). To test whether our ABIs could overcome P-gp-mediated multi-drug resistance, Dr. Li obtained one P-gp overexpressing human melanoma cell line, MDA-MB-435/LCCMDR1, and the matching sensitive parent cell line from Dr. Robert Clarke at Georgetown University. I then tested three representative compounds ABI-270, -274, and -288 on these two cell lines together with colchicine, paclitaxel, and vinblastine. The dose response curves are shown in **Figure 5-2.**The IC_{50} values and calculated resistance index are shown in **Table 5-5**. Big distance between two curves for paclitaxel, vinblastine, and colchicine means they were substrates for P-gp. The two curves of each ABI compound overlapped means they were not substrates for P-gp and overcame multi-drug resistance.

The results clearly showed that cell line MDA-MB-435/LCCMDR1 was very resistant to colchicine, paclitaxel, and vinblastine. But our ABIs showed equal potency to the drug resistant cell line and the sensitive parent cell line. This result strongly suggests that ABIs are not substrate for P-gp. Thus, they overcame the multi-drug resistance found in MDA-MB-435/LCCMDR1 cells. Note that ABI-274 has a resistance index of 3, meaning that MDA-MB-435/LCCMDR1 cells have some resistance to this compound. I believe that the reason may be that ABI-274 has a trimethoxy-phenyl group, which makes it partially chemically similar to colchicine.

5.3.4 ABIs Inhibit Melanoma Colony Formation in Soft Agar

Colony formation assay has been generally used to measure the sensitivity of tumors to anticancer drugs. Results reflect the therapeutic efficacy of a drug (146). To further measure ABIs' anti-melanoma efficacy, I tested ABI-270, -274, and -288 on melanoma colony formation in soft agar. Three different concentrations - 20, 100, 500 nM - were tested. Representative photos are shown in **Figure 5-3**. Quantified results are shown in **Figure 5-4**. After 14 days of incubation, about 130 detectable colonies (diameter larger than 100μm) were formed in controls (no treatment). Compounds ABI-270 and -274 effectively inhibited B16-F1 melanoma colony formation even at the lowest tested concentration, 20 nM ($p < 0.05$ compared with control). ABI-288 showed effective inhibition at 100 nM. All three tested compounds showed complete inhibition of colony formation at 0.5 μM, further proving ABIs' anti-melanoma efficacy.

5.3.5 ABIs Inhibited Melanoma Tumor Growth *In Vivo*

Encouraged by ABIs' good activity against melanoma cells and inhibition of melanoma colony formation in soft agar, *in vivo* anti-melanoma activity of ABIs was

الــمـــنارة للاستشارات

www.manaraa.com
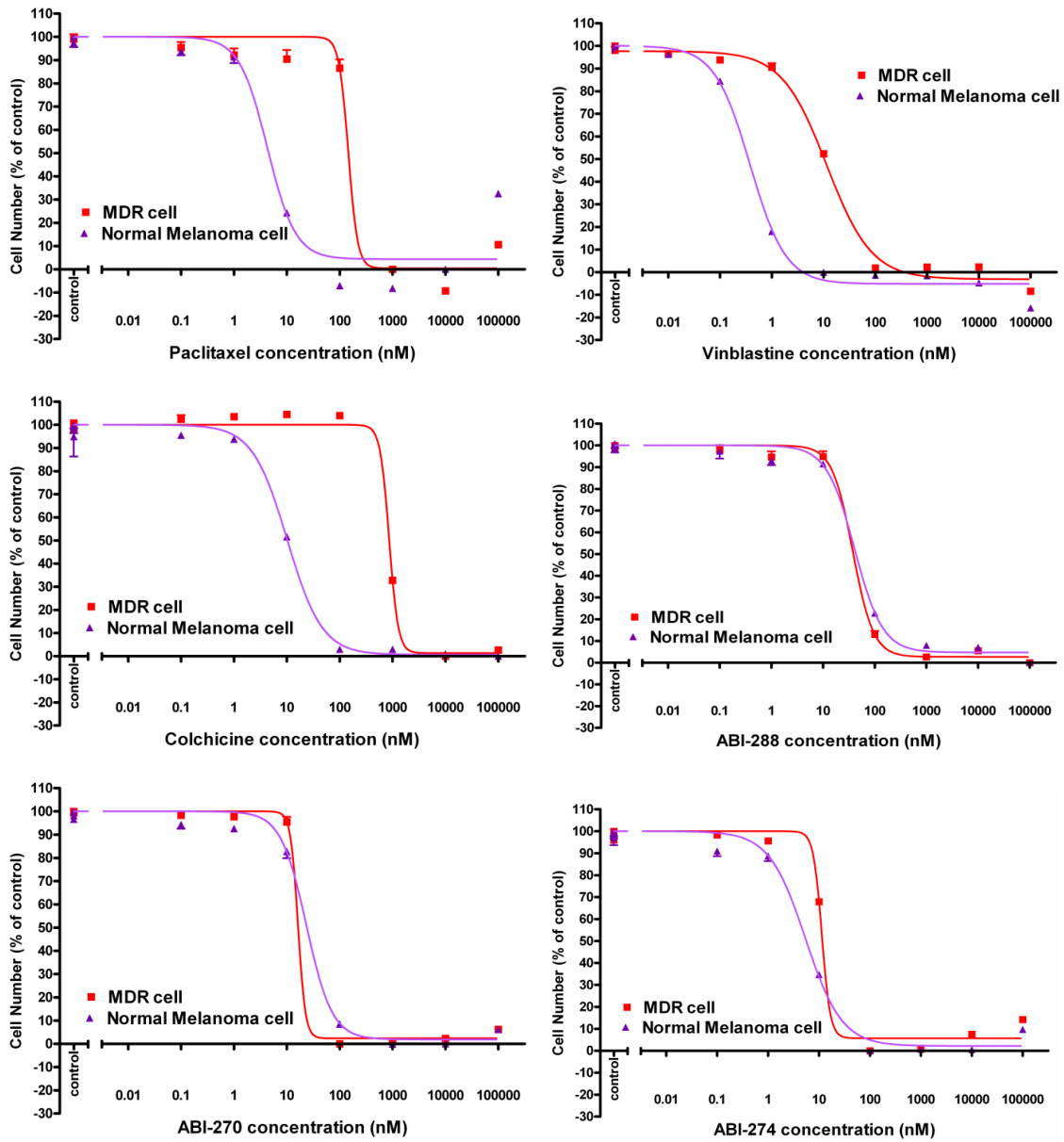
Figure 5-2. Dose-response curves showed ABI compounds overcome multi-drug resistance for melanoma compared with other anticancer drugs.

Table 5-5. *In vitro* cytotoxic activity comparison of ABI compounds with other anticancer drugs on multi-drug resistant melanoma cell line.

Compound name	$IC_{50}\pm SEM$ (nM) (n=3)		Resistance index (R)*
	MDA-MB-435	MDA-MB-435 /LCC6MDR1	
Colchicine	10±1	658±50	66
Paclitaxel	4±1	277±41	69
Vinblastine	400±100 pM	11±1	28
ABI-274	5±1	15±2	3
ABI-270	24±2	30±4	1
ABI-288	41±2	38±2	1

* Resistance indexes were calculated by dividing IC_{50} values on multi-drug resistant cell line MDA-MB-435/LCC6MDR1 by IC_{50} values on the matching sensitive parent cell line MDA-MB-435.

114
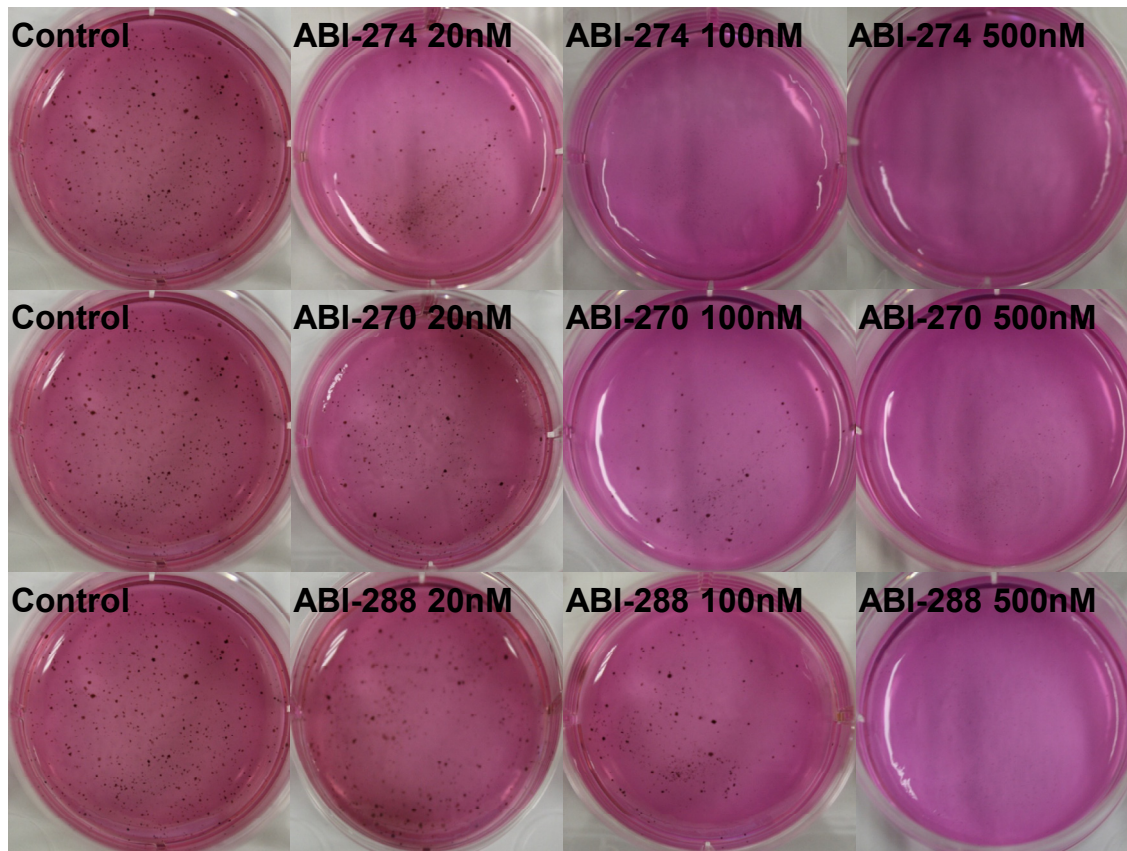
Figure 5-3. B16-F1 melanoma colony formation assay in soft agar for ABI compounds. Compounds ABI-270 and 274 effectively inhibited B16-F1 melanoma colony formation even at the lowest tested concentration 20 nM ($p<0.05$ compared with control). ABI-288 showed effective inhibition at 100 nM. All three tested compounds showed complete inhibition for colony formation at 0.5 μM.
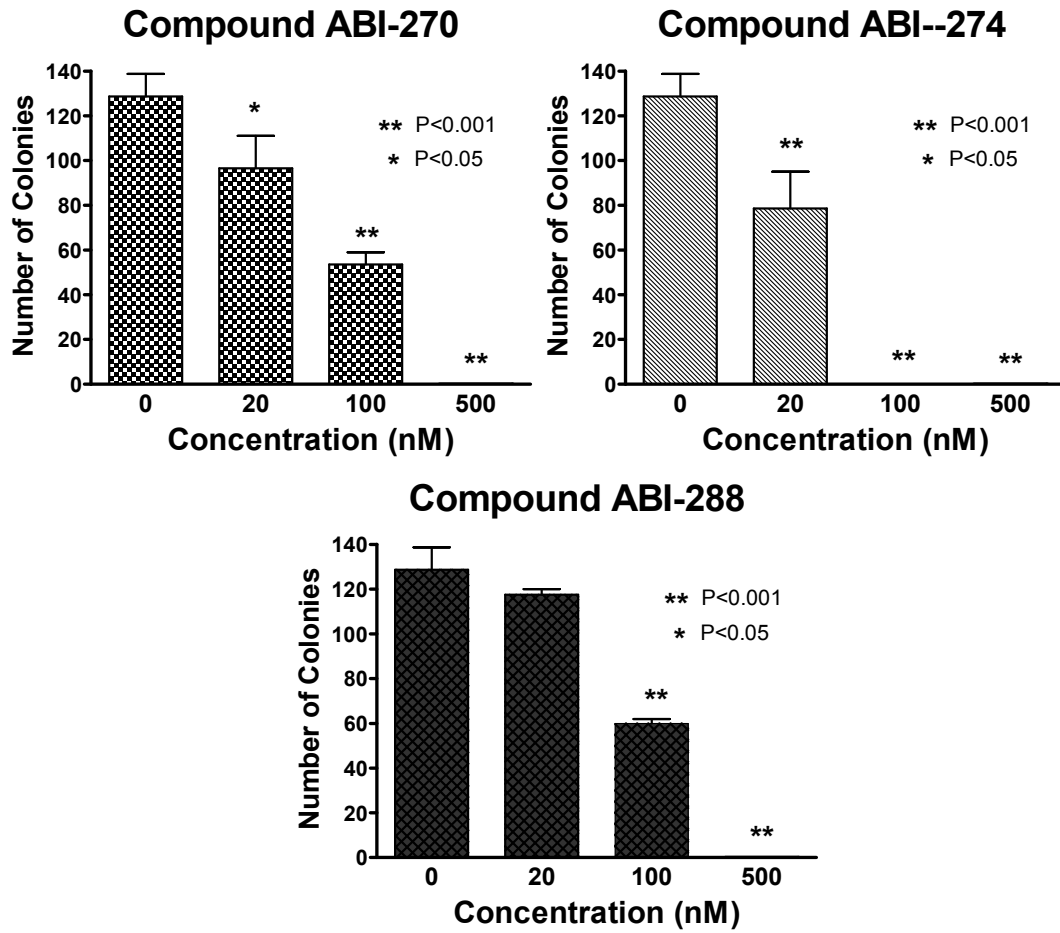
Figure 5-4. Quantified representation of colony formation assay using colony counter.
*p<0.05 compared with control. **p<0.001 compared with control.

tested. Compound ABI-288 was chosen because it does not have a trimethoxy group and its solubility is better than that of the others. Based on our previous study experience, two dose levels, 15 and 45 mg/kg, were chosen. DTIC at 60 mg/kg was used as a positive control according to the literature (109). B16-F1 melanoma allograft model on C57BL/6 mice was first chosen for study. After 13 days of treatment (**Figure 5-5**), ABI-288 inhibited melanoma tumor growth (TGI value) by 32% at 15 mg/kg and 82% at 45 mg/kg. Student's *t* test p value of ABI-288 at 45 mg/kg compared with control was less than 0.001, indicating a significant difference. The *t* test p value of ABI-288 at 15 mg/kg compared with control was 0.08, suggesting that this dose was not effective. Comparing ABI-288 at 45 mg/kg with DTIC at 60 mg/kg, which had a TGI of 51%, the *t* test p value was about 0.001, suggesting that ABI-288 had substantially better activity than did DTIC. I also observed a continuous average body weight loss in the ABI-288 45 mg/kg treatment group. For the control and ABI-288 15 mg/kg treatment groups, average body weight increased slightly throughout the experiment period.

To further confirm ABIs' *in vivo* activity, A375 human melanoma xenograft model on SHO mice was used, and ABI-288 at 25 mg/kg was tested. DTIC at a dose of 60 mg/kg was used as a positive control again. After 31 days of treatment (**Figure 5-6**), ABI-288 inhibited melanoma tumor growth (TGI value) by 69%, whereas DTIC inhibited growth by 52%. The *t* test p value of ABI-288 treatment versus control was less than 0.001, suggesting that ABI-288 significantly inhibited melanoma tumor growth at 25 mg/kg. The *t* test p value of ABI-288 treatment versus DTIC was less than 0.05, suggesting again that ABI-288 had better activity than did DTIC. Average body weight of all groups increased slightly throughout the experiment period. Physical activities for the mice also looked normal, suggesting that 25 mg/kg was a well tolerated dose for SHO mice.

5.3.6 ABIs Target Cell Tubulin at the Colchicine Binding Site

The cellular target of ABIs was determined by the following five experiments.

5.3.6.1 Cell Cycle Analysis

After identifying the great anti-melanoma potency of ABIs and their capability for overcoming multi-drug resistance, our next goal was to determine the cellular target of this class of compounds. Based on their high potency and behavior similarity with other tubulin binding agents on melanoma cells, I hypothesized that these compounds may also target tubulin. If our hypothesis were right, ABIs should arrest cells in the G2/M phase, so I did a cell cycle analysis. I tested ABI-270, -274, and -288 together with colchicine as a positive control on A375 cells. Four different concentrations - 10, 50, 200, and 1000 nM - of each compound were chosen to show the dose effect (**Figure 5-7** and **Figure 5-8**). For controls (no treatment) without interference, about 16% of A375 cells were distributed in the G2/M phase. For the colchicine treatment group, as concentration increased from 10 nM to 50 nM, the percentage of cells distributed in the G2/M phase

117
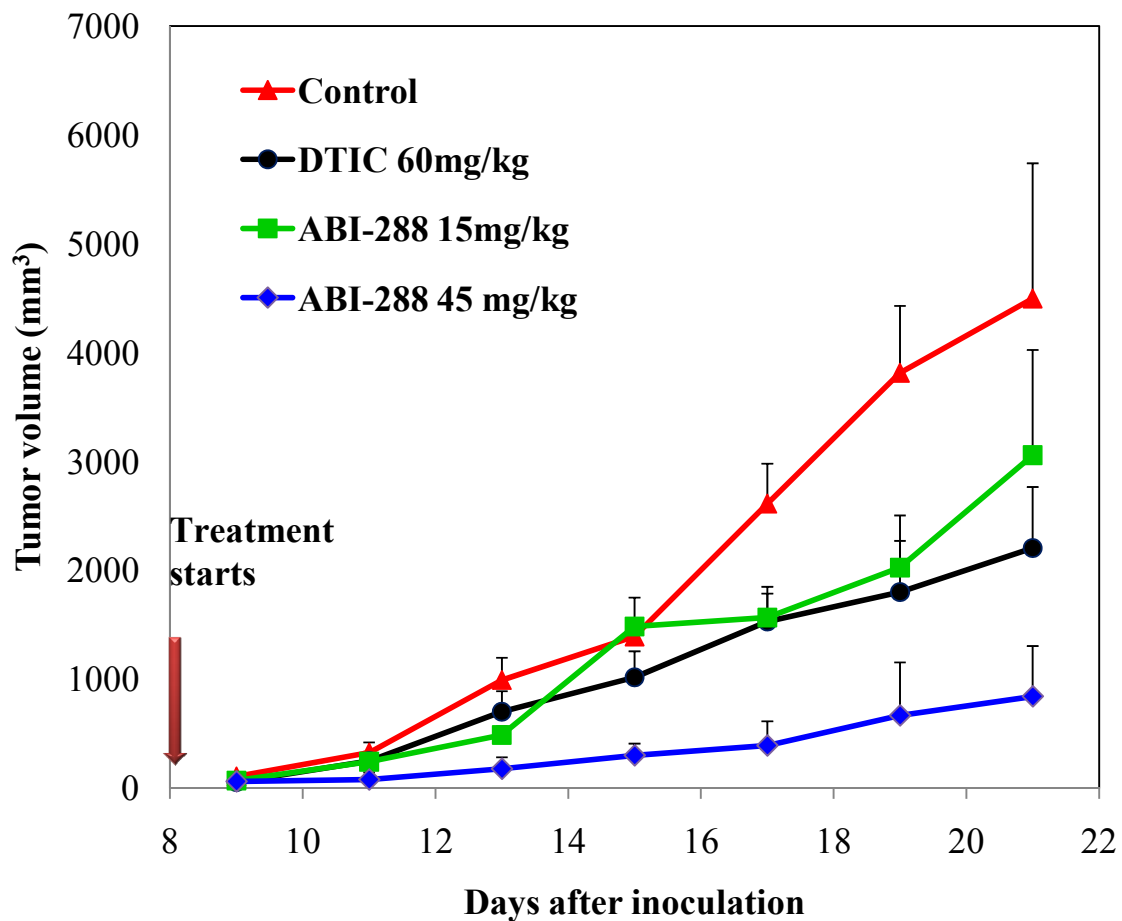
Figure 5-5. *In vivo* studies on C57BL/6 mice bearing B16-F1 melanoma allograft for ABI-288.

ABI-288 inhibited melanoma tumor growth in a dose-dependent manner. Each mouse received 0.5×10^6 cells by s.c. injection into the flank. 30 µL i.p. daily treatments were started when tumor size reached ~100 mm^3. Control, vehicle solution only; points, means; bars, SD. n=5 per group.

118
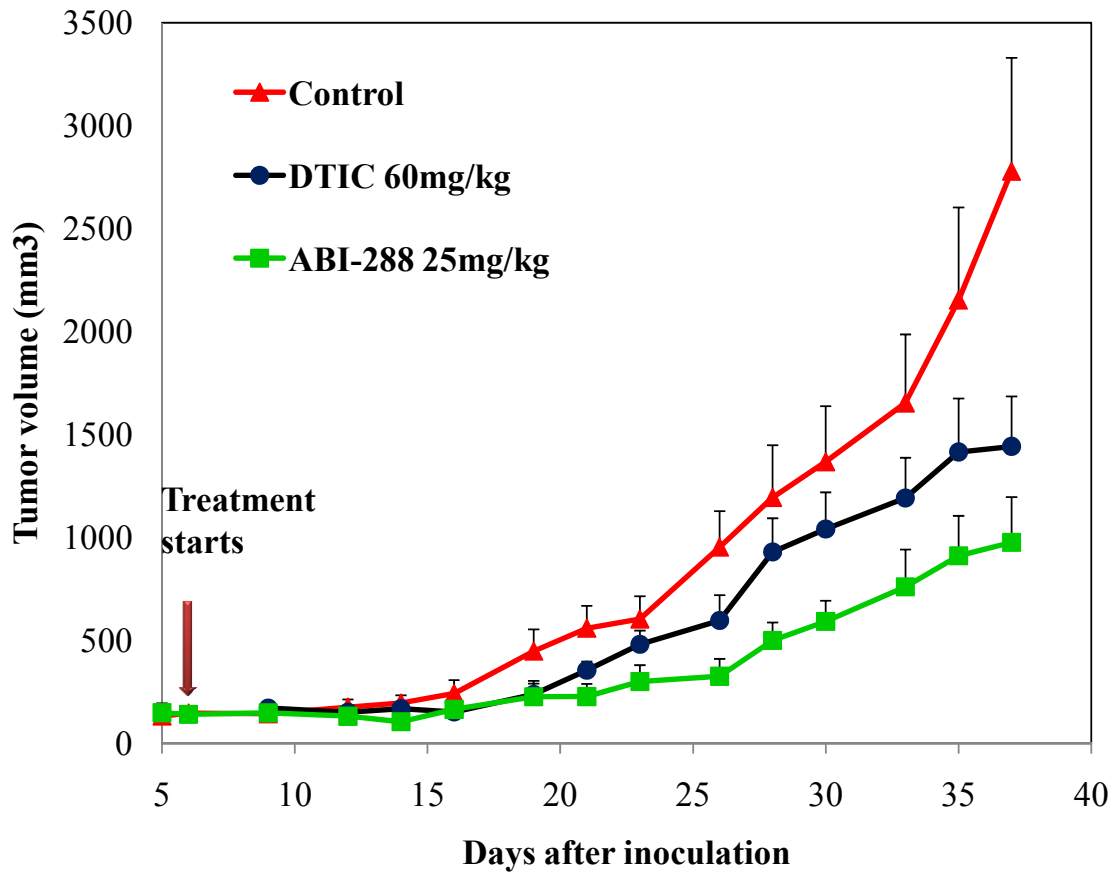
Figure 5-6. *In vivo* studies on SHO nude mice bearing A375 human melanoma xenograft for ABI-288.
ABI-288 inhibited melanoma tumor growth in a dose-dependent manner. Each mouse received 2.5×10^6 cells by s.c. injection into the flank. 30 µL i.p. daily treatments were started when tumor size reached ~150 mm^3. Control, vehicle solution only; points, means; bars, SD. n=5 per group.

119
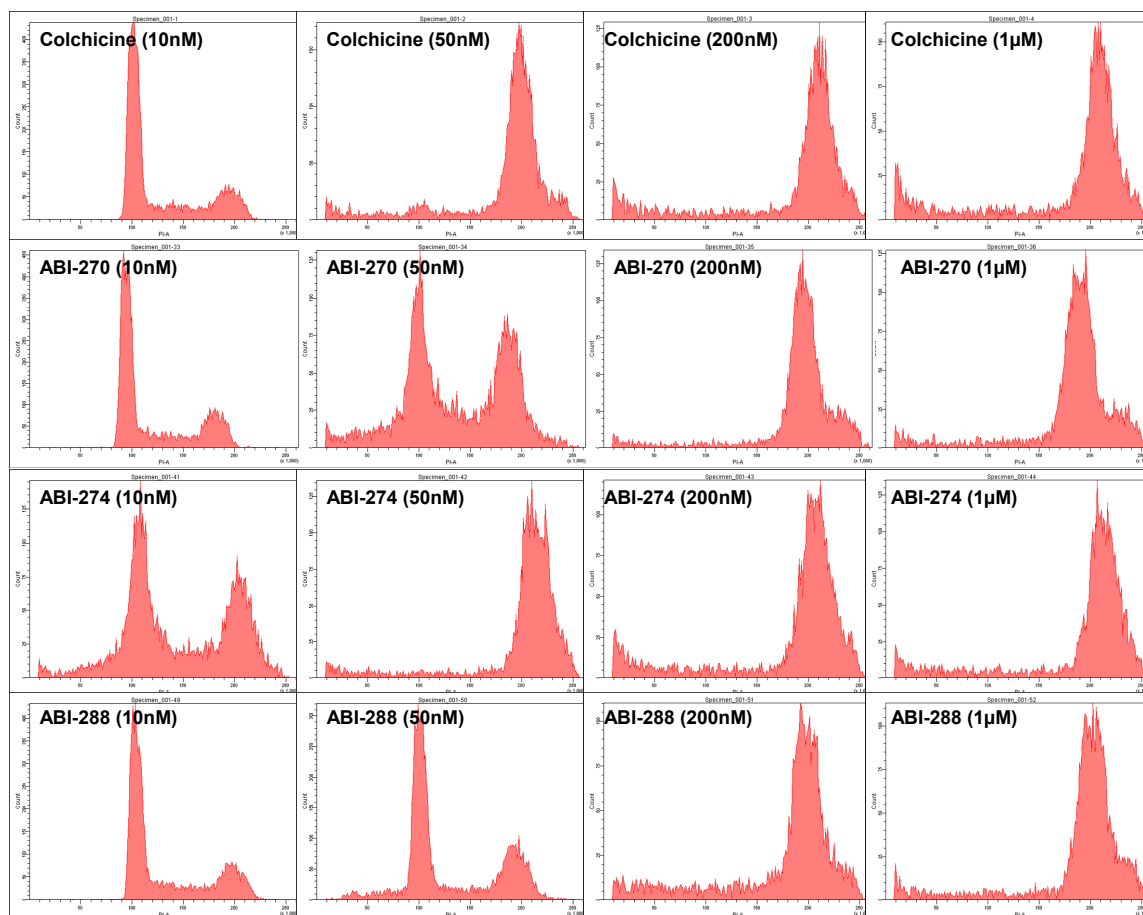
Figure 5-7. Cell cycle analysis of A375 cells after incubation with ABI compounds and colchicine.

Colchicine arrested most cells into G2/M phase starting from 50 nM. ABI-270, 274, and 288 also arrested most cells into G2/M starting from 200, 50, and 200 nM respectively.
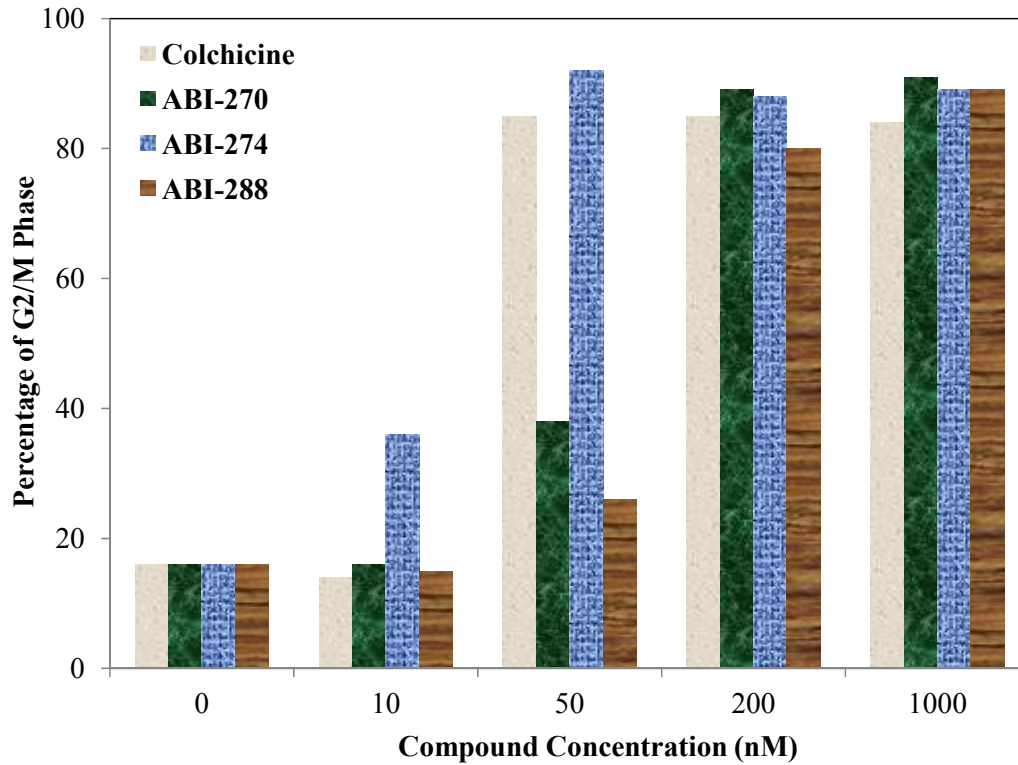
Figure 5-8. Quantified graphic depiction of cell cycle analysis.
ABI-274 showed greater potency than colchicine in arresting cells into G2/M phase.
Although ABI-270 and 288 showed lower potency, they also arrested most cells into
G2/M phase at higher concentration.

increased from 14% to 85%. ABIs had similar results for A375 cells, in arresting them in the G2/M phase in a dose-dependent manner. The potency of the different concentrations in arresting cells in the G2/M phase positively correlated with *in vitro* activity.

5.3.6.2 *In Vitro* Tubulin Polymerization Assay

The findings of the cell cycle analysis strongly supported our hypothesis and guided us to test ABIs' direct effect on tubulin polymerization. I conducted an *in vitro* tubulin polymerization assay by using purified bovine brain tubulin monomer (**Figure 5-9**). Three tested compounds - ABI-270, -274, and -288 - all showed a strong inhibitory effect on tubulin polymerization. At a concentration of 10 µM and 15 min of incubation, the compounds inhibited tubulin polymerization to 17%, 3%, and 22%, respectively, compared with control (5% DMSO was used in controls as a promoter for tubulin polymerization and to compensate DMSO usage in compound testing). This microtubule destabilization effect was similar to that of colchicine and vinblastine but was opposite to that of paclitaxel. The results not only confirmed that ABIs can directly interact with tubulin but also suggested that they may share the same binding site with colchicine or vinblastine. Our next goal was to determine the exact binding site for our compounds.

5.3.6.3 Molecular Modeling

Based on the structure similarity of ABI compounds with colchicine and using molecular modeling techniques, Dr. Li first tested whether our compounds could bind to the colchicine binding site on tubulin (147, 148). All three compounds showed excellent docking scores and their binding poses overlaps with the native ligand very well. As an example, the binding mode of ABI-288 (stick model) is shown in **Figure 5-10**. For comparison, he also displayed the native ligand DAMA-colchicine as a wire model in the α/β-tubulin heterodimer. The overall structure of ABI-288 and DAMA-colchicine overlapped very well. The *p*-Fluoro phenyl moiety overlaps with the trimethoxylpheny moiety which is interacting with the T7 loop in the β-subunit. Similarly, the *p*-Chloro phenyl moiety occupies the other side of the pocket where the seven-member ring of the DAMA-colchicine is, with the chlorine atom occupying the pocket where the methoxy moiety interacts. This exciting finding encouraged us to search further for more solid experimental proof to confirm the binding.

5.3.6.4 Tubulin Colchicine Site Binding Assay

After comparison, rapid [3H]colchicine competition-binding scintillation proximity assay (SPA) was chosen to confirm the binding site and to measure binding affinity (131). This method uses SPA technology and requires a close association between a solid-phase scintillant (the beads) and the radioligand for a signal to be emitted and subsequently detected. Biotin tubulin was the reagent that brings the radioligand and the scintillant into close association. When using tritiated colchicine as radioligand, the

122
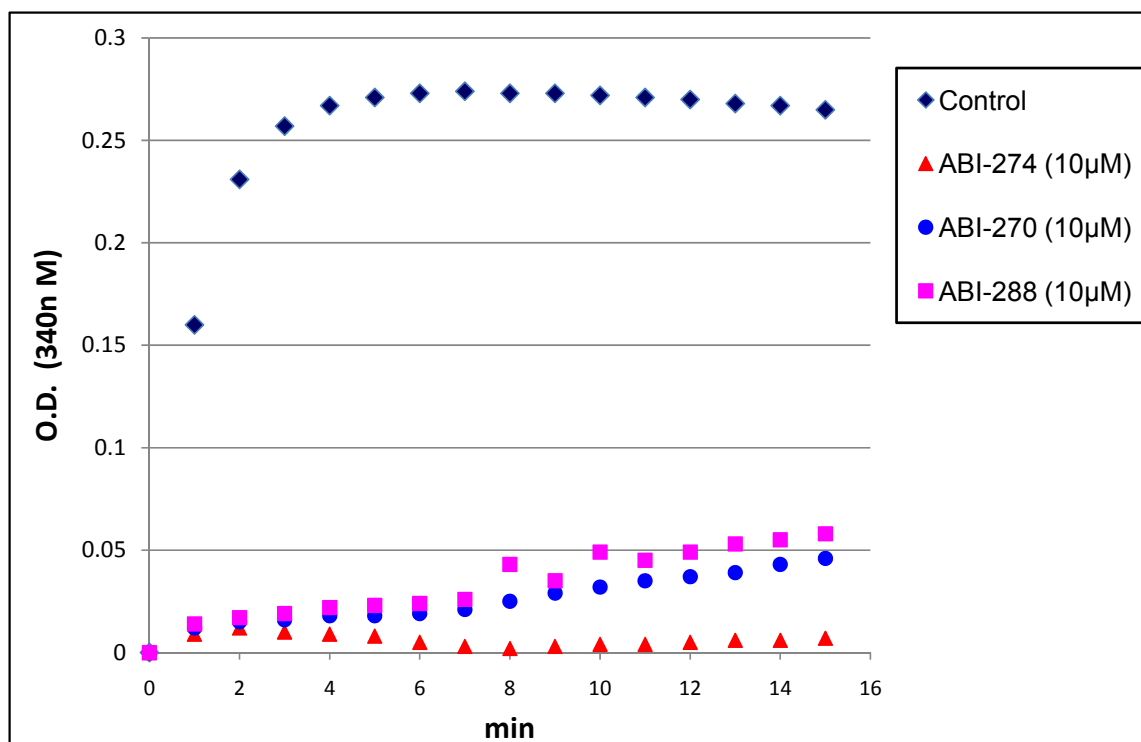
Figure 5-9. Three representative ABI compounds inhibited *in vitro* tubulin polymerization at a concentration of 10 μM.
After 15 min incubation, ABI-274, 288, and 270 inhibited tubulin polymerization to 3%, 17%, and 22% respectively compared with control (5% DMSO in general tubulin buffer). This experiment was done by Mr. Chien-Ming Li, Division of Pharmaceutics, College of Pharmacy, the Ohio State University.

123
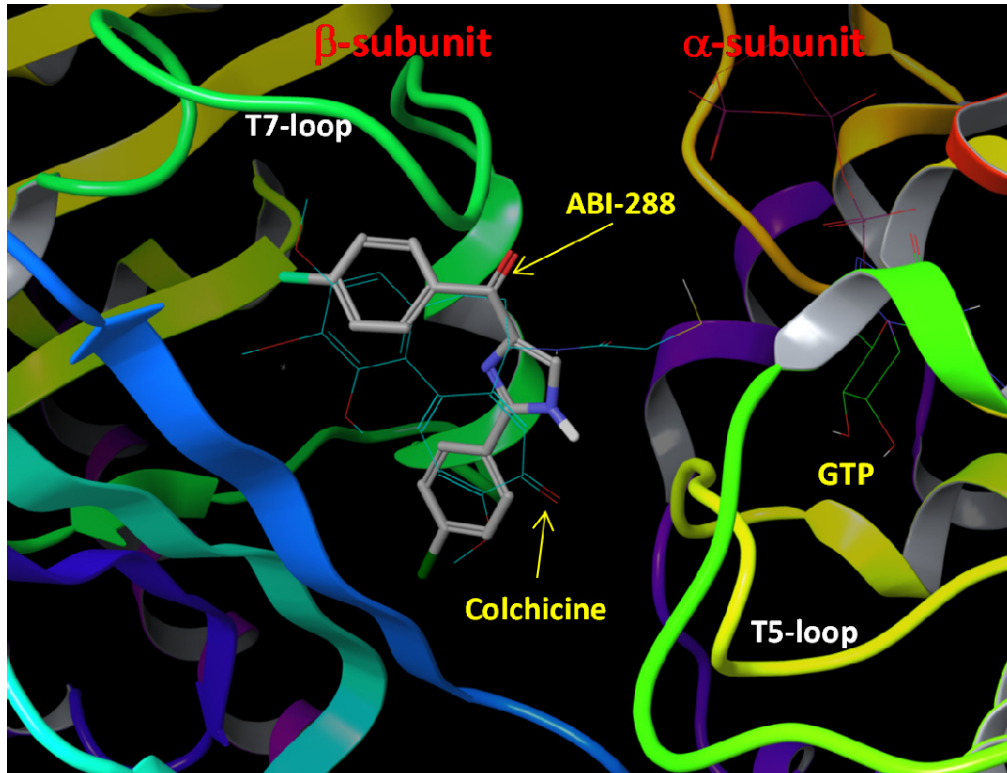
Figure 5-10. Docking of ABI-288 into tubulin crystal structure at the colchicine binding pocket.
Only the related secondary structures in tubulin are shown; ABT-751 is shown as a wire model. The overall structure of ABI-288 and ABT-751 overlapped very well in the binding pocket. The multiple interactions between ABI-288 and tubulin dimer suggested that this compound may have high binding affinity to this pocket. This experiment was done by Dr. Wei Li.

amplitude of signal was proportional to the number of colchicine binding sites that were occupied by this radioligand. When adding a competitor of radio-labeled colchicine, *e.g.*, cold (unlabeled) colchicine, to the mixture, the signal amplitude decreased proportionately with the concentration of the competitor. This method is very specific for tubulin colchicine site binding competitors.

The binding graph (**Figure 5-11**) clearly shows that ABIs can competitively bind to the tubulin colchicine binding site. As the concentration of the three tested compounds increased from 0.03 µM to 100 µM, increased tritiated colchicine was competitively stripped away from tubulin and emitted lower SPA counts. The negative control, paclitaxel, gave only a flat line, because theoretically it should not bind to the colchicine binding site on tubulin. Second, ABIs have relatively high binding affinity to the tubulin colchicine binding site (**Table 5-6**). GraphPad Prism calculated IC_{50} values for binding showed that ABI-274 has the highest binding affinity among the three tested compounds. Its binding affinity was even higher than that of colchicine. The other two compounds, ABI-270 and ABI-288, showed a little lower affinity to this site than did the natural ligand colchicine, but they were still very close. Third, the binding affinity was positively correlated to *in vitro* anti-melanoma activity; the higher the binding affinity, the higher the anti-melanoma activity.

According to the Cheng-Prusoff equation, $Ki=IC_{50}/(1+D/Kd)$, where Ki is the inhibition constant, D is the concentration of the radioligand, the Kd is the dissociation constant of the radioligand to tubulin (149). In our experiment, the D value was 0.08 µM, and the Kd value was around 1 µM according to the literature (131). So the IC_{50} was very close to the Ki value. Our result was comparable with the Ki value reported in the literature for colchicine binding to tubulin.

5.3.6.5 Microtubule Imaging Using Immunofluorescence Microscope

To obtain visual proof of ABIs interacting with tubulin inside the cells, I examined microtubule arrangement in human melanoma WM-164 cells upon treatment with different compounds (**Figure 5-12**). The microtubule images clearly showed that all five tested compounds resulted in cytoskeleton rearrangement. There was a significant difference between paclitaxel and the other four compounds (colchicine, ABT-751, ABI-270, and 274). Treatment with paclitaxel resulted in a condensation of microtubules orderly lying around the nuclei compared with controls, consistent with its mechanisms of action for stabilizing microtubules. On the contrary, treatment with colchicine, ABT-751, ABI-270, or 274 had similar effects on microtubules and resulted in some degree of microtubule fragmentation, consistent with their common mechanism of action for destabilizing microtubules. These results also confirmed that ABIs shared the same cellular target with colchicine and induced the same cellular effect.

125
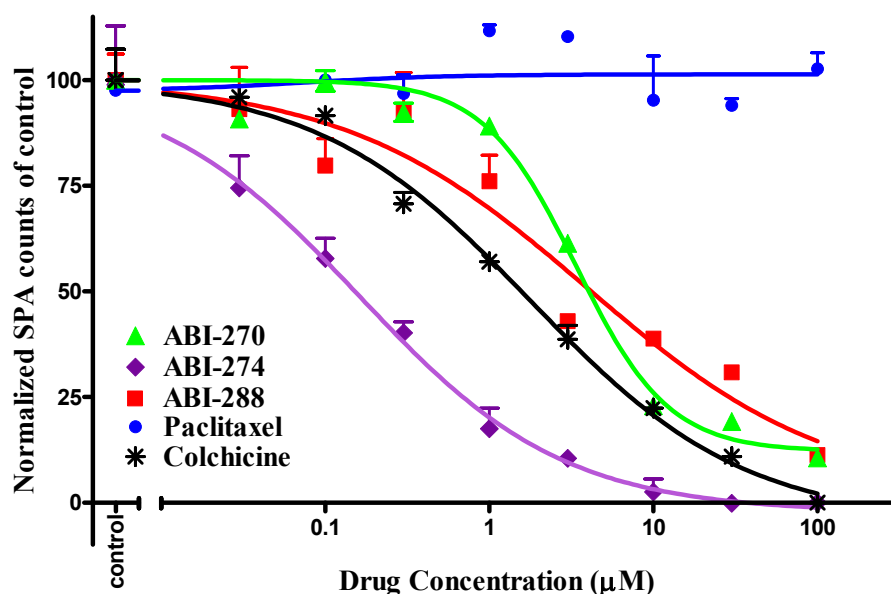
Figure 5-11. [3H]colchicine competition-binding assay confirmed ABI compounds competitively bound to tubulin at the colchicine binding site.
As concentration of these compounds increased from 0.03 µM to 100 µM, more and more tritiated colchicine were competitively stripped away from tubulin. Thus gave out lower and lower SPA counts. The negative control paclitaxel just gave out a flat line because it didn't bind to the colchicine binding site on tubulin. Each data point represents an average of three replicates.

Table 5-6. Comparison of tubulin binding affinity and *in vitro* cytotoxic activity between ABI compounds and known tubulin interacting drugs.

Compound name	IC$_{50}$±SEM (n=3)	
	For tubulin binding (µM)	On A375 (nM)
ABI-270	3±2	31±5
ABI-274	200±100 nM	9±2
ABI-288	4±2	52±4
Colchicine	2±1	20±3
Paclitaxel	N/A	12±3

N/A: not available

126
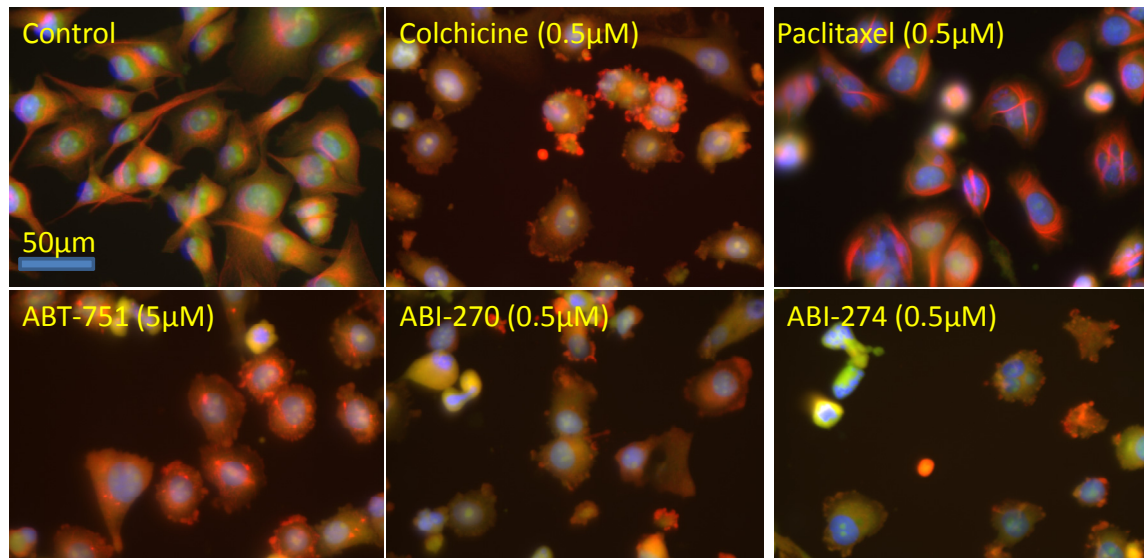
Figure 5-12. Microscopic images of immunofluorescence labeled microtubules inside melanoma cells after compounds treatment.

Treatment with paclitaxel resulted in condensation of microtubules nicely laying around the nuclei compared with control, consistent with its mechanisms of action for stabilizing microtubules. On the contrary, treatment with colchicine, ABT-751, ABI-270 or -274 all had similar effect on microtubules, and resulted in some degree of microtubule fragmentations, consistent with their common mechanism of action for destabilizing microtubules.

127

5.4 Conclusions

Our team synthesized a set of novel 2-aryl-4-benzoyl-imidazole (ABI) derivatives that showed potent activity in a number of melanoma cell lines, as well as in a xenograft model. The compounds inhibited tubulin polymerization by binding to the colchicine binding site. Structure-activity-relationships were investigated by introducing different substituents into the A and C rings. Compared with the earlier SMART compounds, ABI analogs showed two improvements. Firstly, ABI compounds showed much better resistance index (1) compared with colchicine (66), paclitaxel (69), and vinblastine (28). The fact that ABIs can overcome multi-drug resistance suggests a promising future development of more drug-like agents. Secondly, our in *vivo* study showed that compound ABI-288 at a dose of 25 mg/kg gave better tumor suppression than that of DTIC at a dose of 60 mg/kg.

LIST OF REFERENCES

1.   Li G, Satyamoorthy K, Herlyn M. Dynamics of cell interactions and communications during melanoma development. Crit Rev Oral Biol Med 2002;13:62-70.

2.   Halaban R. The regulation of normal melanocyte proliferation. Pigment Cell Res 2000;13:4-14.

3.   Miller AJ, Mihm MC. Melanoma. N Engl J Med 2006;355:51-65.

4.   Gray-Schopfer V, Wellbrock C, Marais R. Melanoma biology and new targeted therapy. Nature 2007;445:851-7.

5.   Jemal A, Thomas A, Murray T, *et al*. Cancer statistics, 2002. Cancer J Clin 2002;52:23-47.

6.   Vries E, Bray FI, Coebergh JW, *et al*. Changing epidemiology of malignant cutaneous melanoma in Europe 1953-1997: rising trends in incidence and mortality but recent stabilizations in western Europe and decreases in Scandinavia. Int J Cancer 2003;107:119-26.

7.   Ries L, Melbert D, Krapcho M, *et al*. SEER cancer statistics review, 1975-2005. Bethesda: National Cancer Institute; 2008.

8.   Lucas R. Global burden of disease of solar ultraviolet radiation, environmental burden of disease series. News release. Report No. 13. World Health Organization; 2006.

9.   Williams DA, Lemke TL, editors. Foye's principles of medicinal chemistry. 6th ed. Philadelphia: Lippincott Williams & Wilkins; 2007.

10.   Falkson CI, Ibrahim J, Kirkwood JM, *et al*. Phase III trial of dacarbazine versus dacarbazine with interferon alpha-2b versus dacarbazine with tamoxifen versus dacarbazine with interferon alpha-2b and tamoxifen in patients with metastatic malignant melanoma: an eastern cooperative oncology group study. J Clin Oncol 1998;16:1743-51.

11.   Chapman PB, Einhorn LH, Meyers ML, *et al*. Phase III multicenter randomized trial of the dartmouth regimen versus dacarbazine in patients with metastatic melanoma. J Clin Oncol 1999;17:2745-51.

12.   Eggermont AM, Kirkwood JM. Re-evaluating the role of dacarbazine in metastatic melanoma: what have we learned in 30 years? Eur J Cancer 2004;40:1825-36.

129

13. Smith FO, Downey SG, Klapper JA, *et al*. Treatment of metastatic melanoma using interleukin-2 alone or in conjunction with vaccines. Clin Cancer Res 2008;14:5610-8.

14. Riker AI, Radfar S, Liu S, *et al*. Immunotherapy of melanoma: a critical review of current concepts and future strategies. Expert Opin Biol Ther 2007;7:345-58.

15. Quan W, Brick W, Vinogradov M, *et al*. Repeated cycles with 72-hour continuous infusion interleukin-2 in kidney cancer and melanoma. Cancer Biother Radiopharm 2004;19:350-4.

16. Kiessling R, Wasserman K, Horiguchi S, *et al*. Tumor-induced immune dysfunction. Cancer Immunol Immunother 1999;48:353-62.

17. Jacinto FV, Esteller M. MGMT hypermethylation: a prognostic foe, a predictive friend. DNA Repa (Amst) 2007;6:1155-60.

18. Newlands ES, Blackledge GR, Slack JA, *et al*. Phase I trial of temozolomide (CCRG 81045: M&B 39831: NSC 362856). Br J Cancer 1992;65:287-91.

19. Middleton MR, Grob JJ, Aaronson N, *et al*. Randomized phase III study of temozolomide versus dacarbazine in the treatment of patients with advanced metastatic malignant melanoma. J Clin Oncol 2000;18:158-66.

20. Strumberg D, Richly H, Hilger RA, *et al*. Phase I clinical and pharmacokinetic study of the novel raf kinase and vascular endothelial growth factor receptor inhibitor BAY 43-9006 in patients with advanced refractory solid tumors. J Clin Oncol 2005;23:965-72.

21. Ahmad T, Pyle L, James M, *et al*. BAY 43-9006 in patients with advanced melanoma: the royal marsden experience. J Clin Oncol 2004;22:7506.

22. Eisen T, Ahmad T, Flaherty KT, *et al*. Sorafenib in advanced melanoma: a phase II randomised discontinuation trial analysis. Br J Cancer 2006;95:581-6.

23. Flaherty KT, Brose BM, Schucter L, *et al*. Phase I/II trial of BAY 43-9006, carboplatin (C) and paclitaxel (P) demonstrates preliminary antitumor activity in the expansion cohort of patients with metastatic melanoma. J Clin Oncol 2004;22:7507.

24. Herlyn M. Recent development in melanoma research (review on literature). Soci Mela Res News 2007;4:3-5.

25. Atkins MB. The treatment of metastatic melanoma with chemotherapy and biologics. Curr Opin Oncol 1997;9:205-13.

130

26. Evans LM, Casper ES, Rosenbluth R. Phase II trial of carboplatin in advanced malignant melanoma. Cancer Treat Rep 1987;71:171-2.

27. Gogas HJ, Kirkwood JM, Sondak VK. Chemotherapy for metastatic melanoma: time for a change? Cancer 2007;109:455-64.

28. Boaziz C, Breau JL, Morere JF, *et al*. Brain metastases of malignant melanomas. Bull Cancer 1991;78:347-53.

29. Quagliana JM, Stephens RL, Baker LH, *et al*. Vindesine in patients with metastatic malignant melanoma: a southwest oncology group study. J Clin Oncol 1984;2:316-9.

30. Bedikian AY, Weiss GR, Legha SS, *et al*. Phase II trial of docetaxel in patients with advanced cutaneous malignant melanoma previously untreated with chemotherapy. J Clin Oncol 1995;13:2895-9.

31. Avril MF, Bonneterre J, Delaunay M, *et al*. Combination chemotherapy of dacarbazine and fotemustine in disseminated malignant melanoma, experience of the french study group. Cancer Chemother Pharmacol 1990;27:81-4.

32. Fletcher WS, Green S, Fletcher JR, *et al*. Evaluation of cisplatin and DTIC combination chemotherapy in disseminated melanoma: a southwest oncology group study. Am J Clin Oncol 1988;11:589-93.

33. Vorobiof DA, Sarli R, Falkson G. Combination chemotherapy with dacarbazine and vindesine in the treatment of metastatic malignant melanoma. Cancer Treat Rep 1986;70:927-8.

34. Legha SS, Ring S, Papadopoulos N, *et al*. A prospective evaluation of a triple-drug regimen containing cisplatin, vinblastine, and dacarbazine (CVD) for metastatic melanoma. Cancer 1989;64:2024-9.

35. Prete SA, Maurer LH, O'Donnell J, *et al*. Combination chemotherapy with cisplatin, carmustine, dacarbazine, and tamoxifen in metastatic melanoma. Cancer Treat Rep 1984;68:1403-5.

36. Flaherty LE, Liu PY, Unger J, *et al*. Comparison of patient characteristics and outcome between a single-institution phase II trial and a cooperative-group phase II trial with identical eligibility in metastatic melanoma. Am J Clin Oncol 1997;20:600-4.

37. Liu YJ. IPC: professional type 1 interferon-producing cells and plasmacytoid dendritic cell precursors. Annu Rev Immunol 2005;23:275-306.

38. Moschos SJ, Edington HD, Land SR, *et al*. Neoadjuvant treatment of regional stage IIIB melanoma with high-dose interferon alfa-2b induces objective tumor regression in association with modulation of tumor infiltrating host cellular immune responses. J Clin Oncol 2006;24:3164-71.

39. Kirkwood JM, Strawderman MH, Ernstoff MS, *et al*. Interferon alfa-2b adjuvant therapy of high-risk resected cutaneous melanoma: the eastern cooperative oncology group trial EST 1684. J Clin Oncol 1996;14:7-17.

40. Kirkwood JM, Ibrahim J, Lawson DH, *et al*. High-dose interferon alfa-2b does not diminish antibody response to GM2 vaccination in patients with resected melanoma: results of the multicenter eastern cooperative oncology group phase II trial E2696. J Clin Oncol 2001;19:1430-6.

41. Gupta A, Kirkwood JM. Melanoma. Kaufman, HL, Wadler S, Antman K, editors. Molecular targeting in oncology. Totowa: Humana Press; 2008.

42. Sangfelt O, Erickson S, Castro J, *et al*. Induction of apoptosis and inhibition of cell growth are independent responses to interferon-alpha in hematopoietic cell lines. Cell Growth Differ 1997;8:343-52.

43. Kirkwood JM, Bender C, Agarwala S, *et al*. Mechanisms and management of toxicities associated with high-dose interferon alfa-2b therapy. J Clin Oncol 2002;20:3703-18.

44. Weber J. Review: anti-CTLA-4 antibody ipilimumab: case studies of clinical response and immune-related adverse events. Oncologist 2007;12:864-72.

45. Reuben JM, Lee BN, Li C, *et al*. Biologic and immunomodulatory events after CTLA-4 blockade with ticilimumab in patients with advanced malignant melanoma. Cancer 2006;106:2437-44.

46. Johnston RL, Lutzky J, Chodhry A, *et al*. Cytotoxic T-lymphocyte-associated antigen 4 antibody-induced colitis and its management with infliximab. Dig Dis Sci 2009;54:2538-40.

47. Mitjans F, Meyer T, Fittschen C, *et al*. *In vivo* therapy of malignant melanoma by means of antagonists of alphav integrins. Int J Cancer 2000;87:716-23.

48. Hersey P, Sosman J, O'Day S, *et al*. A phase II, randomized, open-label study evaluating the antitumor activity of MEDI-522, a humanized monoclonal antibody directed against the human metastatic melanoma (MM). Proc Am Soc Clin Oncol 2005;23:711.

49. Hersey P, Sosman J, O'Day S, *et al*. A randomized phase 2 study of etaracizumab, a monoclonal antibody against integrin alpha(v)beta(3), +/- dacarbazine in patients with stage IV metastatic melanoma. Cancer 2010;116:1526-34.

50. Ward S, Casey D, Labarthe MC, *et al*. Immunotherapeutic potential of whole tumour cells. Cancer Immunol Immunother 2002;51:351-7.

51. Hsueh EC, Morton DL. Antigen-based immunotherapy of melanoma: Canvaxin therapeutic polyvalent cancer vaccine. Semin Cancer Biol 2003;13:401-7.

52. Market Wire. CancerVax announces results of phase 3 clinical trials of Canvaxin(TM) in patients with stage III and stage IV melanoma. http://ajaxworld.com/node/198642. Accessed February 12, 2010.

53. Sondak VK, Liu PY, Tuthill RJ, *et al*. Adjuvant immunotherapy of resected, intermediate-thickness, node-negative melanoma with an allogeneic tumor vaccine: overall results of a randomized trial of the Southwest Oncology Group. J Clin Oncol 2002;20:2058-66.

54. News Feature. Rethinking therapeutic cancer vaccines. Nat Rev Drug Discov 2009;8:685-6.

55. Berd D, Sato T, Maguire HC, *et al*. Immunopharmacologic analysis of an autologous, hapten-modified human melanoma vaccine. J Clin Oncol 2004;22:403-15.

56. Avax Technologies. Harnessing the patient's immune system for the treatment of cancer. http://www.avax-tech.com/about/pdfs/avaxfactsheet.pdf. Accessed February 13, 2010.

57. Riker AI, Panelli MC, Kammula US, *et al*. Development and characterization of melanoma cell lines established by fine-needle aspiration biopsy: advances in the monitoring of patients with metastatic melanoma. Cancer Detect Prev 1999;23:387-96.

58. Rosenberg SA, Yang JC, Schwartzentruber DJ, *et al*. Immunologic and therapeutic evaluation of a synthetic peptide vaccine for the treatment of patients with metastatic melanoma. Nat Med 1998;4:321-7.

59. Pipeline Review. Pipeline insight: therapeutic cancer vaccines - prospect of first approval set to reinvigorate interest from major companies. http://www.the-infoshop.com/report/dc105049-cancer-vaccine.html. Accessed February 13, 2010.

60. Kruit W, Suciu S, Dreno B, *et al*. Immunization with recombinant MAGE-A3 protein combined with adjuvant systems AS15 or AS02B in patients with unresectable and progressive metastatic cutaneous melanoma: a randomized open-label phase II study of the EORTC melanoma group. J Clin Oncol 2008;26:9065.

61. Rosenberg SA, Yang JC, Restifo NP. Cancer immunotherapy: moving beyond current vaccines. Nat Med 2004;10:909-15.

62. Slingluff CL, Petroni GR, Yamshchikov GV, *et al*. Clinical and immunologic results of a randomized phase II trial of vaccination using four melanoma peptides either administered in granulocyte-macrophage colony-stimulating factor in adjuvant or pulsed on dendritic cells. J Clin Oncol 2003;21:4016-26.

63. Albert ML, Sauter B, Bhardwaj N. Dendritic cells acquire antigen from apoptotic cells and induce class I-restricted CTLs. Nature 1998;392:86-9.

64. Ridgway D. The first 1000 dendritic cell vaccinees. Cancer Invest 2003;21:873-86.

65. Nestle FO, Alijagic S, Gilliet M, *et al*. Vaccination of melanoma patients with peptide- or tumor lysate-pulsed dendritic cells. Nat Med 1998;4:328-32.

66. Schadendorf NF, Broecker EB, Enk A, *et al*. Dacarbacine (DTIC) versus vaccination with autologous peptide-pulsed dendritic cells (DC) as first-line treatment of patients with metastatic melanoma: results of a prospective-randomized phase III study. J Clin Oncol 2004;22:7508.

67. Rosenberg SA, Dudley ME. Cancer regression in patients with metastatic melanoma after the transfer of autologous antitumor lymphocytes. Proc Natl Acad Sci U S A 2004;101 Suppl 2:14639-45.

68. Sotomayor MG, Yu H, Antonia S, *et al*. Advances in gene therapy for malignant melanoma. Cancer Contr 2002;9:39-48.

69. Piechocki MP, Pilon SA, Wei WZ. Complementary antitumor immunity induced by plasmid DNA encoding secreted and cytoplasmic human ErbB-2. J Immunol 2001;167:3367-74.

70. Ulmer JB, Donnelly JJ, Parker SE, *et al*. Heterologous protection against influenza by injection of DNA encoding a viral protein. Science 1993;259:1745-9.

71. Trisciuoglio D, Desideri M, Ciuffreda L, *et al*. Bcl-2 overexpression in melanoma cells increases tumor progression-associated properties and *in vivo* tumor growth. J Cell Physiol 2005;205:414-21.

134

72. Jansen B, Wacheck V, Heere-Ress E, *et al*. Chemosensitisation of malignant melanoma by BCL2 antisense therapy. Lancet 2000;356:1728-33.

73. Millward MJ, Conry RM, Gore ME, *et al*. Randomized multinational phase 3 trial of dacarbazine (DTIC) with or without Bcl-2 antisense (oblimersen sodium) in patients (pts) with advanced malignant melanoma (MM): analysis of long-term survival. J Clin Oncol 2004;22:7505.

74. Medical News Today. FDA advisory committee reviews Genasense(reg) for use in advanced melanoma. http://www.medicalnewstoday.com/articles/7929.php. Accessed February 14, 2010.

75. Vical Inc. Vical completes enrollment in Allovectin-7(r) phase 3 trial for metastatic melanoma. http://ir.vical.com/releasedetail.cfm?ReleaseID=441001. Accessed February 14, 2010.

76. Richards AB, Gonzalez R, Atkins MB, *et al*. High-dose Allovectin-7 in patients with advanced metastatic melanoma: final phase 2 data and design of phase 3 registration trial. J Clin Oncol 2005;23:7543.

77. Senzer NN, Kaufman H, Amatruda T, *et al*. Updated results of a phase II clinical trial with a second generation, enhanced potency, immune-enhanced, oncolytic herpesvirus in unresectable metastatic melanoma. http://www.biovex.com/downloads/ASCO_melanoma_poster_2009.pdf. Accessed February 14, 2010.

78. BioVex Inc. Biovex commences OncoVEX (GM-CSF) phase 3 trial in metastatic melanoma. http://www.biovex.com/04_14_09.htm. Accessed February 14, 2010.

79. Dothager RS, Putt KS, Allen BJ, *et al*. Synthesis and identification of small molecules that potently induce apoptosis in melanoma cells through G1 cell cycle arrest. J Am Chem Soc 2005;127:8686-96.

80. Fernandez Y, Verhaegen M, Miller TP, *et al*. Differential regulation of noxa in normal melanocytes and melanoma cells by proteasome inhibition: therapeutic implications. Cancer Res 2005;65:6294-304.

81. Smalley KS, Herlyn M. Targeting intracellular signaling pathways as a novel strategy in melanoma therapeutics. Ann N Y Acad Sci 2005;1059:16-25.

82. Gududuru V, Hurh E, Dalton JT, *et al*. Discovery of 2-arylthiazolidine-4-carboxylic acid amides as a new class of cytotoxic agents for prostate cancer. J Med Chem 2005;48:2584-8.

83. Li W, Lu Y, Wang Z, *et al*. Synthesis and antiproliferative activity of thiazolidine analogs for melanoma. Bioorg Med Chem Lett 2007;17:4113-7.

135

84.   Chen J, Wang Z, Lu Y, *et al*. Synthesis and antiproliferative activity of imidazole and imidazoline analogs for melanoma. Bioorg Med Chem Lett 2008;18:3183-7.

85.   Li W, Wang Z, Guduru V, *et al*. Structure-activity relationship studies of arylthiazolidine amides as selective cytotoxic agents for melanoma. Anticancer Res 2007;27:883-8.

86.   Guduru V, Zeng K, Tsukahara R, *et al*. Identification of Darmstoff analogs as selective agonists and antagonists of lysophosphatidic acid receptors. Bioorg Med Chem Lett 2006;16:451-6.

87.   Guduru V, Hurh E, Sullivan J, *et al*. SAR studies of 2-arylthiazolidine-4-carboxylic acid amides: a novel class of cytotoxic agents for prostate cancer. Bioorg Med Chem Lett 2005;15:4010-3.

88.   Bankston D, Dumas J, Natero R, *et al*. A scaleable synthesis of BAY 43-9006: a potent raf kinase inhibitor for the treatment of cancer. Org Proc Res Dev 2002;6:777-81.

89.   Slominski A, Ermak G, Wortsman J. Modification of melanogenesis in cultured human melanoma cells. *In Vitro* Cell Dev Biol Anim 1999;35:564-5.

90.   Rubinstein LV, Shoemaker RH, Paull KD, *et al*. Comparison of *in vitro* anticancer-drug-screening data generated with a tetrazolium assay versus a protein assay against a diverse panel of human tumor cell lines. J Natl Cancer Inst 1990;82:1113-8.

91.   Slominski A, Pisarchik A, Zbytek B, *et al*. Functional activity of serotoninergic and melatoninergic systems expressed in the skin. J Cell Physiol 2003;196:144-53.

92.   Ormerod MG, editor. Flow cytometry, a practical approach. 3rd ed. Oxford: Oxford University Press; 2000.

93.   Zmijewski MA, Li W, Zjawiony JK, *et al*. Photo-conversion of two epimers (20R and 20S) of pregna-5,7-diene-3beta, 17alpha, 20-triol and their bioactivity in melanoma cells. Steroids 2009;74:218-28.

94.   Guo W, Wu S, Liu J, *et al*. Identification of a small molecule with synthetic lethality for K-ras and protein kinase C iota. Cancer Res 2008;68:7403-8.

95.   Chen J, Smith M, Kolinsky K, *et al*. Antitumor activity of HER1/EGFR tyrosine kinase inhibitor erlotinib, alone and in combination with CPT-11 (irinotecan) in human colorectal cancer xenograft models. Cancer Chemother Pharmacol 2007;59:651-9.

136

96. Daidone G, Maggio B, Raffa D, *et al*. Synthesis and *in vitro* antileukemic activity of new 4-triazenopyrazole derivatives. Farmaco 2004;59:413-7.

97. Wilhelm S, Carter C, Lynch M, *et al*. Discovery and development of Sorafenib: a multikinase inhibitor for treating cancer. Nat Rev Drug Discov 2006;5:835-44.

98. McFadyen MC, Melvin WT, Murray GI. Cytochrome P450 enzymes: novel options for cancer therapeutics. Mol Cancer Ther 2004;3:363-71.

99. Rooseboom M, Commandeur JN, Vermeulen N. Enzyme-catalyzed activation of anticancer prodrugs. Pharmacol Rev 2004;56:53-102.

100. Lu Y, Li CM, Wang Z, *et al*. Discovery of 4-substituted methoxybenzoyl-aryl-thiazole as novel anticancer agents: synthesis, biological evaluation, and structure-activity relationships. J Med Chem 2009;52:1701-11.

101. Brugarolas A, Gosalvez M. Treatment of cancer by an inducer of reverse transformation. Lancet 1980;1:68-70.

102. Liu J, Qu S, Li B, *et al*. Synthesis and antitumor activity of timonacic derivatives. Yiyao Gongye 1988;19:203-5.

103. Williams DA, Lemke TL, editors. Foye's principles of medicinal chemistry. 5th ed. Philadelphia: Lippincott Williams & Wilkins; 2002.

104. Meyskens FL, Moon TE, Dana B, *et al*. Quantitation of drug sensitivity by human metastatic melanoma colony-forming units. Br J Cancer 1981;44:787-97.

105. Von Hoff DD, Casper J, Bradley E, *et al*. Association between human tumor colony-forming assay results and response of an individual patient's tumor to chemotherapy. Am J Med 1981;70:1027-41.

106. Zmijewski MA, Li W, Zjawiony JK, *et al*. Synthesis and photo-conversion of androsta- and pregna-5,7-dienes to vitamin D3-like derivatives. Photochem Photobiol Sci 2008;7:1570-6.

107. Zbytek B, Janjetovic Z, Tuckey RC, *et al*. 20-Hydroxyvitamin D3, a product of vitamin D3 hydroxylation by cytochrome P450scc, stimulates keratinocyte differentiation. J Invest Dermatol 2008;128:2271-80.

108. Constantinides PP, Marcello J, Chiossone DC, *et al*. Enhanced intestinal absorption of an RGD peptide from water-in-oil microemulsions of different composition and particle size. J Contr Rele 1995;34:109-16.

109. Povlsen CO, Jacobsen GK. Chemotherapy of a human malignant melanoma transplanted in the nude mouse. Cancer Res 1975;35:2790-6.

110. Lu Y, Li CM, Wang Z, *et al*. Discovery of 4-substituted methoxybenzoyl-aryl-thiazole as novel anticancer agents: synthesis, biological evaluation, and structure-activity relationships. J Med Chem 2009;52:1701-11.

111. Zhou D, Alelyunas Y, Liu R. Scores of extended connectivity fingerprint as descriptors in QSPR study of melting point and aqueous solubility. J Chem Inf Model 2008;48:981-7.

112. Yoon S, Smellie A, Hartsough D, Filikov A. Surrogate docking: structure-based virtual screening at high throughput speed. J Comput Aided Mol Des 2005;19:483-97.

113. Hert J, Willett P, Wilton DJ, *et al*. Comparison of topological descriptors for similarity-based virtual screening using multiple bioactive reference structures. Org Biomol Chem 2004;2:3256-66.

114. Shellman YG, Ribble D, Miller L, *et al*. Lovastatin-induced apoptosis in human melanoma cell lines. Melanoma Res 2005;15:83-9.

115. Li W, Lu Y, Wang Z, *et al*. Synthesis and antiproliferative activity of thiazolidine analogs for melanoma. Bioorg Med Chem Lett 2007;17:4113-7.

116. Longui CA, Santos MC, Formiga CB, *et al*. Antiproliferative and apoptotic potencies of glucocorticoids: nonconcordance with their antiinflammatory and immunosuppressive properties. Arq Bras Endocrinol Metabol 2005;49:378-83.

117. Hadfield JA, Ducki S, Hirst N, *et al*. Tubulin and microtubules as targets for anticancer drugs. Prog Cell Cycle Res 2003;5:309-25.

118. Honore S, Pasquier E, Braguer D. Understanding microtubule dynamics for improved cancer therapy. Cell Mol Life Sci 2005;62:3039-56.

119. Jordan A, Hadfield JA, Lawrence NJ, *et al*. Tubulin as a target for anticancer drugs: agents which interact with the mitotic spindle. Med Res Rev 1998;18:259-96.

120. Jordan MA, Kamath K. How do microtubule-targeted drugs work? Curr Cancer Drug Targets 2007;7:730-42.

121. Uppal SO, Li Y, Wendt E, *et al*. Pattern analysis of microtubule-polymerizing and depolymerizing agent combinations as cancer chemotherapies. Int J Oncol 2007;31:1281-91.

122. Photiou A, Shah P, Leong LK, *et al*. *In vitro* synergy of paclitaxel (Taxol) and vinorelbine (navelbine) against human melanoma cell lines. Eur J Cancer 1997;33:463-70.

123. Germann UA. P-glycoprotein--a mediator of multi-drug resistance in tumour cells. Eur J Cancer 1996;32A:927-44.

124. Dumontet C, Sikic BI. Mechanisms of action of and resistance to antitubulin agents: microtubule dynamics, drug transport, and cell death. J Clin Oncol 1999;17:1061-70.

125. Mohan R, Banerjee M, Ray A, *et al*. Antimitotic sulfonamides inhibit microtubule assembly dynamics and cancer cell proliferation. Biochemistry 2006;45:5440-9.

126. Chaplin DJ, Horsman MR, Siemann DW. Current development status of small-molecule vascular disrupting agents. Curr Opin Investig Drugs 2006;7:522-8.

127. Sampath D, Discafani CM, Loganzo F, *et al*. MAC-321, a novel taxane with greater efficacy than paclitaxel and docetaxel *in vitro* and *in vivo*. Mol Cancer Ther 2003;2:873-84.

128. Liberatore AM, Coulomb H, Pons D, *et al*. IRC-083927 is a new tubulin binder that inhibits growth of human tumor cells resistant to standard tubulin-binding agents. Mol Cancer Ther 2008;7:2426-34.

129. Li W, Shao Y, Hu L, *et al*. BM6, a new semi-synthetic vinca alkaloid, exhibits its potent in vivo anti-tumor activities via its high binding affinity for tubulin and improved pharmacokinetic profiles. Cancer Biol Ther 2007;6:787-94.

130. Liou JP, Hsu KS, Kuo CC, *et al*. A novel oral indoline-sulfonamide agent, N-[1-(4-methoxybenzenesulfonyl)-2,3-dihydro-1H-indol-7-yl]-isonicotinamide (J30), exhibits potent activity against human cancer cells *in vitro* and in vivo through the disruption of microtubule. J Pharmacol Exp Ther 2007;323:398-405.

131. Tahir SK, Kovar P, Rosenberg SH. Rapid colchicine competition-binding scintillation proximity assay using biotin-labeled tubulin. Biotechniques 2000;29:156-60.

132. Gursoy RN, Benita S. Self-emulsifying drug delivery systems (SEDDS) for improved oral delivery of lipophilic drugs. Biomed Pharmacother 2004;58:173-82.

133. Amir E, Rozen S. Easy access to the family of thiazole N-oxides using HOFx CH_3CN. Chem Commun (Camb) 2006:2262-4.

134. Gourdeau H, Leblond L, Hamelin B, *et al*. Species differences in troxacitabine pharmacokinetics and pharmacodynamics: implications for clinical development. Clin Cancer Res 2004;10:7692-702.

135. Bhattacharyya B, Panda D, Gupta S, *et al*. Anti-mitotic activity of colchicine and the structural basis for its interaction with tubulin. Medi Res Rev 2008;28:155-83.

136. Romagnoli R, Baraldi PG, Sarkar T, *et al*. Synthesis and biological evaluation of 1-methyl-2-(3',4',5'-trimethoxybenzoyl)-3-aminoindoles as a new class of antimitotic agents and tubulin inhibitors. J Med Chem 2008;51:1464-8.

137. Romagnoli R, Baraldi PG, Carrion MD, *et al*. Synthesis and biological evaluation of 2- and 3-aminobenzo[b]thiophene derivatives as antimitotic agents and inhibitors of tubulin polymerization. J Med Chem 2007;50:2273-7.

138. Lavelle F, Gueritte-Voegelein F, Guenard D. Taxotere: from yew's needles to clinical practice. Bull Cancer 1993;80:326-38.

139. Nelson RL. The comparative clinical pharmacology and pharmacokinetics of vindesine, vincristine, and vinblastine in human patients with cancer. Med Pediatr Oncol 1982;10:115-27.

140. Beerepoot LV, Radema SA, Witteveen EO, *et al*. Phase I clinical evaluation of weekly administration of the novel vascular-targeting agent, ZD6126, in patients with solid tumors. J Clin Oncol 2006;24:1491-8.

141. Bross PF, Kane R, Farrell AT, *et al*. Approval summary for bortezomib for injection in the treatment of multiple myeloma. Clin Cancer Res 2004;10:3954-64.

142. Galmarini CM. ABT-751 (Abbott). Curr Opin Investig Drugs 2005;6:623-30.

143. Bellina F, Cauteruccio S, Monti S, *et al*. Novel imidazole-based combretastatin A-4 analogues: evaluation of their *in vitro* antitumor activity and molecular modeling study of their binding to the colchicine site of tubulin. Bioorg Med Chem Lett 2006;16:5757-62.

144. Wang L, Woods KW, Li Q, *et al*. Potent, orally active heterocycle-based combretastatin a-4 analogues: synthesis, structure−activity relationship, pharmacokinetics, and *in vivo* antitumor activity evaluation. J Med Chem 2002;45:1697-711.

145. Gottesman MM, Fojo T, Bates SE. Multi-drug resistance in cancer: role of ATP-dependent transporters. Nat Rev Cancer 2002;2:48-58.

146. Salmon SE. Human tumor clonogenic assays: growth conditions and applications. Cancer Genet Cytogenet 1986;19:21-8.

147. Gigant B, Wang C, Ravelli RB, *et al*. Structural basis for the regulation of tubulin by vinblastine. Nature 2005;435:519-22.

148. Ravelli RB, Gigant B, Curmi PA, *et al*. Insight into tubulin regulation from a complex with colchicine and a stathmin-like domain. Nature 2004;428:198-202.

149. Cheng Y, Prusoff WH. Relationship between the inhibition constant (K1) and the concentration of inhibitor which causes 50 per cent inhibition (I50) of an enzymatic reaction. Biochem Pharmacol 1973;22:3099-108.

APPENDIX

Tubulin Ligand (Colchicine) Competition Assay Protocol

The basic approach to the assay is as follows

1. Set-up scintillation plate reader and warm plate in reader to 37°C.
2. Prepare compounds to 20x strength (1 mM) in G-PEM buffer plus 10% DMSO.
3. Prepare tritiated colchicine. Assay life 24 h.
4. Prepare biotin tubulin on ice. Assay life 4 h.
5. Prepare streptavidin beads. Assay life 24 h.
6. Prepare bead/tubulin mixture. Assay life 24 h.
7. Pipette 10 µL of compound into the wells.
8. Pipette 10 µL of tritiated colchicine into the wells.
9. Pipette 180 µL of bead/tubulin into the wells.
10. Incubate for 45 min at 37°C.
11. Read plate.
12. Extract the raw data and calculate percent inhibition.

Preparation of compounds

This step is performed before the tubulin is rehydrated because if there is an unforeseen error or precipitation occurs, then the experiment can be aborted before rehydrating tubulin. Prepare compound stocks at 20x final concentration (usually 1 mM) in 50% DMSO, 50% Ethanol or G-PEM plus one of these solvents from 5~50% at room temperature. The final organic solvent concentration should not exceed 2.5% (v/v). Solubilizing agents such as SDS or Triton X100 can be used up to 0.1% and 1.0% respectively. The concentration of compounds may vary depending on the nature of the screen, 50 µM final concentration is recommended. The necessary controls are zero compound concentration, 1mM colchicine for competition, and 1mM vinblastine for noncompetitor.

Preparation of buffers

1. Reconstitute General Tubulin Buffer (BST01-010) with 100 mL of Milli-Q water and place at 4°C for storage.
2. Resuspend GTP vial with 100 µL of water, aliquot into 10x10 µL and freeze at -70°C for storage.

Preparation of tubulin protein, in 50 assay aliquots

1.   Prepare 1 mL of ice cold G-PEM buffer: On ice, mix 1mL of General Tubulin Buffer with 10 µL of GTP stock.
2.   Resuspend 500 µg of T333 in 60 µL of ice cold G-PEM and place back on ice.
3.   Microfuge for 5 min at 14,000g at 4°C.
4.   Carefully pipette 55 µL of supernatant (avoiding the location where a very small pellet might be located) into a clean tube on ice.
5.   Pipette into 10x5 µL aliquots on ice, and drop freeze all of them into liquid nitrogen.
6.   Store at -70°C, where they are stable for 6 months.

Preparation of beads, enough for 50 assays

This step should be performed just prior to the assays because the change of buffer decreases the shelf life of the beads to 24 h.

1.   Pipette 4.4 mg of Streptavidin-SPA beads into a 15 mL Falcon tube, centrifuge 3000 rpm for 10 min to pellet the beads.
2.   Carefully pipette off the sup, leaving 100 µL liquid volume above the beads.
3.   Resuspend in 5 mL of General Tubulin Buffer and centrifuge again.
4.   Carefully pipette off the sup, leaving 100 µL liquid volume above the beads.
5.   Resuspend the beads thoroughly in 9.5 mL of General Tubulin Buffer.

Preparation of tubulin-beads, enough for 50 assays

These tubulin loaded beads should be made just prior to assay because they will have a life time of 24 h at 4°C.

1.   Prepare 1mL of ice cold G-PEM buffer: On ice, mix 1 mL of General Tubulin Buffer with 10 µL of GTP stock.
2.   Rapidly defrost one vial of biotin tubulin by warming in Milli-Q water for 30 secs, then place on ice.
3.   Dilute the vial of biotin tubulin with 500 µL of G-PEM buffer.
4.   Pipette the entire volume of biotin tubulin into the 9.5 mL of beads, mix thoroughly incubate on a slow 10 rpm rotator at 4°C for 30 min), then use immediately, or up to 24 h thereafter if necessary (activity may drop by 40% during this time). The tubulin-beads must be kept rotating if aliquots are going to be used continuously over the 24 h period.

143

Preparation of tritium colchicine, enough for 50 assays

Dilute 50 µL of [3H]colchicine (specific activity 20~80 Ci/mmole, 1.0 µCi/µL, original stock concentration 5~10 µM) into 500ul of General Tubulin Buffer and mix well. This makes a sub-stock of 0.5~1.0 µM and a final concentration in the reaction of 25~50 nM. If the signal is too low this component can be increased upto fourfold this level, this is particularly useful for non-HTS applications where more signal is required.

Material and equipment required

Material

Tritiated Colchicine
Streptavidin SPA beads
96-well plates Low PB Corning Costar Inc.

Equipment

Scintillation Counter Packard Instrument Inc. Tel: 1-800-762-4000 Topcount Microtplate Reader

Scintillation counter plate reader set-up

Measurement type: Top
Sensitivity: Highest.
Read time per well: 10 seconds per read.
Shaking: 5 s medium, orbital.
Plate template: Griener GRE96fb (flat, black).

Soft Agar Colony Assay Protocol

Preparation of 1.6% agar

1.   Pre-warm 50 mL autoclave-safe glass bottles in a 40°C water bath.
2.   Heat 1800 mL of deionized H_2O in a 4 L flask with 2 L calibration to 80~90°C on a hot plate. Use a glass petri cap to prevent evaporation.
3.   Add 25 g of dry Agar to the flask containing the 80~90°C water. Stir with a glass rod until lumps disappear.
4.   While the flask is still being heated, adjust the volume to 2000 mL with H2O. Stir until thoroughly mixed.
5.   Add 40 mL of the 1.6% agar solution to each of the 100 mL bottles previously held at 40°C. Cap bottles loosely.
6.   Autoclave for 15 min on slow exhaust. Allow bottles to cool for a few minutes then tighten caps. Store at room temperature or at 4°C.

Preparation of the 0.5% agar growth medium dishes

The directions provided below are for 100 mL of 0.5% Agar Growth Medium—enough to prepare about 14~60 mm dishes. Volumes may be adjusted for larger sized dishes as needed.

1.   Prepare the Growth Medium at the desired concentration of FBS, and warm in a 44°C water bath.
2.   Melt 40 mL of 1.6% agar in a microwave oven until just molten, swirling intermittently. Remove the bottle as soon as the agar solution becomes clear.
3.   Cool the 1.6% agar at room temperature for 2 to 3 min.
4.   Place the bottle containing the agar in the 37°C water bath.
5.   When both the Growth Medium and the 1.25% agar have reached 37°C, mix the 1.6% agar with the Growth Medium to make a 0.5% Agar Growth Medium solution.
6.   Pipette 6 mL of the 0.5% Agar Growth Medium mixture into each sterile 60 mm petri dish. Avoid forming bubbles and spread the mixture evenly by slowly rotating the dish. Note: Reagents such as TPA) or EGF should be added to the 0.5% Agar Growth Medium just before pipetting it into the petri dishes. Typically, a final concentration of 10 ng/mL TPA or EGF is used. Control plates to which the solvent (DMSO or water) for the TPA or EGF is added should also be prepared.
7.   Allow the 0.5% Agar Growth Medium layer to harden for 30 to 40 min at room temperature in a sterile laminar flow hood.
8.   Store the dishes overnight in a 37°C incubator or seal in a bag and store at 4°C. The dishes can be stored this way for several days. Note: Refrigerated dishes should be warmed to 37°C before use.

Preparation of cell suspension and performing the over-agar assay

1. Two or three days before the experiment, plate the cells in a screw-cap T-25 or T-75 flask in a final volume of 10 to 15 mL of Cell Growth Medium.
2. Grow the cells in a 37°C, 5% CO_2 humidified incubator until the cells are 80 to 90% confluent.
3. Wash the monolayer of cells in T-25 flask or T-75 flask twice with 1~2 mL of Ca^{2+}, Mg^{2+} free PBS, aspirating the PBS after each wash.
4. Add 1 mL of 0.03% Trypsin.
5. Incubate in a 37°C, 5% CO_2 humidified incubator for 3 to 6 min or until 90% of the cells are detached.
6. Add 1 mL of DMEM containing 10% heat-inactivated FBS (DMEM-FBS).
7. Gently resuspend cells with a sterile pipette three or four times to make a single-cell suspension. Note: Observe a sample of the suspension with a microscope to confirm that it consists of single cells rather than clumps.
8. Determine the concentration of cells and adjust the suspension to 1×10^3 cells/mL in DMEM-FBS. Note: If the cells are to be plated on the TPA- or EGF-containing 0.5% Agar Growth Medium, then TPA or EGF should be added to the cell suspension just before transferring them onto the plates. The final concentration of TPA or EGF should be 10 ng/mL.
9. Transfer 3 mL of the cell suspension (containing a total of 3×10^3 cells) to the 0.5% Agar Growth Medium plate and incubate at 37°C, 5% CO_2.
10. Culture the cells on the 0.5% Agar Growth Medium plate for 14 to 21 days, during which time colonies of transformed cells will form in the TPA- or EGF-treated dishes.
11. Count the number of cells in each colony and the number of colonies using a microscope. Note: Each colony should contain more than eight cells.

Cell Cycle Analysis Protocol

1.   Human melanoma cells A375 were cultured into 10 cm tissue culture dishes till 80% confluence.
2.   Serum starved for 24 h. Media was then replaced with media containing testing compounds at different concentration or vector only in triplicates.
3.   Cells were incubated with compounds for 6 h, trypsinized, and harvested by centrifugation.
4.   Cells were then washed with 1×PBS 3 times and resuspended in ice-cold 70% ethanol at 4°C overnight.
5.   Ethanol was removed by centrifugation and washing with 1×PBS 3 times.
6.   Finally, cells were pelleted out of PBS and resuspended in 1mL PBS buffer containing 100 µg/mL RNase A. cells were incubated at 37°C for 1 h.
7.   After centrifuging cells and aspirating supernatant, resuspend cells in 500 µL of propidium iodide (50 µg/mL) in PBS.
8.   Cell cycle was determined using a BD LSR-II (BD Biosciences, San Jose, CA USA) with a 10,000 cells scored. Data were analyzed and graphs were prepared using the Modfit 2.0 program (Verity Software House, Topsham, ME).

Tubulin Imaging Protocol

Solution preparation (per 96-well plate)

1. 1X Wash Buffer: Add 30 mL 10X Wash Buffer to 270 mL ultrapure water. Store buffer at 4°C for up to 7 days.
2. Fixation Solution: Add 5 mL of 16% formaldehyde solution to 15 mL of 1X Wash Buffer and heat to 37°C in a water bath just before use. Pre-warming the Fixation Solution is critical for maintaining cell integrity. Prepare solution just before each assay.
3. 1X Permeabilization Buffer: Add 2 mL of 10X Permeabilization Buffer to 18 mL of the 1X Wash Buffer. Store this buffer at 4°C for up to 7 days.
4. 1X Blocking Buffer: Add 10 mL of the 10X Blocking Buffer to 90 mL of 1X Wash Buffer. Store buffer at 4°C for up to 7 days.
5. Primary Probe Solution: Reconstitute DY554-phalloidin (F-actin kits) by adding 110 μL for 10 units (550 μL for 50 units) of pure methanol and gently mixing. Use the DY554-phalloidin immediately and promptly store any unused portion at -20°C.
6. F-actin and tubulin kits (8402401, 8402402): Add 100 μL of DY554-phalloidin and 6 μL of Tubulin Primary Antibody to 5.9 mL of 1X Blocking Buffer. Prepare solution just before each assay. F-actin kits (8402501, 8402502): Add 6 μL of DAPI, 100 μL of DY554-phalloidin to 5.9 mL of the 1X Blocking Buffer. Prepare solution just before each assay.
7. For the tubulin kits (8402601, 8402602): Add 6 μL of Tubulin Primary Antibody to 6 mL of the 1X Blocking Buffer. Prepare solution just before each assay.
8. Staining Solution (Secondary Antibody): F-actin and tubulin kits (8402401, 8402402): Add 6 μL of DAPI, 6 μL of the DyLight 649 Goat Anti-Mouse to 6 mL of 1X Blocking Buffer. Prepare solution just before each assay.
9. For the tubulin kits (8402601, 8402602): Add 6 μL of DAPI and 6 μL of the DyLight 549 Goat Anti-Rabbit to 6 mL of 1X Blocking Buffer. Prepare solution just before each assay.
10. Whole Cell Stain Solution: Just before use, reconstitute the Whole Cell Stain Green by adding 50 μL of DMSO to the tube and mixing. Add 12 μL of the stain in DMSO to 12 mL of 1X Wash Buffer. Prepare solution just before each assay. Use the Whole Cell Stain Solution immediately and discard the unused solution. Whole Cell Stain Green in DMSO may be stored at -20°C for <1 week.

Protocol for the cytoskeletal rearrangement kit

1. Dilute the cytochalasin D stock solution (*e.g.*, 3 mM in DMSO) to 30 μM, or other test compounds to appropriate concentration, in culture medium. Add 50 μL of culture medium to the control wells. Add 50 μL of cytochalasin D in culture medium to each treatment well (150 μL final). Incubate for 3 h at 37°C in 5% CO_2.

148

2. Aspirate culture medium and add 100 μL/well of warmed Fixation Solution. Incubate plate in a fume hood at room temperature for 15 min. Using warm (37°C) Fixation Solution is critical for maintaining cell integrity.
3. Aspirate Fixation Solution and wash plate twice with 100 μL/well of 1X Wash Buffer.
4. Aspirate Wash Buffer, add 100 μL/well of 1X Permeabilization Buffer and incubate for 15 min at room temperature.
5. Aspirate Permeabilization Buffer. Add 100 μL/well of 1X Blocking Buffer. Incubate at room temperature for 15 min.
6. Aspirate Blocking Buffer and add 50 μL/well primary probe solutions. Incubate for 1 h at room temperature. Note: For whole cell stain and F-actin kits, skip step 7 and 8.
7. Aspirate Primary Probe Solution and then wash twice with 100 μL/well of 1X Blocking Buffer.
8. Aspirate Blocking Buffer and add 50 μL/well of Staining Solution (secondary antibody). Incubate for 30 min protected from light at room temperature.
9. Aspirate solution and then wash plate three times with 100 μL/well of 1X Wash Buffer.
10. Add 100 μL/well of Whole Cell Stain Solution. Incubate for 15 min protected from light at room temperature.
11. Aspirate Whole Cell Stain Solution and wash plate three times with 100 μL/well of 1X Wash Buffer.
12. Aspirate Wash Buffer and replace with 150 μL/well of 1X Wash Buffer.
13. Seal plate and evaluate on the ArrayScan HCS Reader. Store plates at 4°C.

VITA

Zhao Wang was born in Shandong Province, China, in 1975. He joined the Shandong University in 1995 and received a Bachelor of Medicine degree in 2000. He joined the joint Master degree program offered by the Peking Union Medical College (PUMC) and the Chinese National Institute for the Control of Pharmaceutical and Biological Products (NICPBP) in 2000. He received his Master of Pharmaceutical Sciences degree in 2003. After graduation, he worked in NICPBP for two years as former employee with a title of Lab Scientist. In the fall of 2005, he joined the graduate program in the Department of Pharmaceutical Sciences, the University of Tennessee Health Science Center, Memphis, from where he will receive his Ph.D. under the supervision of Prof. Wei Li.